eChem
https://www.sciltp.com/journals/eChem

Review

Electrolyte Design for Low-Temperature Lithium-Ion Batteries: Solvation Regulation and Interfacial Chemistry

Dandan Yu [1,*], Kexin Li [1], Tianyi Yu [1], Jingyun Mou [1], Tianqi Ge [1], Jiawei Luo [1], Wenlong Song [2,*], Khatam Ashurov [3] and Da Chen [1,*]

[1] College of Materials and Chemistry, China Jiliang University, Hangzhou 310018, China
[2] Tianneng Battery Group Co., Ltd., Changxing 313100, China
[3] Arifov Institute of Ion-Plasma and Laser Technologies, Academy of Sciences of the Republic of Uzbekistan, Tashkent 100125, Uzbekistan
* Correspondence: yudandan@cjlu.edu.cn (D.Y.); songwl@tianneng.com (W.S.); chenda@cjlu.edu.cn (D.C.)

How To Cite: Yu, D.; Li, K.; Yu, T.; et al. Electrolyte Design for Low-Temperature Lithium-Ion Batteries: Solvation Regulation and Interfacial Chemistry. *eChem* **2026**, *2*(1), 2. https://doi.org/10.53941/echem.2026.100002

Received: 23 February 2026
Revised: 20 April 2026
Accepted: 23 April 2026
Published: 7 May 2026

Abstract: The development of high-performance lithium-ion batteries (LIBs) that operate efficiently at subzero temperatures, particularly below −20 °C, has garnered considerable attention due to their increasing demand in cold environments. Electrolyte engineering plays a pivotal role in ensuring reliable battery performance at low temperatures. However, the relationship between the solvation structure of electrolytes and interfacial chemistry at subzero temperatures remains inadequately understood. A comprehensive investigation of the synergistic effects between electrolyte solvation and the composition and structure of interphase layers is essential for optimizing low-temperature (LT) performance. This review consolidates recent advancements in electrolytes designed for LT LIBs, beginning with a discussion on how temperature reduction influences the physicochemical properties of electrolytes. Electrolytes are classified into four categories: aqueous, organic, solid-state, and ionic liquid-based, with key performance limitations at LT outlined for each type. We further explore design principles aimed at overcoming these limitations, emphasizing the interplay between solvation structures and interphases at subzero temperatures. Finally, we propose future research directions to drive advancements in electrolyte engineering for LT applications. This review serves as a comprehensive roadmap for advancing battery technologies in ultra-low temperature environments.

Keywords: lithium-ion batteries; electrolyte design; interfacial chemistry; subzero temperatures; solvation

1. Introduction

1.1. Backgrounds

As the world strives toward carbon neutralization, rechargeable batteries play a vital role in revolutionizing portable electronics, electric vehicles (EVs), and energy storage systems. Low-temperature (LT) battery technologies are urgently needed for electric vehicles operating in cold regions (e.g., −20 to −40 °C), aerospace systems exposed to extreme thermal cycling (−60 °C to +80 °C), unmanned polar research equipment, and grid storage in high-latitude regions [1–5]. These applications demand reliable power output, fast charging, and high safety under subzero environments, making the development of robust electrolytes indispensable. Lithium-ion batteries (LIBs) perform well within a temperature range of 0~40 °C. However, the harsh reality is that even commercial LIBs suffer rapid degradation in reversible capacity and fast charging capability at subzero temperatures, particularly below −20 °C [6–10]. Such degradation is primarily caused by slow ion transport in the

bulk electrolyte, difficulty of the desolvation process, slow ion migration at the electrode/electrolyte interphase (EEI) layers, sluggish ion diffusion within the electrodes, the increased polarization voltage ($E = E^{\theta} - \frac{RT}{nF}\ln Q$, where E, E^{θ}, and F represent the actual potential, standard potential, Faraday constant, while n and Q denote the electron migration number and the concentration of substances, respectively) and even lithium metal plating as the temperature decreases (Figure 1).

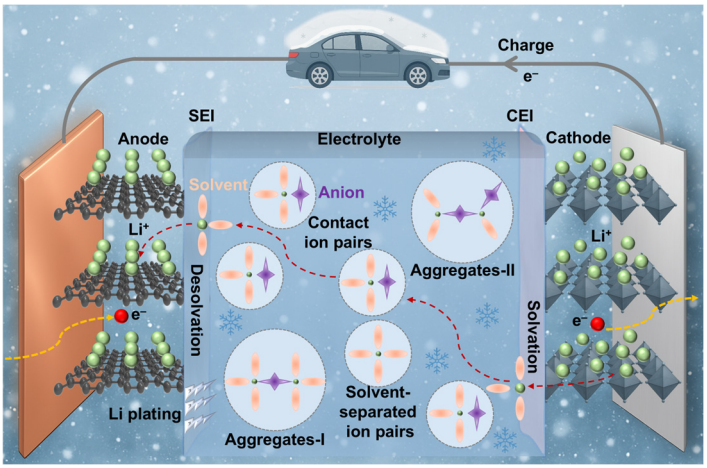

Figure 1. Key steps that limit the LT performance of LIBs.

Electrolytes are critical for extending battery operating capabilities from room temperature (RT) to extreme temperature conditions. According to the Stokes Law, the transport rate of ions in electrolytes is heavily influenced by the electrolyte viscosity. The LT environment generally induces the increased viscosity and reduced ion conductivity, hindering the mass transfer process and electrode wettability, which inevitably leads to higher battery internal resistance. When the temperature drops below subzero Celsius, a high desolvation energy barrier must be overcome, imposing a limitation to the charge transfer at the EEI [11]. The composition and structure of EEI layers are closely associated with the electrolyte formulations, which can also influence the charge-transfer kinetics [12]. With the growing demand for electrolytes that can meet the stringent requirements for ion transport properties, interfacial kinetics, and EEI stability at subzero temperatures, significant efforts have been dedicated to developing new design principles aimed at improving LT battery performance. Therefore, a comprehensive review and outlook on electrolyte design is essential for advancing the development of LT batteries.

1.2. History and Development of Low-Temperature Electrolytes

The pursuit of LT LIBs has been driven by the growing demand for energy storage systems operable in extreme temperature environments (Figure 2). Early efforts in 1983, Abraham et al. [13] introduced tetrahydrofuran (THF) as a co-solvent to improve the ionic conductivity of the base electrolyte (1.4 M lithium hexafluoroarsenate ($LiAsF_6$)/2-methyltetrahydrofuran (2MeTHF)) at LTs. The 1.4 M $LiAsF_6$/THF-2MeTHF (1:1 by volume) electrolyte-based Li||TiS_2 cells exhibit 70% of the theoretical capacity when discharged at –10 °C and 2 mA cm^{-2}, while the baseline electrolyte-based cell shows practically no discharge capacity. For almost all commercial LIBs, ethylene carbonate (EC) is a common co-solvent in carbonate-based electrolytes, while its high freezing point limits the effective LT battery operation when using a high EC-content electrolyte. Ein-Eli et al. [12] investigated the LT performances of Li||graphite cells by using 1 M $LiAsF_6$/methyl formate (MF)-EC electrolytes with different MF contents. Although the electrolyte with a higher MF content exhibits higher ionic conductivity at LTs, Li||graphite cells with the MF-EC (1:3 by volume) electrolyte retain 49% of the room-temperature capacity at –2 °C, significantly higher than the MF-EC (3:1 by volume) counterpart, which is attributed to the poor film-forming ability of MF. After that, Smart et al. [13] found that the EC-based ternary carbonate electrolytes were preferred for LTs compared to the binary analogues in terms of ion conductivities and surface passivating films. Nevertheless, commercial LIBs only preserved 5% of its energy density at –40 °C by using the 1 M lithium hexafluorophosphate ($LiPF_6$) dissolved in EC-propylene carbonate-diethyl carbonate (EC-PC-DEC, 1:1:1 by volume) electrolyte [1]. Smart et al. [14] reported low EC-content quaternary carbonate electrolytes for three-electrode MCMB-carbon||$LiNi_{0.8}Co_{0.2}O_2$ cells which could operate well at the low temperature down to –60 °C. Subsequently, carboxylic ester co-solvents such as methyl acetate (MA), ethyl acetate (EA), methyl butyrate (MB), methyl propionate (MP), and ethyl propionate (EP) with low melting points and low viscosity are added to further improve the ionic conductivity of multi-component carbonate electrolytes at LTs [2,11].

It has been recognized that the significant increase in charge-transfer resistance (R_{ct}) is the primary limitation for LT battery operation, while the low ionic conductivity of bulk electrolytes at subzero temperatures is not the predominant factor that influences the LT performance unless electrolyte solidification or salt precipitation happens. Appropriate solutes have been developed to improve the LT adaptability [3,15–17]. Zhang et al. [3] chose $LiBF_4$ instead of $LiPF_6$ in the mixed solvent of PC-EC-ethylmethyl carbonate (EMC, 1:1:3 by weight) with the 1 m (mol kg^{-1}) concentration for LT LIBs. Despite the lower ionic conductivity of the $LiBF_4$ electrolyte, Li-ion cells with this electrolyte maintain 80% of the room-temperature capacity at –30 °C, higher than that of the $LiPF_6$ counterpart, which is attributed to the much lower R_{ct}. Zhang et al. [18] investigated the impedance of Li-ion cells and symmetric cells as the temperature decreased, and found that the R_{ct} was most significantly increased and became predominant below −10 °C. Besides, film-forming additives have been introduced to improve the LT battery performance by building low-resistance EEIs. Difluoromethyl acetate (MFA) was utilized as the additive to prepare 1 M of lithium perchlorate ($LiClO_4$)/EC-DEC-PC-MFA (1:1:1:0.15 by volume) electrolyte for Li||fluorinated natural graphite cells, which effectively induced a stable solid-electrolyte interphase (SEI) with a lower resistance and better charge transfer across EEI at −10 °C [19]. Typically, the introduction of fluoroethylene carbonate (FEC) additive in the 1 M $LiPF_6$/EC-DMC-EMC-FEC (1:1:1:0.02 by volume) electrolyte effectively improves the reversible capacity of Li||graphite cells at −20 °C, resulting from the reduced R_{ct} and lower-impedance SEI film with a higher LiF content [6].

Importantly, Zhang et al. [18] disclosed that charging of LIBs was more difficult than discharging at the temperature below −10 °C because of a much higher R_{ct}. Nevertheless, the charging process of LIBs at subzero temperatures is often accompanied by severe lithium plating on the anode, which can significantly degrade battery performance and safety. In the early stages of LT battery research, efforts primarily focus on enhancing the LT discharge capacity of LIBs after charging at the RT. As the application scenarios of LIBs continue to expand, many now require not only LT discharge but also efficient rechargeability under cold conditions. Especially since 2017, improving the LT rechargeability of LIBs through electrolyte regulation has emerged as a hot research focus. For example, Fan et al. [7] designed an all-temperature battery electrolyte by dissolving all-fluorinated carbonate electrolyte into highly fluorinated non-polar solvents (like tetrafluoro-1-(2,2,2-trifluoroethoxy)ethane, D2) to regulate the affinity between solvents and Li^+. The designed 1.28 M lithium bis(fluorosulfonyl)imide (LiFSI)/FEC-methyl (2,2,2-trifuoroethyl) carbonate (FEMC)-D2 (1:2:7 by volume) electrolyte exhibits a high ionic conductivity (>1 × 10^{-2} mS cm^{-1} at −80 °C), a wide voltage window up to 5.6 V, and non-flammability, and thus Li||$LiNi_{0.8}Co_{0.15}Al_{0.05}O_2$ cells deliver a discharge capacity of 96 mAh g^{-1} even at −85 °C and 1/15 C after the room-temperature charging at 1/3 C.

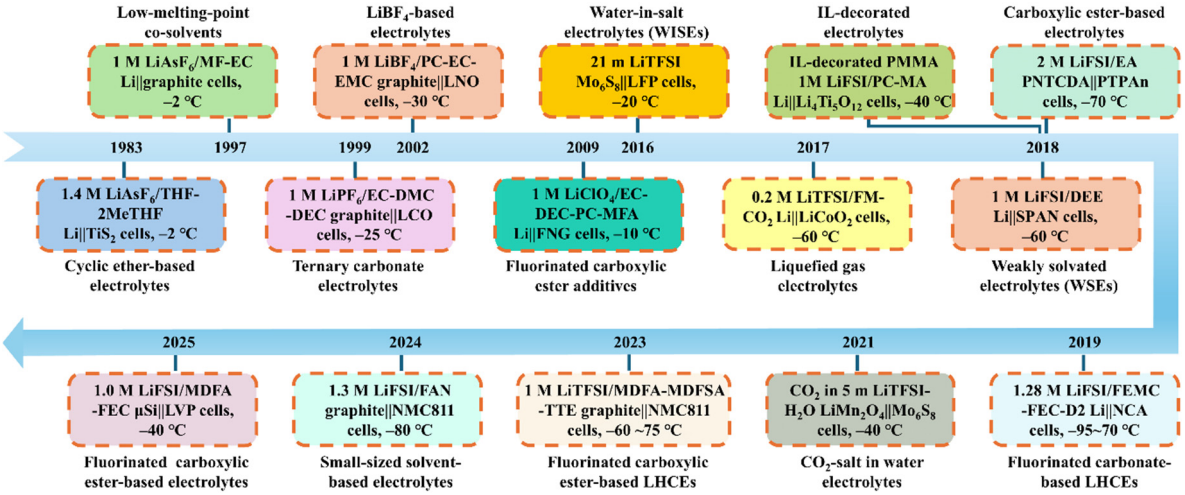

Figure 2. The research history and milestones of electrolytes for LT LIBs [3,4,7,12,19–27].

Aqueous electrolytes have garnered growing attention for LT operation due to their low cost, environmental friendliness, and excellent ionic conductivity. It was discovered that aqueous electrolytes enabled the remarkable performance of intercalation cathodes for LIBs at −40 °C compared to traditional organic electrolytes, which was mainly caused by no significant increase in R_{ct} at subzero temperatures [8]. Suo et al. [24] designed a CO_2-salt in water (SIW, CO_2 in 5 m LiTFSI-H_2O) electrolyte, where the introduction of CO_2 as an interphase-forming additive contributed to forming the Li_2CO_3-rich interphase in a dilute SIW electrolyte, effectively preventing the crystallization of super-concentrated water-in-salt electrolytes at LTs. The $LiMn_2O_4$||Mo_6S_8 aqueous full cells shows a stable capacity above 70 mAh g^{-1} at 0.5 C and −40 °C.

Furthermore, innovative non-aqueous electrolyte systems have played a pivotal role in sustainably improving the LT performance of LIBs. Meng et al. [22] developed liquefied gas electrolytes for ultra-LT battery operation, which possessed high electrolytic conductivities at LTs due to the low melting point and superior dielectric-fluidity factor of liquefied gas solvents like fluoromethane (FM). The FM-based Li||$LiCoO_2$ (LCO) batteries show a high discharge capacity retention of 60.6% at −60 °C and 0.1 C. Ionic liquids (ILs), which consist entirely of cations and anions, have been recognized as promising components for LT electrolytes due to their wide liquidus temperature, nonflammability, low saturated vapor pressure, and superior thermal/electrochemical stability. Kunze et al. [28] found that binary mixtures of Nbutyl-N-methyl pyrrolidinium-bis(trifluoromethanesulfonyl)imide (Pyr_{14}TFSI) and N-methyl-N-propyl pyrrolidinium-bis(fluorosulfonyl)imide (Pyr_{13}FSI) exhibited higher ionic conductivity than pure IL materials at −40 °C. Although ILs offer the improved safety and high-temperature performance compared to conventional organic electrolytes, their high viscosities, high costs, and low ionic conductivities hinder the practical application at LTs. Li et al. [4] designed ionic liquid (IL)-decorated poly(methyl methacrylate (PMMA) nanoparticles with 1 M lithium bis(trifluoromethylsulfonyl)imide (LiTFSI)/PC-MA as the electrolyte which demonstrated a remarkable ionic conductivity of 9.15×10^{-4} S cm^{-1} at −40 °C, enabling excellent reversible capacity and rate capability of Li||$Li_4Ti_5O_{12}$ cells under subzero conditions. Compared to organic electrolytes, solid-state electrolytes (SSEs) offer several advantages, including low flammability, excellent flexibility, a wide electrochemical stability window (ESW), superior thermal stability, leakage prevention, and enhanced safety. However, they also have notable drawbacks, such as low ionic conductivity, limited electrochemical interface activity, and high interfacial resistance. The incorporation of solid polymer electrolytes (SPEs) with special structure presents a promising strategy to overcome these challenges. Lin et al. [9] synthesized a starch-based SPE (BStSi) through two cross-linking reactions to produce –B–O–C– and –O–Si–O– bonds for sufficient salt dissociation, which possessed superior flexibility, outstanding ionic conductivity (3.10×10^{-5} S cm^{-1}), high Li^+ transfer number of 0.72, and excellent oxidation stability up to 5.5 V at −20 °C, enabling stable cycling performance of Li||$LiFePO_4$ (LFP) batteries for 300 cycles at −20 °C and 0.1 C.

In this review, we focus on electrolyte design to enhance the LT performance of LIBs through regulation of solvation structures and interfacial chemistry. Recent advances and ongoing challenges in LT LIBs are systematically summarized (Scheme 1). We begin by outlining the practical requirements for LT applications and the electrolyte-related failure mechanisms that limit battery performance at subzero temperatures. We analyze how physico-chemical properties of bulk electrolytes, solvation structures, and interphase characteristics collectively govern electrochemical performance, particularly under ultralow temperatures (≤−40 °C). Key design principles for LT electrolytes are subsequently highlighted, offering guidance for improving the temperature adaptability of LIBs in cold environments. Building on these principles, we review recent progress in the rational design of aqueous, organic, solid-state, and ionic liquid-based electrolytes. Special attention is given to the correlation between electrolyte solvation structures and the formation and stability of EEI films at low temperatures. Finally, we discuss the remaining challenges and propose future research directions to advance the development of high-performance LT electrolytes.

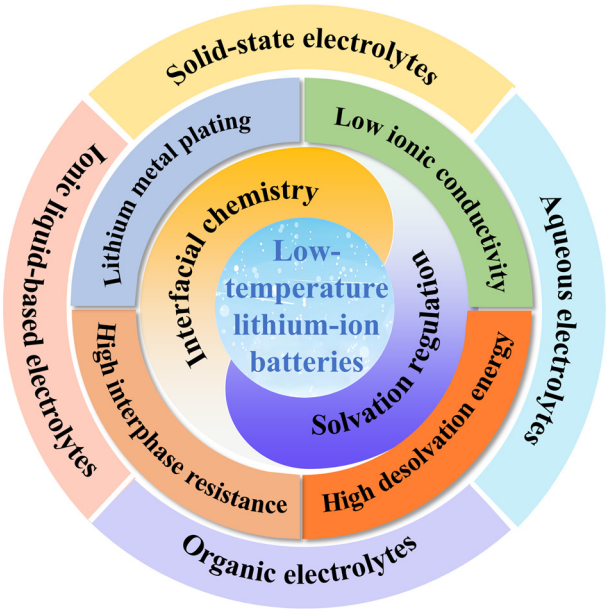

Scheme 1. Challenges faced by LIBs for LT operations and summary of advanced electrolyte systems.

2. Fundamentals and Challenges of Electrolytes under Low-Temperature Conditions

2.1. Impact of Electrolyte Properties on Low-Temperature Performance

2.1.1. Physico-Chemical Properties of Bulk Electrolytes

Physico-chemical properties of bulk electrolytes, such as ionic conductivity, viscosity, liquid range, and ion transference number, are critical to the LT performance of LIBs. The ionic conductivity (σ) can be described using the Nernst-Einstein equation: $\sigma = \frac{F^2 cD}{\mathrm{RT}}$, where *F*, *c*, *D*, *R*, and *T* represent the Faraday constant, ion concentration, diffusion coefficient, universal gas constant, and absolute temperature, respectively. Moreover, the temperature-dependence of conductivity is often modelled via an Arrhenius-type equation: $\sigma = \sigma_0 e^{(\frac{-E_a}{k_B T})}$, where σ_0 represents the pre-exponential factor, E_a *is* the activation energy, and k_B *is* the Boltzmann constant. This relationship underscores the exponential decline of ionic conductivity at lower temperatures due to the thermally activated nature of ion transport.

The viscosity (η) *of* electrolyte can be linked to *D* through the Stokes-Einstein equation: $D = \frac{kT}{6\pi\eta \mathrm{r}}$, with *r* being the effective ionic radius, which is inversely related to temperature and plays a pivotal role in ion diffusion. Thus, the decreased ionic conductivity of electrolytes at lower temperatures can be primarily attributed to the increased viscosity and reduced ion mobility, leading to a rise in internal resistance and the voltage polarization and insufficient capacity output. In 2023, Wang et al. [29] designed a colloid liquid electrolyte (CLE) by mixing the trace amount of lithium thiocarbonate (LTC) colloids with the 1 M $LiPF_6$/EC-DMC (1:1 by volume) for fast-charging LT LIBs. The competitive coordination of LTCs with anions and solvents facilitates the ion dissociation, dramatically enhancing the ion conductivity (4.5 mS cm^{-1} at −20 °C), and accelerates the Li^+ desolvation.

A liquid range determined by the melting and boiling points of the electrolyte components defines the operational temperature range of LIBs. The liquid-phase range at LTs is a critical bulk property of the electrolyte, as crystallization can severely compromise battery performance. Multisolvent systems, commonly incorporating co-solvents or eutectic formulations, are frequently utilized to extend the operational temperature range and preserve electrolyte fluidity at subzero temperatures. Additionally, the ion transfer number (t_+), defined as $t_+ = \frac{I_+}{I_+ + I_-}$, quantifies the fraction of current carried by alkali metal ions, which is directly correlated with polarization resistance and dendrite growth in operating batteries. And t_+ is crucial for reducing concentration polarization under LT conditions. Recent studies suggest that the t_+ in typical LIB electrolytes tends to decline as temperature decreases [30]. This reduction can lead to enhanced polarization, potentially causing the early onset of voltage drop commonly observed during LT discharge. Smart strategies including the use of single-ion conductors, weakly coordinating anions, anion-immobilizing additives (e.g., polymer matrices) can effectively enhance t_+ to mitigate ion transport limitations.

The above parameters play a critical role in electrolyte design because they directly influence the solvation structure, ion transport, and interfacial characteristics within LIBs. These factors become especially significant under LT conditions, where reduced thermal energy challenges ion mobility and interfacial stability.

2.1.2. Solvation Structures

The solvation structure determines the desolvation barrier and interphase chemistry at low temperatures. A raised energy barrier for ion desolvation is observed at EEIs under LT conditions, where the interfacial charge transfer process plays a pivotal role in governing overall battery performance. This process is largely dominated by the solvation structure of electrolytes, which typically consists of SSIPs, CIPs (one anion coordinated with one cation), and AGGs (one anion coordinated with two or more cations). The formation of these solvated structures is highly sensitive to the environmental conditions, thereby significantly influencing the desolvation kinetics [27].

In general, the formation of solvation structure depends on the intricate interplay among cation-anion (ion-ion), cation-solvent and anion-solvent (ion-dipole), and solvent-solvent (dipole-dipole) interactions. When the relative intensity of cation-solvent interaction is stronger than that of the cation-anion interaction, more solvent molecules can enter the solvation sheath with anions being dismissed, which induce the SSIP configuration. Nevertheless, the ion conductive pathways enabled by SSIPs are notably vulnerable to LT, with ion transport being severely impeded by robust intermolecular interactions. At reduced temperatures, desolvation kinetics are adversely affected, leading to an increased participation of solvent molecules in forming organic-rich EEIs. For instance, strongly solvating carbonate solvents form solvent-rich primary shells, leading to sluggish desolvation and the formation of organic-rich interphase films. In contrast, the strong cation-anion interaction compared to the cation-solvent counterpart enables more anions participate in the solvation, which contributes to forming anion-

dominated solvation structures (CIPs and AGGs). This solvation configuration can promote the formation of inorganic species at EEIs, resulting in the decreased desolvation energy.

More exactly, anion-coordinated or weak-solvation structures promote the formation of inorganic, ion-permeable interphases, which greatly facilitate charge transfer under subzero temperatures. Nevertheless, electrolytes dominated by large solvated AGG ion clusters exhibit diminished ion conduction efficiency owing to serious steric hindrance. By comparison, the CIP-dominated solvation structure is preferred for LT electrolytes to avoid large-sized AGGs by balancing cation-anion and cation-solvent interactions. Additionally, the dipole-dipole interaction, which denotes an interaction with the electron-rich region on the solvent in the adjacent solvation shell, show much higher temperature sensitivity than ion-solvent interactions, and it has significant influences on the solvation structure and properties of electrolytes, especially over a wide temperature range.

2.1.3. Interfacial Chemistry

Beyond electrolyte solvation, interfacial structure plays a pivotal role in determining LT performance of AMIBs, which are determined by competitive interactions among cation-solvent, cation-anion, and anion-solvent complexes, particularly within the Helmholtz layer. The interfacial chemistry at both the anode and cathode critically influences the formation and integrity of EEIs. The composition of EEIs, whether organic- or inorganic-rich, is closely associated with the solvation structure of electrolytes, which depends on the above competitive coordination. Both solvents and anions act as ligands, interacting with cations through ion-dipole or ion-ion interactions, thereby influencing the interfacial decomposition pathways and ultimately determining the interfacial chemistry.

Recently, electric double layer (EDL) has attracted significant attention as a critical reaction region in electrolytes due to its pivotal role in governing the process of electrochemical reaction at EEIs. For instance, Zhao et al. [5] proposed an electrolyte design concept with dual salts (LiFSI-LiDFOB) and strongly solvated solvent (dimethyl sulffte, DMS) to balance the Li^+ conductivity and desolvation for wide-temperature fast-charging Li-ion pouch cells. LiFSI provides ultrahigh ionic conductivity, whereas weakly dissociated LiDFOB promotes Li^+ desolvation by regulating the solvation structure, thus preventing the DMS co-intercalation into graphite anode. The interphase stability at both electrodes can be improved by the formation of inorganic-rich EEIs and the enrichment of $DFOB^-$ in the EDL region of cathode which also significantly widens the ESW. The designed 0.6 M LiFSI-0.4 M LiDFOB/DMS electrolyte endows the 1 Ah graphite||LCO (2 mAh cm^{-2}) pouch cell with 96% capacity retention after 300 cycles at –20 °C and 1 C. Zhang et al. [31] designed an unconventional EDL with adaptive and passivating characteristics by incorporating voltage-stimulated responsive additives into an ether-based electrolyte (Figure 3a). The selected anionic additives (e.g., NO_3^-), characterized by their small ionic size and strong coordination ability with cations and free solvents (Figure 3b), facilitate the formation of a cation-rich, branched-chain-like supramolecular polymer structure within the inner layer of the EDL, which departs significantly from the traditional EDL rearrangement theory. The tailored EDL properties guarantee high electrochemical stability and effectively suppress anodic decomposition of bulk solvents, enabling ultra-fast charging and LT capability of high-voltage Li||$LiNi_{0.8}Co_{0.1}Mn_{0.1}O_2$ (NCM811) batteries.

Based on the frontier molecular orbital theory, the electrochemical window, which is defined by the oxidative and reductive decomposition limits, determines the electrolyte stability. The complex with the higher energy level of highest occupied molecular orbital (HOMO) are more prone to oxidation, while those with lower energy levels of lowest unoccupied molecular orbital (LUMO) are more susceptible to reduction. EEIs, arising from thermodynamic equilibrium driven by various electrochemical and chemical reactions within the battery, are determined by the energy difference between the electrode and the electrolyte. The formation of the SEIdepends on the alignment between the electrochemical potentials of anodes and the LUMO levels of electrolytes. When the anode potential falls below the LUMO level of the electrolyte, reduction reactions are initiated through electron injection into the electrolyte [32]. These reactions continue until a passivating SEI layer forms, which subsequently inhibits further electron transfer. The composition of the SEI is closely influenced by the solvation structure of the electrolyte. Typically, in carbonate-based electrolytes, the SEI formed on alkali metal anodes is often rich in organic components, relatively thick, and mechanically fragile, making it ineffective in maintaining interfacial stability. These issues are exacerbated at LTs, where reduced ion transport and sluggish interfacial kinetics further undermine integrity of SEI, impairing the cycling stability of alkali metal batteries in cold environments. Compared to carbonate electrolytes, ether-based electrolytes generally produce more inorganic species with higher elastic moduli, owing to the lower binding energies of ether-based solvent molecules than carbonates. At lower temperatures, the electrodeposited Li in ether-based electrolytes exhibits smaller particle sizes, and the resulting SEI formed at –40 °C is significantly thinner, rich in LiF, and shows lower resistance compared to the SEI formed at 20 °C, which contains Li_2O and Li_2CO_3 [33].

Similarly, the formation of CEI is also highly sensitive to operating temperature. Under ambient conditions, the higher HOMO energy level of the electrolyte relative to the cathode potential facilitates electron transfer from the cathode surface, which stimulates oxidative decomposition and the subsequent formation of a thin organic-inorganic hybrid CEI [34]. At LTs, sluggish interfacial reaction kinetics and limited ion mobility often lead to a heterogeneous, resistive, and chemically unstable interphase. Additionally, as the cathode potential increases during charging, electrolyte components undergo further oxidative decomposition, which exacerbates under subzero conditions due to weakened passivation capability. Furthermore, the LT environment imposes severe limitations on viscosity and ionic conductivity of electrolytes, ionic diffusion coefficients, and overall electrode kinetics, collectively suppressing the formation of inorganic species-rich CEI which is indispensable for interfacial stability. Thus, a comprehensive understanding of EEIs from both thermodynamic and kinetic perspectives is essential to elucidate the mechanism of side reactions (such as the dissolution of transition metal ions and gas generation) and their impact on interfacial charge transport under LT conditions [35,36].

2.2. Limitations and Challenges of Electrolytes under Low-Temperature Conditions

The reversible capacity of LIBs generally decreases with the decreasing temperature, especially below –20 °C, and the capacity loss is typically reversible when the temperature upon restoration to ambient conditions. LT charging may also lead to irreversible capacity loss, primarily due to lithium metal plating on the anode surface. This phenomenon is only partially reversible and becomes more pronounced under high-rate charging conditions. Both types of capacity losses may be largely attributed to the increased internal resistance of LIBs at sub-zero temperatures, primarily arising from hindered ion transport, which is strongly influenced by the electrolyte composition.

2.2.1. Limited Ion/Mass Transport and Charge Transfer Kinetics

Most electrochemical processes in LIBs conform to the Arrhenius relationship, wherein the kinetics of each process exhibit an exponential decline as the temperature decreases. Within the operating temperature range, the ion conductivity of electrolytes shows a significant drop as temperature decreases, primarily due to increased viscosity and reduced wettability, which inevitably leads to the increased internal resistance. Although a high content of linear carboxylates can lower the melting point and viscosity of the electrolyte, carbonate co-solvents such as FEC with a volume ratio of 20% is still required to ensure the formation of stable and low-resistance EEIs [37]. As the temperature decreases, ion transport between the cathode and anode is hindered, which can be quantitatively described by the Arrhenius equation: $D = D_0 e^{(\frac{-E_a}{RT})}$, where D, D_0, E_a, R, and T represent the diffusion coefficient, the pre-exponential factor, the activation energy, the gas constant, and the absolute temperature, respectively. A lower temperature leads to a reduced diffusion coefficient, slowing down the ion migration within both the electrolyte and EEI. In addition, the ion diffusivity is significantly influenced by the composition of the solvent, primarily due to the modulation of the electric field shielding effect which alters the charge distribution at the electrode surface, influencing the adsorption energy and diffusion barriers of lithium ions. The preferential adsorption of cations can induce localized electrostatic shielding, which promotes uniform metal deposition and reduces the interfacial adsorption and diffusion energy barriers. Notably, the shielding effect exhibits strong temperature dependence, adding complexity to its mechanism under varying thermal conditions. Therefore, rational design of solvation structures to optimize the interfacial electric field environment is essential for achieving efficient ion transport and uniform deposition of lithium metal, especially under LT conditions.

At subzero temperatures, the rate-limiting step in the charge transfer process has been identified as the desolvation of lithium ions, rather than ion transport through the EEI or across the EEI–active material boundary. Although both the desolvation process and ion transport through the EEI are critical for LT performance, desolvation is generally recognized as the dominant factor governing the sluggish reaction kinetics under these conditions. Electrochemical impedance spectroscopy (EIS) serves as an effective tool for investigating the electrochemical kinetics of LIBs. Within the EIS framework, the total impedance of LIBs can be deconvoluted into several physically meaningful components, mainly including the ohmic resistance (R_b), solid electrolyte interphase resistance (R_{SEI}), and charge-transfer resistance (R_{ct}). Here, R_b originates from the bulk electrolyte and electrodes, while R_{SEI} and R_{ct} are generally associated with interfacial processes and collectively contribute to the polarization resistance. Zhang et al. [38] investigated the temperature dependence of these three resistance components in graphite||$LiNiO_2$ full cell at 3.87 and 3.45 V, respectively, over the temperature range from 20 to –60 °C. The variations of R_b and R_{SEI} with temperature are quite similar, since both are predominantly determined by the ionic conductivity of electrolyte. In contrast, R_{ct} increases sharply with decreasing temperature and becomes the dominant contributor to the total impedance below −20 °C. As revealed by Abe et al. [39], R_{ct} mainly originates from the desolvation process at the EEI, especially for graphite anode. Follow-up studies show that R_{ct} exhibits an

Arrhenius-type dependence on temperature, with the corresponding activation energy ($E_{a,ct}$) being strongly influenced by electrolyte composition. This $E_{a,ct}$ was found to vary independently of bulk ion transport resistance. Abraham et al. [40] reported similar $E_{a,ct}$ trends in binder- and carbon-free $Li_{4/3}Ti_{5/3}O_4$||$LiMn_2O_4$ cells, despite the lack of interfacial layers.

Recent studies have reinforced that the desolvation process is the rate-limiting step at LTs. Xu et al. [41] confirmed that the $E_{a,ct}$ on $Li_4Ti_5O_{12}$ without the existence of EEIs changed with the electron donicity of the solvent, which is a major factor to reflect solvation strength, reporting 40 kJ mol^{-1} for LiTFSI/THF vs. 50 kJ mol^{-1} for LiTFSI/poly(ethylene glycol). For graphite anode, the presence of SEI that originates from decomposition of carbonate solvents contributes an additional ~20 kJ mol^{-1} to $E_{a,ct}$. Li et al. [42] compared the EIS result of Li||graphite and Li||LFP cells across the temperature range from 25 to −40 °C, and found that interfacial processes including charge transfer and interfacial transport play a more dominant role in limiting the LT performance of graphite, whereas ionic conductivity of electrolyte is more critical for LFP. Li et al. [43] compared graphite||graphite, $LiNi_{0.80}Co_{0.15}Al_{0.05}O_2$ (NCA)||NCA, and lithiated spinel titanate (LTO)||LTO symmetric cells with the carbonate electrolytes. Despite different configurations, these cells show similar impedance spectra at –40 °C, which indicate that the resistance from Li^+ desolvation is the predominant factor, surpassing the influence of all other components. However, the EIS measurements obtained from the two-electrode configuration are influenced by the counter electrode, which may compromise the accuracy and reliability of the impedance data. To address this issue, distribution of relaxation times (DRT) technique combined with a three-electrode system has been developed to decouple the complex and overlapping electrochemical processes, while effectively minimizing the influence of the counter electrode [44].

Besides, the pronounced variation in LT discharge capacities of cells with identical interfacial chemistry in different electrolytes suggests that bulk solvation structure, rather than interphase chemistry, predominantly governs the LT performance of LIBs. Nonetheless, it remains unresolved whether desolvation is determined solely by the bulk solvation environment. The EEIs and intrinsic electrode properties may also influence desolvation by interacting with solvent molecules or coordinated lithium ions within the solvation sheath. These hypotheses warrant validation through advanced characterization techniques.

2.2.2. High-Resistance Electrode/Electrolyte Interface

After desolvation, bare lithium ions need to diffusion across the EEIs layers to reach the electrode surface. Compared to ion transport in electrolytes, diffusion through EEIs is considerably more sluggish at LTs. Enhancing ion transport within the EEIs is crucial for improving battery performance under such conditions. Although ion transport within the EEIs occurs through solid-state diffusion, the composition and structure of EEIs determines the rate of ion diffusion, which are directly influenced by the electrolyte components and their decomposition behavior during initial cycling. Generally, the decomposition of anions tends to generate inorganic components, while organic solvent decomposition favors the formation of organic species on the electrode surface. And their decomposition sequence depends not only on the electrolyte formulation but also on its solvation structure.

At LTs, the formation of EEIs is significantly delayed compared to room-temperature conditions. The combined effects of limited ion diffusion and sluggish electrochemical reactions cause the development of an initially EEI with less stability, which promotes inhomogeneous nucleation of lithium metals on the electrode surface, leading to increased overpotentials and diminished stability of the EEIs. Although the influence of EEIs on the charge transfer process remains unclear, their involvement in mass transfer process of the ionic transport introduces a notable R_{SEI} that significantly contributes to the overall cell impedance. The magnitude of R_{SEI} can vary from negligible to comparable with the R_{ct} depending on the specific system and operating conditions. However, at temperatures below 0 °C, R_{SEI} is unlikely to be the dominant component of internal resistance. Wang's group [45] found that the large R_{SEI} and high cathodic/anodic overpotential of Li metal at subzero temperatures led to the unreliable LT evaluation of working electrodes in half cells (Figure 3c). To address this, they proposed a LiC_6@Li composite electrode for the first time to replace Li metal as the counter electrode. In this design, Li^+ preferentially de-intercalate from the LiC_6 component due to its lower interfacial resistance compared to Li metal (Figure 3d,e). Notably, the LiC_6@Li composite electrode (Figure 3f,g) maintains an almost constant potential throughout operation, owing to the rapid replenishment of Li^+ from the metallic Li into LiC_6 (Figure 3h).

Although R_{SEI} may not be the primary factor limiting LT capacity, the critical role of the interphase in maintaining cell stability should not be overlooked. For example, to ensure the reliable LT operation of graphite-based LIBs, the electrolyte must form a mechanically stable interphase that mitigates continuous decomposition and prevents the exfoliation of graphitic layers. Furthermore, solvent co-intercalation and gas evolution can severely destabilize the EEI even at LTs, leading to a rapid degradation in the cycling stability of LIBs. Beyond

the SEI, greater attention should be directed to the chemical composition and structure of the CEI, particularly when aiming to enhance the energy density of LT LIBs by integrating with high-voltage cathodes.

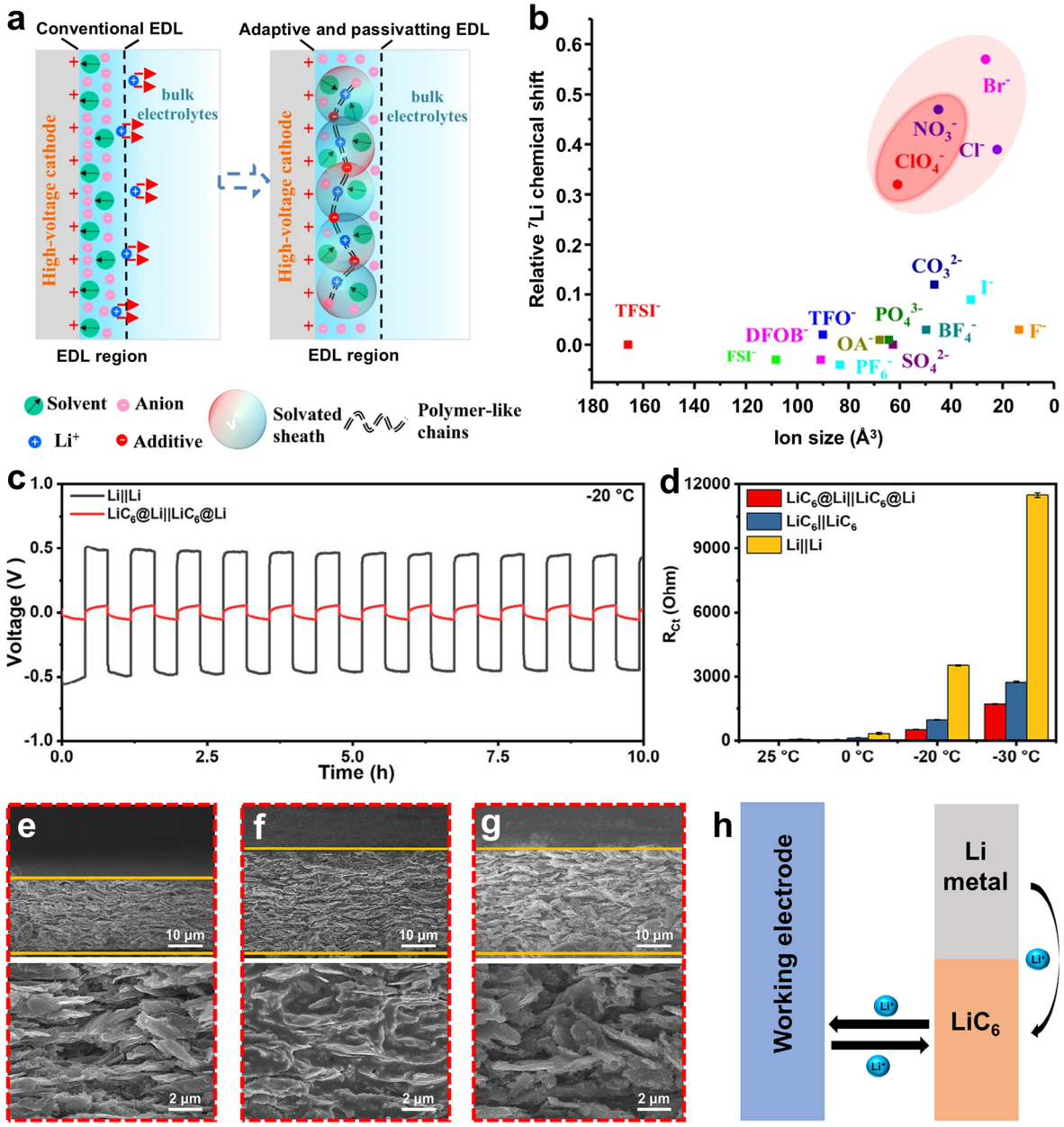

Figure 3. (**a**) Proposed mechanism for constructing a dynamic high-voltage resistance EDL. (**b**) The selection of stimulus-response additives depends on ion volume and relative ^{7}Li chemical shift. Reproduced from [31]. Copyright 2022 with permission from Springer Nature. (**c**) Galvanostatic cycling of Li||Li and LiC_6@Li||LiC_6@Li symmetric cells at −20 °C. (**d**) R_{ct} of Li||Li, LiC_6||LiC_6 and LiC_6@Li||LiC_6@Li symmetrical cells at 25~−30 °C. Cross-sectional SEM images of (**e**) LiC_6, (**f**) LiC_6@Li and (**g**) LiC_6@Li foils after removing Li metal. (**h**) Schematic diagram of the working mechanism of LiC_6@Li. Reproduced with permission [45]. Copyright 2025 with permission from Wiley-VCH GmbH.

2.2.3. Lithium Metal Plating

The use of anode materials such as graphite, which exhibit low working potential plateaus (~0.1 V) at RT, substantially increases the risk of lithium metal plating and even dendrite formation under LT and/or fast-charging conditions [25]. Once the anode's electrochemical potential drops below 0 V, lithium metal deposition becomes thermodynamically favorable. This phenomenon leads to electrolyte depletion and loss of active lithium ions, thereby accelerating capacity degradation and elevating safety concerns. At LTs, the limited mass transport and charge transfer kinetics lead to the large polarization even at the low rate. This polarization is characterized by a rapid decrease in anode potential below 0 V, which can further promote unwanted lithium metal plating on the

anode surface. Additionally, the reaction between the deposited lithium metal and electrolyte generates substantial gas evolution, which imposes additional mechanical stress on the electrodes and can ultimately lead to cell failure. Furthermore, the additional SEI construction, dendritic formation, and the accumulation of dead lithium metals further aggravate the capacity degradation [46].

Cell polarization can be classified into three main types: ohmic, electrochemical, and concentration polarization. Ohmic polarization originates from the resistance within cell components, electrochemical polarization reflects the charge-transfer kinetics at the EEIs, and concentration polarization is driven by ionic concentration gradients across the electrolyte and electrodes. In particular, factors including ion transport within the bulk active material and electrolyte, the desolvation at EEIs, and ion diffusion through EEIs all contribute to the aggravation of lithium metal plating. Thus, a well-designed electrolyte system can significantly mitigate the risk of lithium metal plating. Wang et al. [47] successfully constructed the SEI enriched with different inorganic components (Li_2CO_3, LiF, and Li_3PO_4) on graphite anode surface by introducing FEC, VC, and lithium difluorophosphate ($LiPO_2F_2$) as the additive into the base electrolyte of 1 M $LiPF_6$/EC-EMC-DMC (1:1:1 by volume), respectively. Importantly, the Li_3PO_4-rich SEI effectively decreases the de-solvation energy because of its ability to weaken the Li^+-solvent interactions, thereby accelerating the de-solvation process. The Li_3PO_4-modified graphite||$LiNi_{0.5}Co_{0.2}Mn_{0.3}O_2$ (NCM523) full cells with the base electrolyte show fast-charging capability at LTs, retaining 88% capacity after 300 cycles at –10 °C under 4 C charge and 0.2 C discharge.

To achieve optimal battery performance at subzero temperatures, it is imperative to address the aforementioned challenges when designing cryogenic electrolytes, with particular focus on overcoming the pivotal desolvation energy barrier of lithium ions.

3. Design Principles of Low-Temperature Electrolytes

3.1. High Ionic Conductivity and Low Viscosity

The ultimate objective in designing LT electrolytes for LIBs is to maintain a liquid phase and ensure high ionic conductivity at LTs. A key strategy involves the selection of solvents with intrinsically low freezing points and viscosities, as the increase in viscosity and even solidification at LTs primarily result from enhanced solvent-solvent interactions. Accordingly, rational electrolyte formulation that disrupts or weakens these intermolecular interactions can effectively suppress viscosity rise and freezing [10]. In addition to physical limitations, LTs also hinder ion migration, degrade electrochemical kinetics, and reduce CE of LIBs. Therefore, the design of LT electrolytes must holistically account for both physical and chemical parameters. Critical physical factors include freezing point, viscosity, dielectric constant, and ionic conductivity, while chemical considerations encompass solvation structure, redox stability, and interfacial film-forming characteristics [48–50]. At the atomic level, an ideal electrolyte should exhibit weak solvent-solvent interactions to reduce freezing point and viscosity, as well as an optimized ion-solvent interaction to promote ion dissociation, enhance conductivity, and lower desolvation energy [51,52]. Furthermore, the electrolyte should facilitate the formation of low-resistance and stable EEIs at LTs. Given the complexity of these interdependent requirements, single-solvent or single-salt systems are typically inadequate; instead, the rational combination of multiple solvents and mixed salts represents a promising approach to achieving the desired balance of properties for LT performance.

The selection of solvents is a critical factor in the design of LT electrolytes. An ideal solvent should exhibit both strong salt solubility and a low freezing point. Specifically, sufficient salt solubility at LTs is a prerequisite for achieving high ionic conductivity, which is fundamentally governed by ion-solvent interactions. For a given salt, its solubility is largely determined by the polarity of the solvent, typically represented by its dielectric constant. High-polarity solvents with high dielectric constant are generally favourable for dissolving salt crystals; however, they also tend to exhibit strong solvent-solvent interactions, which in turn lead to elevated freezing points and poor LT solubility. To address the high viscosity of such polar solvents under LT conditions, a widely adopted approach is to incorporate low-polarity co-solvents into conventional electrolytes [53]. In aqueous electrolyte systems, water molecules can function as both electron donors and acceptors. Introducing multi-hydroxyl solvents or polymers offers an effective strategy to disrupt the hydrogen bonding network among water molecules, which weakens water-water interactions and consequently enhances the LT performance of aqueous LIBs.

3.2. Low Desolvation Energy

At LTs, the energy barrier for lithium-ion transport across the interface is primarily determined by the characteristics of the solvation sheath and the EEI. In such conditions, slow charge transfer process at the EEIs arises from two key steps: the desolvation of solvated lithium ions and their subsequent diffusion through EEIs. The desolvation step is significantly hindered by strong cation-solvent and cation-anion interactions within the

solvation shell, while the subsequent diffusion is influenced by the composition and structure of EEIs [54]. Once the EEI is established, ion desolvation becomes essential for interfacial charge transfer and usually requires a high activation energy, especially under subzero conditions. Lowering the coordination strength and number of solvent molecules in the solvation shell can effectively reduce this energy barrier and improve desolvation kinetics. In addition, introducing more anions into the solvation environment to form anion-rich structures (CIPs and AGGs) can further weaken solvent binding, which facilitate easier ion release from the solvated molecules. Consequently, tailoring the solvation structure has become a promising strategy to enhance ion transport at LTs. For instance, Yin et al. [55] reported isoxazole (IZ) to substitute EC for LT operation of graphite anode. Benefiting from the five-membered heterocyclic conjugated structure, IZ with dispersed charge distribution exhibits weaker interactions with Li^+ than EC, inducing relatively more anions participated in the solvation to form CIPs and AGGs. The optimized 0.9 M LiFSI-0.1 M LiDFOB/IZ-FEC (7:3 by volume) electrolyte endows graphite anode with a high reversible capacity of 263 mAh g^{-1} at 0.1 C under −30 °C.

Although solvent ligands with multiple coordination sites (known as chelation effects) can enhance ion conductivity of electrolytes through strong ion-solvent interactions, the desolvation kinetics is impeded simultaneously, leading to the compromised battery performance at LTs. Adjusting the coordination environment of lithium ions is an effective approach to promote the desolvation process under cold climates. For example, Fan et al. [26] developed a novel electrolyte consisting of 1.3 M LiFSI in fluoroacetonitrile (FAN), which achieved an ultrahigh ionic conductivity of 11.9 mS cm^{-1} at −70 °C. Remarkably, graphite||$LiNi_{0.8}Mn_{0.1}Co_{0.1}O_2$ pouch cells deliver a reversible capacity of 0.62 Ah even at −65 °C. The above excellent performance is attributed to the small-sized solvent molecules forming a compact solvation shell around Li^+ and creating fast ion-conduction ligand channels. And this tiny solvent with the low solvation energy also allows the entrance of anions into the first Li^+ solvation sheath, enabling rapid desolvation and the formation of inorganic-rich interphase. Besides, fluorination is the most widely used molecular-level design strategy of solvent structures in LT electrolytes. The introduction of highly electronegative fluorine atoms reduces the electron density around the coordinating oxygen atoms, which weakens cation-solvent interactions and promotes the desolvation process [7,37]. The decomposition of fluorinated solvents contributes to the formation of inorganic-rich EEIs, which enhance ion diffusion across the interface under cold conditions. Moreover, fluorinated solvents typically have low melting points due to their reduced polarizability, which ensures good fluidity at LTs.

In addition to electrolyte design, interfacial engineering can further enhance desolvation. Introducing nano-confined channels at the interface creates a spatial environment that favors the aggregation of solvation structures into CIPs and AGGs. Materials with sub-nanometer pore (such as 3 Å zeolite molecular sieves, covalent organic nanosheets [56], metal-organic frameworks [57], polymer brushes [58], and graphene oxide laminar membranes [59]) are especially effective at regulating solvation behaviour and enabling distinctive interfacial ion transport mechanisms.

3.3. Anion-Derived Interphase Layers

Ion diffusion within EEIs generally proceeds via the "knock-off" pathways through inorganic domains because these components exhibit faster ion mobility than organic ones [60]. The construction of stable and ionically conductive EEIs is essential for improving the LT electrochemical performance of LIBs. Theoretical calculations indicate that Li^+ diffuse efficiently along grain boundaries between inorganic phases such as Li_2O, LiF, and Li_2CO_3, enabling high ion diffusion rates [61]. Such an enhanced ion transport is attributed to space charge accumulation at the Li_2CO_3-LiF interface, which generates higher ion carrier concentration [62]. Therefore, inorganic-rich EEIs layers are considered optimal for LT LIBs, which are generally derived from anion decomposition and strong cation-anion interactions serve as a prerequisite. In order to promote the desolvation step at LTs, it is necessary to achieve weak ion-solvent coordination. Thus, LT electrolytes should be featured with anion-rich solvation structures. Besides, electrolyte additives benefit the formation of inorganic-rich EEI layers to facilitate ion diffusion at LTs. The content of such additives is generally low, resulting in weak impact on the bulk solvation structure. Instead, their primary role is to act as sacrificial agents that promote favourable EEI formation.

The current mainstream view is that anion-derived inorganic-rich EEI shows better stability, more uniform ion transport, and more effective dendrite inhibition than the organic-rich EEI. Nevertheless, the inorganic-rich EEIs may not be the best choice for LT LIBs owing to the low-resistance requirement. Specifically, the high polarity of inorganic-rich EEI can attract lithium ions and thereby decrease the ion-solvent coordination. Inorganic-rich EEIs also exhibit strong solvent adsorption, resulting in more solvent molecules involved in the interfacial solvation structure and thus increased ion-solvent coordination. These two synergetic effects may impede the desolvation process in some electrolytes. On the contrary, the weak polarity of organic components can avoid attracting solvents and maintain the anion-dominated solvation structure. Compared to the inorganic-rich EEI with

dense structure, the organic-rich EEI produces typical pore diffusion mechanism, enabling significantly enhanced ion diffusion rate [63].

By tuning the SEI components formed at different temperatures, Yin et al. [64] reported such an abnormal phenomenon for LT lithium metal batteries (LMBs) by using a WES of 1.5 M LiFSI/dimethyl dimethoxy silicane featured with the CIP-dominated solvation structure. Because of the variation in temperature-responsive solvation structures, organic-rich SEI containing Si–O fragments can be formed on Li metal during initial cycling at the low temperature, while the inorganic-rich SEI enriched with LiF and Li_3N can be constructed under the room-temperature condition. *In-situ* Raman detection shows that the signal of FSI^- in the near-interfacial region decreases when the deposition time increases. Notably, the organic-rich SEI can help keep more CIPs and AGGs compared to the inorganic-rich SEI during this working process, suggesting its less influence on the solvation structure. Even with the lean DMS-based electrolyte (2.5 mL Ah^{-1}), the 1.2 Ah Li (20 μm)‖NCM811pouch cells still maintain 92.1% capacity retention after 50 cycles at −20 °C under 0.05 C charge and 0.1 C discharge.

Beyond the electrolyte formulation, low temperature significantly impacts the composition and structure of EEIs, primarily through changes in the solvation structure of the electrolyte. As temperature decreases, intensified solvent-solvent interactions lead to increased electrolyte viscosity and weakened solvent-ion coordination, thereby reducing salt solubility. Thus, cation-anion interactions are enhanced, as evidenced by the salting-out phenomenon observed at LTs. Before salt precipitation occurs, the strengthened ion-ion interactions promote the formation of more CIPs, which in turn facilitate preferential anion decomposition and the construction of inorganic-rich EEIs. Xu et al. [65] reported that the solvation structure of the 1.3 M LiTFSI/dimethyl dodecanedioate (DDCA)-DME (3:1 by volume) electrolyte transformed from SSIPs to CIPs upon cooling, accompanied by a phase change from liquid to solid. Conversely, Dong et al. [66] observed that increasing the temperature from −20 to 45 °C led to a higher proportion of AGGs and fewer SSIPs in the 1 M LiFSI/ethyl difluoroacetate (EDFA)-FEC (9:1 by volume) electrolyte. This shift is attributed to enhanced Li^+-anion interactions and weakened Li^+-solvent coordination in the primary solvation sheath at elevated temperatures. On the other hand, LTs also influence the onset potential and reaction kinetics of interfacial processes during EEI formation. Besides, the formation of low-resistance and ionically conductive EEIs can be effectively regulated by optimizing the formation temperature and charge current during the initial charge/discharge stage, which is critical for enhancing interfacial ion transport at LTs [66].

To sum up, an ideal LT electrolyte should possess sufficient salt dissociation, high ionic conductivity, low viscosity, low desolvation energy, and the ability to form a thin yet robust inorganic-rich SEI layer under subzero conditions. At the atomic level, this requires a delicate balance of multiple interactions. First, strong solvent-ion interactions are necessary to ensure sufficient salt dissociation, which is a prerequisite for high ionic conductivity. At the same time, weak solvent-solvent interactions are essential for achieving low viscosity and a low freezing point which are both critical for electrolyte fluidity at LTs. Furthermore, strong cation-anion interactions can promote the preferential decomposition of anions at the electrode interface, resulting in the formation of inorganic-rich EEIs that enhances interfacial ion transport. Additionally, weak cation-solvent and cation-anion interactions are beneficial for reducing the desolvation energy barrier at the EEI interface to improve charge transfer kinetics. Clearly, these interaction requirements are complex and, in some cases, inherently contradictory. It is unlikely that any single solvent-salt pair can simultaneously meet all these demands. Future strategies for developing LT electrolytes will therefore focus on the rational design and optimization of multi-component systems, in which the composition and ratio of each component are precisely tuned to achieve a functional balance among these fundamental interactions.

3.4. Designing Low-Temperature Electrolytes Based on Thermodynamics

In view of thermodynamics, the dissolution of salts in solvents to form homogeneous electrolytes can be simplified into the dissociation or splitting of the crystalline salt lattice and the subsequent ion solvation. The inherent driving force is the solvation energy to overcome the lattice energy of salts, which can be described by their Gibbs free energy of solvation (ΔG_{mix}) that depends on the balance between enthalpy change (ΔH_{mix}) and entropy change (ΔS_{mix}) of mixing ($\Delta G_{mix} = \Delta H_{mix} - T\Delta S_{mix}$) [67,68]. It should be mentioned that the melting point of crystalline salts is usually employed to reflect their lattice energy.

In general, the ΔG_{mix} varies with the content of different solvation structures. The enthalpy change, which is determined by the binding energy, could be released when the ion-solvent or cation-anion coordination structure is formed. The formation of characteristic coordination depends on which configuration can cause more enthalpy release to realize minimized ΔG_{mix}. The weakened binding between the cation and the solvent incorporated with electron-withdrawing groups decreases the enthalpy release by forming a cation-solvent coordination structure, leading to the shift of the enthalpy change-affected competitive coordination equilibrium towards anion-dominant

solvation structures, and thus benefits the inorganic-rich SEI formation [27]. The ΔH_{mix} for desolvation can be reduced by weakening ion-solvent interactions [69,70]. For example, Dong's group [37] investigated the fluorination degree of carboxylate ester-based solvents on the solvation capability for realizing the fast-charging performance of graphite-based LIBs under cryogenic conditions. The introduction of F atoms in the acetyl group of EA can effectively modulate the binding energy between the fluorinated-EA and Li^+, and the increased amount of F atoms (from 1 to 3) induce the formation of larger Li^+-anion aggregates. They ultimately selected the moderate fluorinated EDFA to balance the ion-solvent affinity and ionic conductivity at subzero temperatures. Thus, low-enthalpy effects provide a new idea for cold-resistance electrolyte design.

In principle, higher ΔS_{mix} play a vital role in reducing ΔG_{mix}. Introducing multiple components to increase the ΔS_{mix} is a feasible strategy to promote the formation of homogeneous electrolytes and even avoid the freezing and crystallization under cryogenic conditions [71]. The eutectic temperature of electrolytes is reduced due to the high-entropy effect, demonstrating their great potential for LT applications. For example, the solubility of $LiNO_3$ in commercial carbonate-based electrolyte of 1 M $LiPF_6$/EC-DMC (1:1 by weight) with 5% FEC is enhanced by introducing three types of lithium salts (LiFSI, LiTFSI, and LiDFOB) [68]. Currently, entropy-driven electrolytes have attracted significantly attention to improve the capacity retention and rate performance of LIBs at extremely LTs. Compared to low-entropy electrolytes, high-entropy electrolytes have advantages of high ion conductivity favoured by small ion clusters and improved EEI properties and ion diffusivity kinetics at LTs [72]. Qu et al. [73] designed the amide-based strong-solvation (SS) and weak-solvation (WS) electrolyte consisting of 0.8 M LiTFSI-0.4 M LiDFOB/2,2,2-trifluoro-N-methoxy-Nmethylacetamide (FMMA)-FEC (7:3 by volume) for high-voltage and LT LMBs.

Besides, low ΔG_{mix} change enables rapid the ion desolvation kinetics at subzero temperatures. Ren et al. [70] designed a Gibbs-free-energy-driven electrolyte (1 M $LiPF_6$-LiDFOB-$LiNO_3$-LiTFSI-LiFSI/DME) with both low ΔH_{mix} and high ΔS_{mix} by incorporating mult-anions to decrease the desolvation barrier and construct anion-derived inorganic-rich SEI with fast interfacial kinetics for guiding uniform Li deposition at LTs.

4. Current Strategies of Low-Temperature Electrolytes

Over the past several decades, research on low-temperature electrolytes (Table 1) has gradually shifted from emphasizing macroscopic properties such as freezing point suppression and ionic conductivity to recognizing the importance of solvation structure evolution and interfacial chemistry. It is now understood that poor performance at subzero temperatures originates not only from sluggish ion transport but also from temperature-induced changes in ion-solvent coordination, desolvation behavior, and the formation of EEI layers. Thus, current electrolyte design strategies increasingly combine solvent optimization, salt selection, and functional additives with deliberate regulation of solvation structures to enable controlled interphase formation. This integrated approach provides a more effective pathway to enhance the reversibility, stability, and energy density of rechargeable batteries operating in cold environments.

Table 1. Comparative summary of four types of LT electrolytes.

Electrolyte Type	Advantages at LT	Limitations	Typical LT Working Range
Aqueous electrolytes	High ionic conductivity; good safety	Freezing risk; narrow stability window	down to −20 °C with additives
Organic electrolytes	Tunable solvents; wide electrochemical window	High viscosity at LT; poor SEI stability	−20 to −60 °C
Ionic liquid–based electrolytes	Low volatility; intrinsic LT fluidity	High cost; moderate conductivity	−40 °C or below
Solid-state electrolytes	Nonflammable; mechanical stability	Grain-boundary resistance; poor interfacial contact at LT	−20 °C (depending on SSE type)

4.1. Aqueous Electrolytes

Three distinct types of electrolytes have been proposed to enable the stable operation of aqueous LIBs at LTs: (1) "water-in-salt electrolytes (WISEs)" with ultrahigh ionic concentrations that disrupt hydrogen bonds through ionic shielding effects, (2) "water-organic hybrid electrolytes" that employs organic solvents to reconstruct hydrogen bonds (HBs) networks via competitive interactions, and (3) "inorganic aqueous electrolytes" which leverage specific ion-water coordination chemistry to stabilize hydration shells.

4.1.1. Water-in-Salt Electrolytes

Water-in-salt electrolytes (WISEs), where the mass and volume of dissolved salt surpass that of water, allow aqueous LIBs to operate reliably at −20 ℃ [21]. Compared to conventional aqueous electrolytes, which suffer from a narrow ESW, reduced ion conductivity and even freezing at LTs, WISE shows superior LT adaptability in both physical and electrochemical properties. In WISEs, the increase in cation concentration enhances the interactions between water molecules and cations, decreasing the number of free water molecules and alter the electronic cloud density of water molecules, thereby expanding the ESW. Traditional aqueous electrolytes contain limited hydrated cations, while high-concentration cations in WISEs confines water molecules within solvation shells, creating an energy barrier for H_2O crystallization.

In diluted aqueous electrolytes, the presence of excessive highly reactive free water molecules leads to continuous side reactions at the EEI, while the crystallization of free water near the freezing point causes phase separation, which disrupts ion transport pathways. The decomposition of free water molecules generates gases which leads to the formation of porous and fragile SEI and other side reactions [74]. In WISEs, the ion-ion interaction becomes more pronounced than the ion-solvent interaction due to the limited average number of water molecules available to solvate each ion, which promotes the formation of numerous salt aggregates, and results in preferential salt decomposition to form stable interphase layers on electrodes [75]. For example, Li^+ ions are fully solvated by water molecules in diluted electrolytes as the primary solvation shell. In the 20 m LiTFSI electrolyte, the reduction of water generates highly active OH^-, which can react with $TFSI^-$ to form a passivating SEI layer that effectively prevents the water reduction [76]. In the 21 m LiTFSI electrolyte, each Li^+ is coordinated with 2.6 water molecules, and $TFSI^-$ enters the Li^+ solvation sheath [77]. The reduction of anion-dominated solvation structures at the anode can form a LiF-rich SEI which serves as an electron barrier preventing the reduction of water while allowing Li^+ migration. The NASICON-type $LiTi_2(PO_4)_3$||$Li_3V_2(PO_4)_3$ full batteries with the 21 M LiTFSI aqueous electrolyte exhibit a high capacity of 111 mAh g^{-1} at –20 ℃ and 0.2 C (1 C = 133 mA g^{-1}) [78].

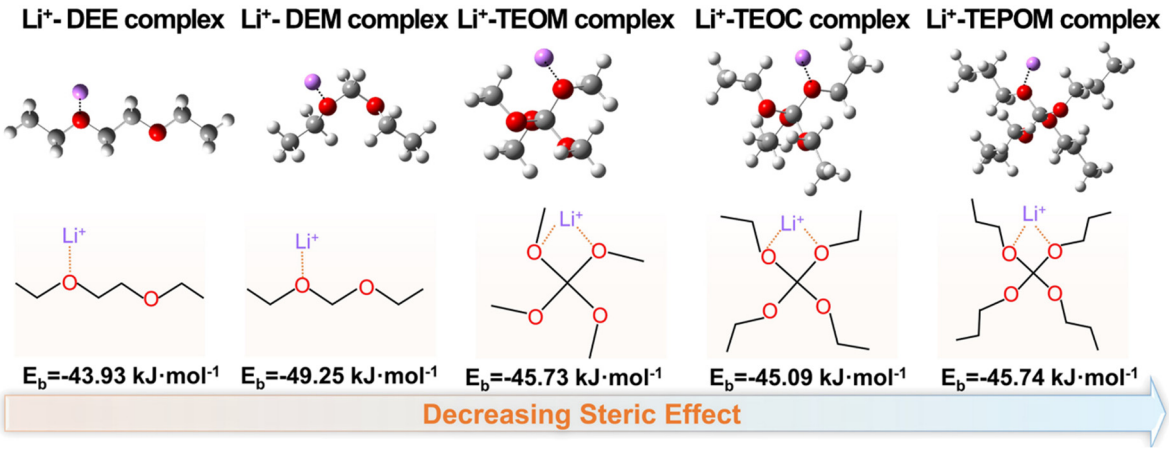

Figure 4. Chemical structure and binding energy (E_b) of different solvents. Reproduced from [79]. Copyright 2025 with permission from Wiley-VCH GmbH.

WISEs provide an innovative solution for the application of electrolytes in extremely LT environments. The incorporation of high concentration salts effectively disrupts the original HBs network between water molecules and limits water molecules within solvation shells of cations to creates an energy barrier for H_2O crystallization. Such characteristics greatly improve the operational stability of aqueous batteries and establish a foundation for the practical deployment of energy storage devices in subzero environments.

4.1.2. Water-Organic Hybrid Electrolytes

To enhance the electrochemcial performance of aqueous batteries in subzero temperature, organic solvents with low melting point and low viscosity can be introduced as co-solvents or cryogenic anti-freeze additives to widen the liquid range of aqueous electrolytes and maintain an appropriate ionic conductivity. Tetramethylene sulfone (TMS) exhibits analogous cryogenic functionality. A hybrid electrolyte composed of LiTFSI, TMS and H_2O at a molar ratio of 1:0.5:1 retains a liquid state even at −85 ℃, which endows $Li_4Ti_5O_{12}$||$LiNi_{0.5}Mn_{1.5}O_4$ full cells with a reversible capacity of 9.5 mAh g^{-1} at −80 ℃ and 3 C [80]. Ma et al. [81] proposed a binary-solvent electrolyte consisting of N,N-dimethylformamide (DMF) and H_2O (1:1 by molar), supplemented with 5 wt.% 3-sulfolene (3SF) in 9 M

LiTFSI. The H_2O solvent ensures nonflammability and high safety, while DMF reduces the freezing point and enhances LT conductivity. Through the incorporation of the 3SF additive along with LiTFSI, a stable bilayer interphase film is formed on the anode surface, which effectively expands the ESW to 4.37 V. Benefiting from these features, the $Li_4Ti_5O_{12}$||$LiMn_2O_4$ full cell retains 98.8% of its initial capacity after 50 cycles at −30 ℃ and 0.3 C (1 C = 175 mA g^{-1}).While conventional co-solvents rely on functional groups such as P=O and S=O to disrupt HBs, Shang et al. [79] recently reported a tiny-ligand solvation electrolyte composed of 2 m LiTFSI in tetraethyl orthocarbonate(TEOC)/H_2O (95:5 by volume) that enabled an ultrasmall Li^+ solvation sheath volume and showed an ionic conductivity of 1.09 mS cm^{-1} at –20 ℃. The steric bulk of TEOC with a molecular radius exceeding 3 Å renders the low binding energy with Li^+ (Figure 4), which forces $TFSI^-$ anions and H_2O molecules into the primary Li^+ solvation sheath to generate an ultrasmall volume cluster of $[(Li^+)(TFSI^-)_{0.4}(H_2O)_{0.56}(TEOC)]$. TEOC forms strong C–O–H···H_2O hydrogen bonds that convert free H_2O into coordinated H_2O and allows the electrolyte to exhibit a wide ESW of 5.7 V as well as the remain liquid even at –80 ℃. In addition, they also proposed an EA-based electrolyte at an optimal EA/H_2O molar ratio of 3.91, where –COO– effectively break the HB network of water and lower the freezing point to −106.95 ℃ [82].

The incorporation of co-solvents and additives has proven effective in depressing the freezing point and enhancing ionic conductivity of aqueous electrolytes under subzero conditions. Nevertheless, significant progress has been made, most aqueous LIBs still face challenges such as limited electrochemical stability and uncertain long-term compatibility with electrode. Future studies should aim to elucidate ion-solvent interactions at the molecular level and develop scalable electrolyte formulations for practical low-temperature energy storage applications.

4.1.3. Inorganic Aqueous Electrolytes

Ions coordinate with water molecules via electrostatic interactions, which disrupts the HB network and inhibits ordered HB formation at LTs. Ions with high charge density (such as Ca^{2+}, Mg^{2+}, and Mn^{2+}) exhibit strong hydration, which can cause water molecules to be orderly arranged and slow down molecular thermal movement than the bulk water. In contrast, ions with low charge density have weak hydration effects but can destabilize the arrangement of water molecules, which increase their disorder and interfere with the formation or maintenance of HBs. These disruptions caused by additional salts play a crucial role in lowering the freezing point of aqueous electrolytes. Therefore, incorporating specific salts into aqueous electrolytes can effectively lower the freezing point.

Eutectic electrolytes, a class of solvent-free ionic systems formed by mixing two or more components, typically promote the formation of complex ion species through strong intermolecular interactions, which reduces lattice energies and allows for the tuning of physicochemical properties. Kim et al. [83] proposed an aqueous eutectic electrolyte (AEE), composed of 5.2 m LiTFSI, could disrupt the HB network of water molecules via high concentration Li^+ and $TFSI^-$ ions and reduce free water content. The AEE exhibits a remarkably low freezing point of −69.3 ℃ and maintains an ionic conductivity of 1.8 mS cm^{-1} at −40 ℃. Consequently, the AC||$LiMn_2O_4$ hybrid supercapacitor delivers 66.4% of its RT capacity (94.6 mAh g^{-1} at −40 ℃ and 2 C, 1 C = 100 mA g^{-1}). Ramanujapuram et al. [8] investigated the aqueous electrolytes based on three low-cost inorganic salts ($LiNO_3$, Li_2SO_4, and LiCl) in symmetric LCO cells at subzero temperatures, and found that the charge transfer resistance is the largest impedance contributor at LTs. Saturated LiCl (≈16 mol kg^{-1} concentration at RT), does not freeze down to −45 or −50 ℃, saturated $LiNO_3$ (≈9 mol kg^{-1} at RT) freezes somewhere between −20 and −30 ℃ and saturated Li_2SO_4 (≈3.5 mol kg^{-1} at RT) between −30 and −35 ℃. It is found that the R_{ct} is the largest impedance contributor at subzero temperatures. All aqueous electrolytes in LCO||LCO exhibit markedly lower charge R_{ct} than the organic electrolyte (1 M $LiPF_6$/EC-DEC) both at RT or subzero, by orders of magnitude. In the saturated LiCl electrolyte, the LCO maintains approximately 72% of the room-temperature capacity at −40 ℃ and 0.2 C.

Jiang et al. [84] designed anti-freezing electrolyte concentrations through the freeze concentration process that concentrates dilute solutions by precipitating ice or hydrates at target LTs (T_t). When the temperature drops to T_t, water in the electrolyte crystallizes, which causes the concentration of certain salts in the remaining liquid to increase. The frozen concentrated electrolyte (FCE), which the liquid-ice mixture yields, maintains the minimum salt concentration that is necessary to remain liquid at T_t. The FCE approach provides two significant advantages over traditional approaches. Firstly, it can accurately design the optimal electrolyte composition for both single and multiple salt electrolyte systems, which eliminate the need to screen a large number of concentration combinations. Secondly, traditional approaches are not only tedious and inefficient but also inaccurate in aqueous solutions when they rely on differential scanning calorimetry (DSC) measurements to determine freezing points. The optimized 7.18 m LiCl electrolyte still remains in the liquid state at −60 ℃ with a high ionic conductivity of 6.09 mS cm^{-1}, which enables the PTCDI||$LiMn_2O_4$ pouch cell to deliver a reversible capacity of 5.4 mAh at −60 ℃ and 0.5 C.

Selection of salts and regulation of electrolyte concentration offers a unique and promising pathway for designing anti-freezing aqueous electrolytes. However, the relationship between the ion effect and the role of anion-inducing vitrification transition is unknown, which hinders the rational design of aqueous batteries with enhanced subzero performance and stability.

4.2. Organic Electrolytes

4.2.1. Localized High-Concentration Electrolytes

High-concentrated electrolytes (HCEs) successfully reduce the solvent molecules and extensively confine anions within the solvation sheath, resulting in the high oxidative stability and anion-derived inorganic-rich EEIs. Although HCEs can widen the operating temperature range of LIBs, the sharply increased viscosity and poor wettability of HCEs depresses the battery performance at fast charging and/or low temperature conditions. Non-polar diluents or low-polar solvents are added into HCEs for developing localized high-concentration electrolytes (LHCEs), which can inherit locally anion-rich solvation structure and maintain the merits of HCEs (such as high voltage stability, Al corrosion resistance, and good compatibility with lithium metal anodes). The introduction of diluents also reduce viscosity and improve wettability of electrolytes, which effectively enhances ion mobility under cold conditions. Compared to conventional electrolytes, LHCEs exhibit a markedly reduced number of solvent molecules in the primary solvation shell. The diluent can be miscible with solvents but scarcely dissociate salts because of its low dielectric constant and electron donating capability. Introducing non-solvating hydrofluoroethers (TTE [85–91], TFTFE [92–94], bis(2,2,2-trifluoroethyl) ether (BTFE) [95], D2 [7], hexafluoroisopropyl methyl ether [96], etc.) may cause salt precipitation, phase separation, and inferior ion-conducting efficiency, owing to the difference in salt solubility ability between a high-polar solvent and the diluent with low polarity. These hydrofluoroether solvents do not coordinate strongly with lithium ions while enhancing cation coordination with the surrounding anions and high-polar solvents, leading to an increase in AGG levels and proportions, thereby driving the preferential decomposition of these species at EEIs [92]. Importantly, non-solvating diluents can disorganize bulk AGG clusters into smaller AGGs by weakening the interactions between the polar solvent molecules, and reduce the electrolyte viscosity. Ether solvents with the relatively strong solvation ability, primarily including cyclic ethers (THF [86–88], 2MeTHF [85,86], and 1,3-dioxolane (DOL) [88,92,97]) and linear ethers (DME [89,90,95,98,99], methyl n-propyl ether (MPE) [100], and diethyl ether [101],) are adopted in LHCE for LT LMBs, benefiting from their benign chelation effect and positive de-solvation energy. For example, Holoubek et al. [95] investigated the impact of BTFE/DME volume ratio on ion-pairing degree in 1 M LiFSI electrolytes, and found a distinct ion-pairing transition when the BTFE/DME volume ratio exceeds 3:1, resulting in significantly improved Li plating/stripping efficiency at LTs (96.9% at −60 °C) and enhanced oxidative stability for pairing with high-voltage cathode.

Classically, TTE with low freezing/high boiling points (−94 to 93 °C) has strong electron-withdrawing $–CF_n$ groups in its molecular structure, which significantly weaken the electronegativity of oxygen in TTE, excluding it from the first solvation sheath of lithium ions [87]. The 1 M LiFSI/DME-TTE (1:2 by volume) LHCE shows the strengthened anion-cation interaction intensity when the temperature decreases from 25 to −20 °C [90]. Benefiting from the weak solvation ability of dibutyl ether (DBE), abundant ion-pair aggregates appeared in the 1 M LiFSI/DBE-TTE (1:1 by volume) LHCE can promote fast Li^+ desolvation, the formation of robust EEIs, and the suppression of shuttle effects, resulting in the impressive stability of lithium||sulfurized polyacrylonitrile batteries over a wide temperature range (−20~60 °C) [102]. Sun et al. [98] designed a multilayer solvated electrolyte, 0.8 M LiFSI-0.2 M $LiNO_3$/DME-TTE (1:3 by volume), for high-rate LMBs at 0 °C by utilizing a major anion with moderate coordination ability and the secondary anion with stronger coordination than the solvent molecule. Li et al. [85] reported the 2 M LiFSI/THF-TTE (1:1 by volume) electrolyte for stable operation of LMBs at LTs. Compared to the 2MeTHF counterpart, this THF-based LHCE with a strong solvation strength exhibits rapid interfacial kinetics for TTE defluorination to form an amorphous and inorganic-rich SEI on the Li metal anode surface, achieving a high CE of ~99.63% for Li plating/stripping and dendrite-free Li deposition at −30 °C. Piao et al. [86] esigned a temperature-insensitive solvated electrolyte (TISE) consisting of 1.5 M LiFSI/THF-2MeTHF (1:1 by molar)-TTE for LT LMBs. The TTE co-solvent can weaken the electronegativity of oxygen in theTHF-2MeTHF mixed solvent through the intermolecular interactions, enabling the involvement of more anions to form AGGs as the primary solvation structure in TISE. The 1 Ah-level Li||LFP pouch cell (N/P = 3) with the TISE delivers 61% of the room-temperature capacity when charged and discharged at −40 °C and 0.1 C. Gu et al. [88] disclosed that the medium concentration (2 M) of LiTFSI/DOL-THF-TTE (3:3:4) electrolytes enabled suitable ion pairing (CIPs/AGGs) solvation structures and facile desolvation, forming an anion-derived organic-inorganic SEI, which could effectively improve the efficiency of ion transport at LTs.

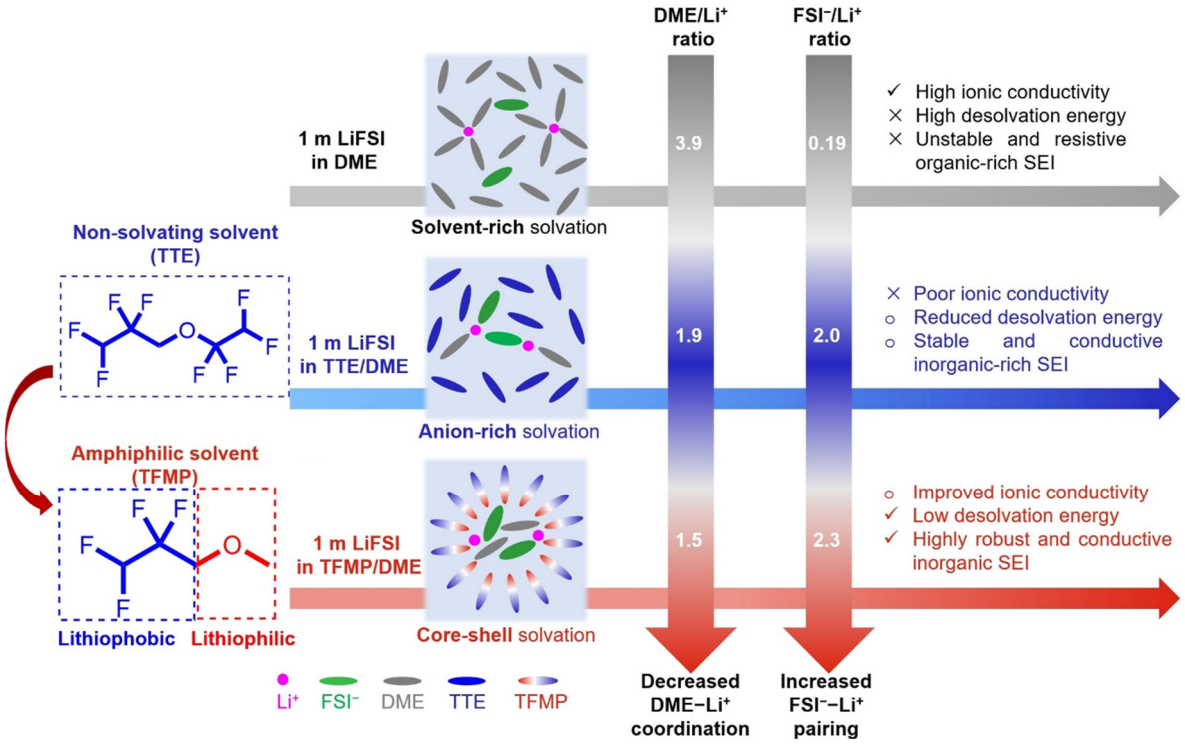

Figure 5. Amphiphilic solvent design strategy for LMB electrolyte. Reproduced from [99]. Copyright 2023 with permission from Wiley-VCH GmbH.

Oxidation-resistant low-polarity hydrofluoroethers exhibit negligible affinity with lithium ions due to the low absolute value of their high electrostatic potential (ESP) minima (>−20.0 kcal mol^{-1}). By leveraging the molecular ESP screening and intermolecular hydrogen bonding chemistry, Cui et al. [103] proposed a push-pull electrolyte design strategy for high-voltage LT LMBs. They screened 2,2-difluoroethyl trifluoromethanesulfonate (DTF) with a moderate ESP minimum (−21.0 kcal mol^{-1}) and a high ESP maximum (37.3 kcal mol^{-1}), signifying its weak coordination with Li^+ (pull) and a strong hydrogen bond donor ability (push) accordingly, as an optimal co-solvent. The optimized 1 M LiFSI/EMC-FEC-DTF (1.5:1.5:7 by volume) electrolyte contributes to the formation of robust inorganic-rich interphases and rapid charge transfer kinetics. Taking three electrolytes including 1 M $LiPF_6$/EMC-EC, 1 M $LiPF_6$/EMC-FEC (1:1), and 1 M $LiPF_6$/EMC-FEC-TFTFE (1:1:1) as an example, Lai et al. [94] demonstrated that more solvent molecules entered the inner solvation sheath at lower temperatures caused by the enhanced ion-solvent interactions. The introduction of a fluorinated solvent, especially non-solvating diluent (TFTFE), can improve the temperature-adaptivity of electrolyte solvation structure owing to its lower dielectric constant. LiFSI/EMC-TTE (2:3.3:3.3) and LiFSI/MA-TFTFE (1:1.5:2 by molar) [44] electrolytes enable the cyclability of graphite-based full cells at subzero temperature even without Li plating during charging. The LiFSI/AN-TTE (1:2.73:5.66 by molar) electrolyte achieves 85.5% capacity retention of Li||NCM811 cells after 95 cycles at −30 °C and 0.3 C [104]. Besides, the addition of 0.02 M lithium difluorobis(oxalato)phosphate (LiDFBOP) into 1 M $LiPF_6$/DMC-TTE (1:1 by volume) electrolyte contributes to forming a stable and low-impedance SEI, which endows graphite anode with a high capacity of 240 mAh g^{-1} and stable 100 cycles at −20 °C and 0.1 C. A sulfonamide-based LHCE comprising of 0.75 M LiFSI/N,N-dimethyltrifluoromethane-sulfonamide (TFMSA) weak solvent and TTE anti-solvent (7:3 by volume) exhibits the AGGs-dominant solvation structure due to the intermolecular interaction between TTE and TFMSA, enabling an excellent cycling performance of graphite||LCO full cells (N/P = 0.75) over 50 cycles at –50 °C and 0.05 C.

Furthermore, 1,1,2,2-tetrafluoroethyl methyl ether (TFME) [100,105] and 1,1,2,2-tetrafluoro-3-methoxypropane (TFMP) [99] are developed as short-chain fluorinated diluents in LHCEs. Zhao et al. [100] proposed an effective strategy to balance the desolvation barrier and ion transport properties by employing the solvent with moderate weakly solvating ability (DME > THF > MPE > DEE) and the diluent with minimal viscosity (TTE > TFTFE > TFME). The optimized LiFSI/MPE-TFME (1:2.3:4.5) electrolyte enables excellent Li reversibility of 99.34% at −40 °C and 98.96% at −60 °C under the current density 0.5 mA cm^{-2}. As an amphiphilic ether, TFMP involves both the polar lithiophilic segment (–O–) to solvate Li^+ and the fluorinated lithiophobic segment (–CF_2CF_2H) which can provide high-voltage tolerance and act as the diluent to retain locally anion-rich solvation structures (Figure 5) [99]. The 1 M LiFSI/DME-TFMP (1:7 by volume) LHCE is featured with a unique core-shell-like

solvation structure, which not only shows relatively high ionic conductivity and low desolvation energy, but also enables the formation of a highly robust and conductive SEI, thereby allowing an average CE of 98.5% for Li plating/stripping at −40 °C and 1 mA cm^{-2}.

More recently, fluorine-containing diluents such as FB [106–109], 1,2-difluorobenzene (DFB) [110], 1,3,5-trifluorobenzene (TFB) [111], hexafluorobenzene (HFB) [112], and flame-retardant ethoxy (pentafluoro) cyclotriphosphazene (PFPN) [113] have been employed in LT LHCEs. By regulating the dipole-dipole interactions between the polar solvent and diluent, the cation-anion interaction can be enhanced. As a representative, Xie et al. [114] applied this design strategy by utilizing intermolecular (dipole-dipole) interactions between fluorobenzene (FB) and PC to weaken Li^+-PC interactions, which promoted desolvation at the graphite interface and ensured excellent interfacial compatibility across a wide temperature range from −90 to 90 °C. Yi et al. [115] designed a flame-retardant 1 M LiFSI/DME-MME (3-methoxyperfluoro(2-methylpentane))-OOE (1,1,2,2,5,5,6,6-octafluoro-3-oxahexane) (salt:DME, 1:3.5; MME:DME, 1:4; salt:OOE, 1:3 by molar) electrolyte with excellent chemical/thermal stability, oxidation resistance, and wide operating temperatures. The introduction of MME with low-solvation ability and non-polar OOE diluent with ultra-low ε and DN contributes to a favorable solvation structure and inorganic-rich SEI. The Li||LFP cells deliver the capacity of 80 mAh g^{-1} after 190 cycles at −20 °C and 200 mA g^{-1}.

Carboxylic ester-based LHCEs have been designed for high-voltage and low temperature lithium batteries [116–119]. For example, Dong et al. [116] reported dichloromethane (DCM) as the diluent in a 5 mol kg^{-1} (5m) LiTFSI/EA HCE, and the optimized electrolyte with the 1:4 by volume remains undisturbed local solvation structure, low viscosity (0.35 Pa s at −70 °C), high ionic conductivity (0.6 mS cm^{-1} at −70 °C), and high compatibility with Li metal anode. By weakening the Li^+-solvent interactions, Su et al. [120] designed the LiFSI/MB-EMC-TTE (1:1.025:0.483:1.1 by molar)-2 wt.% 1,3-propylenesulfate (PCS) with the compact ion-pair aggregates (CIPAs)-dominated solvation structures for stable cycling of graphite||NCM811 cells at −40 °C for 200 cycles at 0.3 C. Although sulfone-based solvents possess high-voltage tolerance, the high viscosity limits their further application. For example, He et al. [111] designed a TMS-based LHCE consisting of LiFSI/TMS-FB-TFB (1:3:2.333:0.167 by molar) for wide-temperature LMBs. The prior decomposition of TFB can assist the formation of LiF-rich EEI to suppress side reactions between TMS and Li, while the FB with low viscosity improves ionic conductivity of the electrolyte at LTs. The optimized dual-salt LHCE of LiTFSI-LiDFOB)/TMS-EA (3:7 by volume)-hydrofluoroether-10 wt.% FEC realizes the LT fast-charging performance of Li||NCM523 cells for 200 cycles at −40 °C and 1 C (1 C = 200 mAg^{-1}) under the charge cut-off voltage of 4.6 V [121].

LHCEs, especially all-fluorinated electrolytes, have significantly promoted the development of high-energy LT LIBs due to the generation of inorganic-rich EEIs and the suppression of side reactions and gas generation on EEIs [112]. More importantly, the physical properties of diluents should be considered for designing LHCEs. Nevertheless, challenges with traditional diluents (such as low boiling points, high volatility, and high cost) may hinder their large-scale applications. To overcome these, researchers are focusing on developing diluents with enhanced electrochemical stability, improved thermal safety, low cost, and environmental friendliness. Efforts are also underway to explore alternative solutions such as ionic liquids and mixed solid-liquid systems.

4.2.2. Weakly Solvated Electrolytes

Weakly solvating electrolytes (WSEs) are considered promising candidates for LT battery applications. First, the reduced ion-solvent interaction lowers the desolvation energy of solvated lithium ions, contributing to the desolvation process, which is often the primary rate-limiting step for ion transport at LTs. Second, the weak solvation effect limits the capability of the solvent to dissociate salt crystals, thereby promoting the involvement of anions in solvation structures. On the other hand, strong cation-anion interactions favor the preferential reduction of anions, resulting in the reduced the solvent decomposition and the formation of inorganic-rich EEI that enhances ion diffusion through the interphase. Finally, the low polarity of such solvents is often accompanied with weak solvent-solvent interactions, which contributes to the low freezing point and viscosity of electrolytes.

Current approaches for designing WSEs mainly focus on identifying or synthesizing solvents with intrinsically low coordination capability. A variety of solvents with intrinsically weak solvation capabilities (mostly associated with low polarity) have been identified and incorporated into electrolyte formulations, including linear ether (e.g., diethyl ether [23], DEE [122,123], dimethoxymethane (DMM) [54], cyclic ether (e.g., dipolyformaldehyde dimethyl ether (DDE) [124], 2-methoxy-1,3-dioxolane (MODOL) [125], 2,2,4,4,5,5-hexamethyl-1,3-dioxolane (HMD) [126]), siloxane [127], sulfonamide [73], carboxylate ester (e.g., MP [128,129], EA [130], methyl trifluoroacetate (MTFA) [131,132], diethyl fluoromalonate (DEFM) [133], ethyl trifluoroacetate (ETFA) [134–136], and ethyl 4,4,4-trifluorobutyrate [137]), and fluorinated carbonate (e.g., difluoroethylene carbonate (DFEC) [138], 2,2-difluoroethyl ethyl carbonate (DFDEC) [139], bis(2,2,2-trifluoroethyl) carbonate (BTC) [140]), etc.

By eliminating one O atom from DME, diethyl ether with weakened solvation is utilized in lithium-sulfur batteries cycled at ultra-LTs, in which the resultant CIP-rich solvation structure is beneficial for Li^+ desolvation and high CE for Li plating/stripping (~99.0% at –40 °C) [23]. By replacing the methoxy groups on DME with larger-sized ethoxy groups, DEE, a linear ether with wide liquid range (−74 to 121 °C), possesses weakened solvation ability due to the increased steric hinderance of its longer carbon chain, while inheriting the good salt solubility and high ionic conductivity [122]. The 1 M LiFSI-0.5 M $LiNO_3$/DEE-FEC (9:1 by volume) electrolyte endows graphite anode with impressive 82.6% capacity retention at −20 °C by realizing the solvent co-intercalation-free behaviour and the formation of LiN_xO_y-rich SEI [123]. Compared to G2 and DME as multidentate ethers, monodentate dibutyl ether (DBE) featured with weak Li^+-solvent affinity, low freezing/high boiling points (−98~142 °C) and low vapor pressure (0.006 atm) ensures reliable wide-temperature of lithium-sulfur batteries [141]. As a branch-chain-rich ether, diisopropyl ether (DIPE) possesses the weak binding interactions of the single oxygen donor ethers and the steric hindrance, which significantly reduce the desolvation energy barrier of the electrolyte [142]. Liu et al. [143] adopted the oxygen-free solvent, n-hexane (HEX), to reduce the Li^+-solvent interactions and enhance the chemical compatibility with Li metal, and matched with monodentate hexyl methyl ether (HME) to fabricate the temperature-immune 1 M LiFSI/HEX-HME (1:1 by volume) electrolyte for realizing dendrite-free Li plating from −30 to 60 °C.

WSEs usually show compromised ionic conductivities compared to traditional carbonate- and ether-based electrolytes, owing to the low ε of most solvents, which restricts the battery's fast-charging capabilities especially at LTs. Cyclopentyl methyl ether (CPME) is a monodentate ether and featured with weak solvating ability due to the single O coordination site and large steric hindrance of the cyclopentane group [144]. For instance, Wei's group [53] utilized low-ε CPME (ε = 4.7) as the main solvent and matched with high-ε FEC (78.4) as the co-solvent to balance the ionic conductivity of electrolytes at LTs. Benefiting from the steric hindrance effect-tuned facile desolvation process and robust LiF-rich SEI, the 1 M LiTFSI/CPME-FEC (7:3 by volume) WSE enables the impressive LT performance of graphite-based full cells under RT charging conditions. Furthermore, the weakly solvated CPME with a wide liquid range (−140~106 °C) have been utilized for Li metal and silicon anodes operating over a wide temperature range [145,146]. Huang et al. [144] designed a 1 M LiFSI/CPME-DME (8.5:1 by molar) electrolyte to realize uniform Li deposition at LTs. The weakly solvated CPME can replace highly solvating DME in the first solvation sheath, and the addition of CPME leads to the coordination of more anions with Li^+ as the temperature decreases to −40 °C. The short residence time of CPME in the solvation shell induces rapid exchange of coordinated CPME with Li^+ as compared with DME and contributes to the desolvation process at LTs. Acetone (DMK) is mainly tridentate due to the strong steric hindrance between $–CH_3$ group, and the DMK-based electrolyte contains SSIPs as the primary solvation structure, which is significantly from the CIPs-dominated solvation shell of linear aprotic MA- and DMC-based electrolytes [147]. Notably, the SIPs content in DMK-based electrolytes increases as the temperature drops, which facilitates high ionic conductivity (>10 mS cm^{-1} at −40 °C) and realizes fast charging at LTs. However, DMK leads to a narrow ESW and cannot solely form a SEI on Li metal. The optimized 1.5 M LiFSI/DMK-VC (7:3 by volume)-5 vol.% FEC endows LFP cathode with 75 mAh g^{-1} at −40 °C and 0.1 C.

Compared to linear ethers, cyclic ethers possess relatively weak solvating abilities, which are further reduced by enlarging the ring structures, resulting in weaker solvating ability of tetrahydropyran (THP) than THF [148]. Despite the weak affinity to Li^+, THP still has a high dissolution ability for lithium salts [149]. THF (a low freezing point of −108.4 °C), one of single-dentate cyclic ether solvents, shows weak interactions towards lithium ions as compared with multi-dentate solvents. Gu et al. [150] reported a thermoresponsive ether-based electrolyte formulation comprising 1 M LiFSI dissolved in THF and 1,3,5-trioxane (TO) at LiFSI:TO molar ratio of 1:0.2 for wide-temperature cyclability of high-voltage LMBs. Importantly, the introduction of TO decreases the Li^+-THF binding energy and contributes to the transformation of the primary solvation structure from SSIPs to CIPs at subzero temperatures, thereby improving Li^+ transport and charge transfer kinetics. Moreover, TO exhibits the low LUMO and high HOMO energy levels compared to THF, enabling its preferential redox decomposition to generate Li-polyoxymethylene (LiPOM) in CEI and SEI. The 1.5-Ah Li||NCM811 pouch cell maintains a specific energy of 317.1 Wh kg^{-1} at −40 °C, retaining 74.7% of its capacity after 60 cycles. Besides, the 1.6 M LiFSI-2 wt.%$LiNO_3$/THF-MeTHF (1:1 by volume) electrolyte enables the formation of LiF/LiN_xO_y-rich SEI, achieving stable operation of LMBs for 100 cycles at −30 °C [151].

Most WSEs show unfavorable oxidation stability, which restricts the energy density of LIBs at subzero temperatures. In view of molecule chemistry, increasing the molecule chain or fluorination of ether solvents is generally adopted to broaden the ESW of electrolyte and weaken the ion-dipole interactions. For instance, compared with diethyl ether, non-polar dipropyl ether molecule has longer alkyl groups and thus weaker coordinating ability due to stronger steric hindrance [152]. Thanks to the electron delocalization effect and the

steric hindrance, Zhu et al. [125] proposed a weakly solvated cyclic ether, 2-methoxy-1,3-dioxolane (MODOL), with better reductive stability for achieving stable operation of LMBs from −20 to 60 °C through the introduction of an electron-donating methoxy group (−OCH_3) onto the DOL solvent. To improve the electrochemical compatibility of ether-based electrolytes with high-voltage cathode and co-intercalation-free graphite anode, Liu et al. [124] managed the length of –O–CH_2–O– segments in polyoxymethylene ether solvents including DMM, DDE, tripolyformaldehyde dimethyl ether (TDE), and tetrapolyformaldehyde dimethyl ether (TTDE). Compared to the strongly solvated DME with five-member ring Li^+ coordination structures, these solvents with four-membered ring coordination show relatively weak desolvation energy and more solvents can be effectively anchored by Li^+ at the same concentration without largely compromising the ionic dissociation capability as the number of −O−CH_2−O− segments increases, thereby improving the oxidation stability of electrolytes. Nevertheless, the viscosity of electrolytes increases with the chain length of polyoxymethylene ethers, leading to the decreased ionic conductivity. Thus, the DDE-based electrolyte is selected as an optimal WSE for Gr||NCM811 Ah-level pouch cells, achieving 75.86% capacity retention after 400 cycles at −20 °C.

The introduction of electron-withdrawing fluorine or chlorine atoms decreases the electron-donating ability of solvents, which is beneficial to the compatibility with lithium metal anode, suppressed corrosion risk, and high-voltage tolerance [153–155]. In carbonate-based electrolytes, lithium ions are typically coordinated with polar solvent molecules through the electronegative carbonyl oxygens. Decreasing the electronegativity of the carbonyl oxygen provides a feasible approach to weaken the ion-solvent coordination without sacrificing the high-ε property of polar solvents. Chen et al. [156] disclosed that a higher fluorination degree and/or ethoxy side fluorination led to a weaker interaction between Li^+ and the solvents, thereby better LT performance. Leveraging both solvents and anions to form interphases, Tan et al. [139] designed the 2.0 M LiFSI/FEC-DFDEC (1:4 by volume) for high-voltage graphite||NMC811 full cells under extreme temperatures. Nevertheless, the fluorination/chlorination of solvent molecules induces weaker ion coordination capability than the non-fluorinated/chlorinated counterpart, which limits the salt solubility and ionic conductivity of electrolytes. Amanchukwu's team [157] adopted the molecular design of fluorinated ethers to optimize the wide-temperature cyclability of LIBs from −40 to 60 °C. With a −CH_2F end group and the decrease in glyme ether chain length, the E1CH2F-based electrolyte achieves low viscosity and high ion diffusivity while maintaining strong ion pairing to form LiF-rich CEI. In contrast, both E3CH2F and E2CH2 solvents enable the SSIP-dominated solvation structure due to the synergetic effect of lower steric hindrance and stronger coordination ability of -CH_2F compared to –CF_3 in E3F1. Chen et al. [158] synthesized a series of fluorinated ethers with weak-solvation ability owing to the duple steric hinderance effect caused by longer carbon chain and the methine group (Figure 6a). The 2 M LiFSI/ethylene glycol (2,2,2-trifluoroethyl-i-propyl) ether (PXEO-CF_3) electrolyte contains high proportion (97.96%) of AGGs and enables a high CE of 98.56% for Li deposition/stripping at −20 °C due to the LiF-rich SEI. Nevertheless, trifluoro- and difluoro-substituted ether-based electrolytes usually suffer from the largely reduced ionic conductivity after the fluorination.

By tailoring the fluorination degree, Zhang et al. [159] successfully synthesized monofluoride bis(2-fluoroethyl) ether (BFE) as the electrolyte solvent for fast-charging LT LMBs. The BFE can strongly coordinate Li^+ with one Li-O and two Li-F interactions to form a five-member ring, resulting in the SSIPs/CIPs-dominated solvation structure of 2 M LiFSI/BFE electrolyte, which simultaneously achieves high ionic conductivity (0.95 mS cm^{-1} at −60 °C), a wide ESW (4.7 V), and good Li cyclability (99.5% at −30 °C) compared to difluoro (-CHF_2) and trifluoro (-CF_3) counterparts. The as-assembled Li||NCM811 coin cells (N/P = 2.8) exhibits a high capacity retention >90% for 150 cycles at −30 °C and 1.75 mA cm^{-2}.

In general, the anti-oxidation capability of solvents follows the sequence of ester > siloxane > ether [127]. Wang et al. [52] designed a DFEC-modified WSE comprising 1 M $LiPF_6$/PC-DEC (1:1)-10% DFEC for high-voltage LT practical graphite-based pouch cells, retaining 91% of room-temperature discharge capacity at −20 °C. Although ether solvents usually have low melting points, most of them suffer from oxidative decomposition at high voltages, owing to the absence of matching and energy-equivalent empty orbitals that can stabilize the non-bonding electrons of oxygen atoms. Decreasing the number of O atom or extending the length of alkyl in ethers can improve oxidation stability [124]. In contrast, carbonyl oxygen in esters contains lone-pair electrons, which can conjugate with the nearby $\pi^*_{C=O}$ anti-bonding orbital, resulting in the formation of a lower-energy filled orbital and thus better oxidative stability of ester solvents. Nevertheless, strong ion-dipole interactions in ester-based electrolytes impede their LT applications. For siloxane solvents, the conjugation between the Si3d empty orbitals and the lone-pair electrons of oxygen atoms decreases the solvation ability (Figure 6b), enabling rapid desolvation at the interface [127]. By regulating the number of Si–O conjugated bonds, the type of anion clusters in the solvation structure can be controlled, balancing fast desolvation and ionic conductivity. For example, among four representative siloxanes with an increasing number of methoxy groups and the negative charges centred on O atoms (Figure 6c), the 1.5 M LiFSI/ethyltrimethoxysilane (MTOS) electrolyte exhibits the highest ionic

conductivity within the temperature ranged from −40 to 20 °C (Figure 6d). The analysis of electrolyte solvation discloses that the proportion of AGGs increases with the increased number of methoxy groups from trimethylmethoxysilane (TMOS) to MTOS, meanwhile, the percentage of more coordinated ion-pair aggregates (AGG+) decreased, whereas a higher content of AGG+ can impede the ionic transport. Besides, these siloxane-based electrolytes show excellent stability to pair with high-voltage cathodes (>4.5 V). Typically, MTOS possesses the highest LUMO and lowest HOMO energy levels, suggesting its good anti-reduction and anti-oxidation electrochemical stability. Based on the 1.5 M LiFSI/MTOS electrolyte, the NCM811 cathode and graphite anode provide reversible capacities of 108 mAh g^{-1} at 0.1 C and 95 mAh g^{-1} at 0.05 C, respectively, when being operated at −40 °C. And the graphite||NCM811 pouch cells still deliver a high discharge capacity of 1.61 Ah at −40 °C and 0.1 C, corresponding to the 67.4% room-temperature capacity, and maintain ~88.85% capacity after 100 cycles at −20 °C and 0.2 C, which far exceeded the LT performance of the full cell containing the commercial EC/EMC electrolyte with a SSIPs-dominated solvation structure. Specifically, the LiF and Si─O-rich interface layer derived from the siloxane solvent and FSI^- anion-rich solvation sheath reduces interfacial resistance for ion transport and suppresses excessive Li dendrite growth on graphite anode at LTs. Notably, Chen et al. [160] revealed that the anion-rich solvation structures of siloxane electrolytes were induced by weak cation-solvent interactions and strong cation-anion interactions.

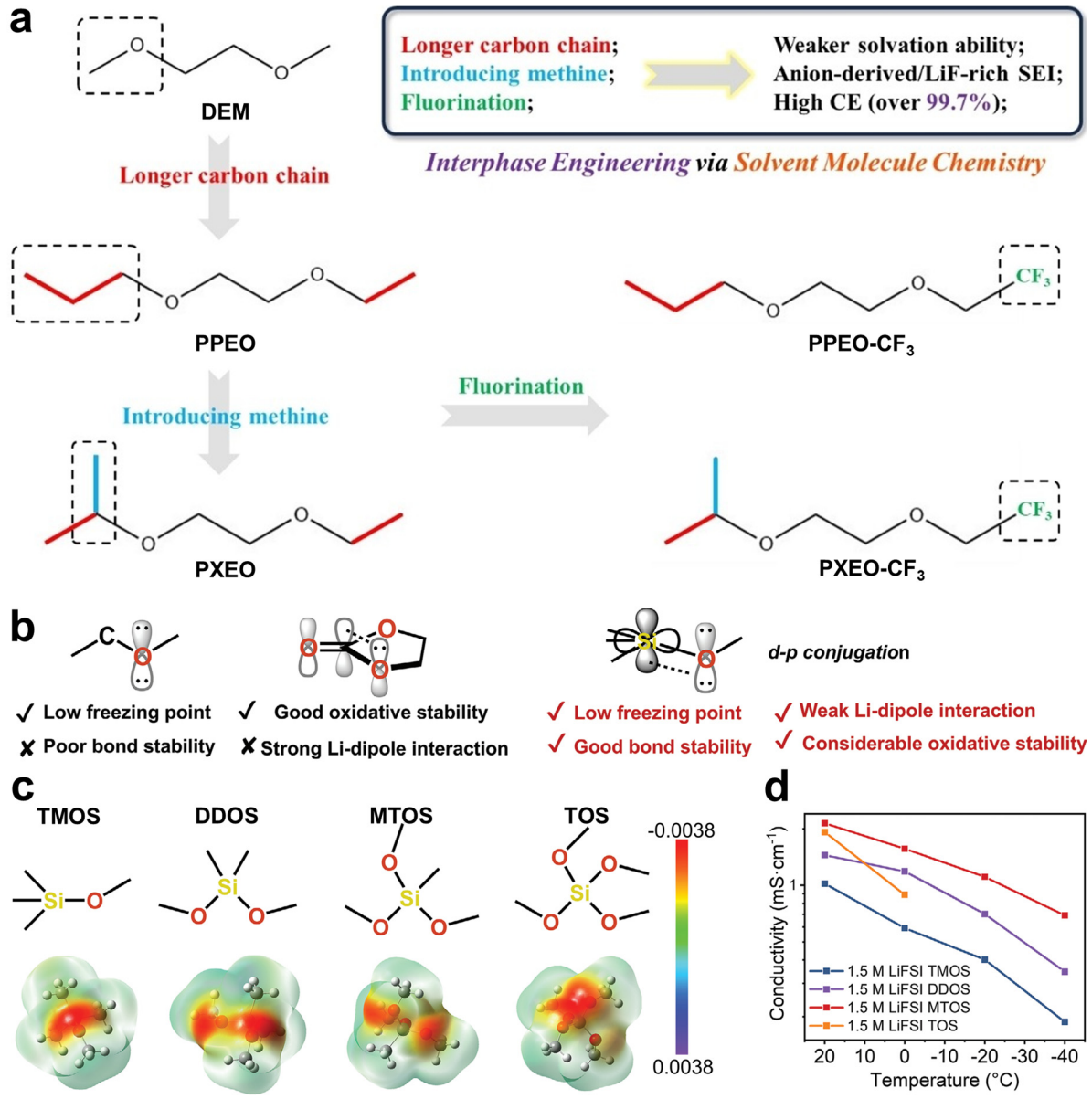

Figure 6. (**a**) Molecular structures of fluorinated ethers and the functional mechanism. Reproduced from [158]. Copyright 2024 with permission from Wiley-VCH GmbH. (**b**) Structures and properties of typical carbonate and ether solvents, and the bonding structures and properties of siloxane solvents. (**c**) Molecular structures and ESP

maps of siloxane solvents. (**d**) Ionic conductivities of prepared siloxane-based electrolytes from 20 to −40 °C. Reproduced from [127]. Copyright 2024 with permission from Wiley-VCH GmbH.

Carboxylic ester-based WSEs have been widely reported in LT LIBs. With a solvent-dominated solvation structure, MTFA in the $LiPF_6$/FEC-DMC-MTFA-1 wt.% LiBOB electrolyte contributes to the formation of thin and robust EEIs [132]. The 1 M LiDFOB/dimethyl sulfite (DMS)-ETFA-FEC (4:4:2 by volume) WSE is featured with the fluoride-rich solvation structures including FEC, ETFA, and $DFOB^-$, which can significantly prevent the corrosion of highly solvated DMS towards electrodes, accelerate the reaction kinetics, and enable uniform Li deposition by forming a highly ionic conductive inorganics-rich SEI [48]. And the assembled Li||NCM811 cell exhibits a capacity of 125.7 mAh g^{-1} with almost no capacity decay after 200 cycles at −40 °C and 0.1 C. Zou et al. [161] designed a non-flammable all-fluorinated electrolyte of $LiPF_6$/methyl difluoroacetate (MDFA)-PFPN-FEC (1:7:0.5:1 by molar) for wide-temperature fast-charging LIBs. The Li^+-PF_6^- interactions can be enhanced after adding PFPN, which avoids the reduction decomposition of MDFA and inhibits the hydrolysis reaction at the anode surface, while they are decreased by further introducing FEC because of the stronger Li^+-FEC interactions. Importantly, the appropriate Li^+-PF_6^- interaction is beneficial for the structural stability of Li^+-solvent-PF_6^- CIPs to inhibit the $LiPF_6$ hydrolysis during cycling. Consequently, the graphite||NCM811 full cells show great capacity retention of 87.4% after 100 cycles at −20 °C and 0.2 C (1.0 C = 2.1 mA cm^{-2}).

Fundamentally, the concept of WSEs arises from the balance between ion-solvent coordination and cation-anion interactions. As such, the design of WSEs can be achieved not only by tuning the solvent, but also by selecting the anion to regulate the solvation environment. Besides, high-entropy WSEs with increased solvation entropy have been widely reported to improve ion transport capabilities without compromising the electrochemical stability with high-voltage cathodes and lithium metal anode. As an important feature, multiple anions- or solvents-induced high entropy effect generally decreases ion clustering while inheriting the anion-rich solvation structure [72,162–164].

4.2.3. Additive-Assisted Electrolytes

Electrolyte additives can significantly improve the LT performance of LIBs due to its closely relationship with interfacial chemistry. Different types of electrolyte additives have been investigated especially for their effects under subzero temperatures because they can accelerate the electrode kinetics, inhibit gas generation, and improve high-voltage stability and/or the flame retardancy of electrolytes.

As a widely used electrolyte additive, FEC has good film-forming ability to construct a fluoride-rich SEI due to its high reaction activity and low LUMO energy level. To stabilize EEIs, FEC has been employed in LT electrolyte formulations. For instance, the addition of 10 vol.% FEC in LiTFSI/DOL-DME (8:2 by volume) electrolyte contributes to the formation of LiF and Li_2CO_3 crystallites in SEI, resulting in the stabilized Li plating/stripping and significantly increased CE even at −60 °C, and enabling relatively high reversible capacity of Li||LFP at −40 °C [165]. More commonly, FEC is used as part of a multi-additive mixture (such as FEC-$LiNO_3$ [149] and FEC-LiDFOB [117]) for LT LMBs. As a highly fluorinated additive, 1,5-difluoro-2,4-dinitrobenzene (FNB) in the 1 M $LiPF_6$/EMC electrolyte contributes to forming LiF and LiN_xO_y-rich EEIs, meanwhile, the interaction between FNB and lithium salt enhances the coordination of anions in Li^+ solvation structures, synergistically improving the operational feasibility of Li||NCM811 cells over a wide temperature range from −30 to 55 °C [166]. Zhu et al. [167] combined the heptafluorobutyric anhydride (HFAA) additive with ethylene glycol bis(propionitrile) ether (DENE) co-solvent to develop the 1 M $LiPF_6$-0.1 M LiDFOB/DENE-TTE-DME (3:5:2 by weight)-5 wt.% FEC-1 wt.% HFAA electrolyte for high-voltage (4.7 V) and high-safety LMBs under extreme temperatures (−30 to 120 °C). HFAA triggers the formation of LiF-rich SEI, ensuring highly reversible Li deposition/stripping with uniform morphology, whereas DENE can restrain lone-pair electrons loss on ether oxygen through the strongly electron-withdrawing –C≡N group to increase the ESW above 5 V. The synergistic effect of HFAA and DENE significantly decreases the coordination number of DME and PF_6^-, promoting Li^+ desolvation process and suppressing interfacial side reactions.

Sulfur-containing additives such as 1,3-propanesultone (PS) can regulate interphase compositions with sulfur-rich substances to facilitate the desolvation step and ionic migration at subzero temperatures. The 1 M $LiPF_6$/EA-FEC (10:1 by volume)-2 vol.% PS electrolyte ensures the operating reliability of Li||NCM811 cells at extensive temperatures from −40 to 60 °C, which is mainly attributed to the participation of PS in the formation of highly ionic conductive CEI with Li_2S, Li_2SO_3, and LiF-rich inner layer and organic-rich outer layer [168]. Furthermore, lithium fluorosulfonate (LFS) as a S- and F-containing additive in the 1 M $LiPF_6$/EC-EMC (3:7 by volume) electrolyte can effectively reduce the R_{ct} of graphite anode by forming a robust and low-resistance SEI composed of inorganic LiF, Li_2SO_4 and organic fluorides/sulfides, enabling the 94% capacity retention of graphite||LFP cells after 100 cycles at −20 °C and 0.5 C [169].

Phosphorus-containing additives possess good film-forming ability and/or excellent flame-retardant ability. PFPN is adopted as the flame-retardant additive to improve the LT battery safety. On the one hand, PFPN with lower LUMO energy level is the main component of anion solvation due to its strong binding energy, forming inorganic-rich EEIs with fast ion transport. On the other hand, PFPN can effectively scavenge combustion radicals (H· and HO·) and avoid HF generation via van der Waals force. With the PFPN as a multifunctional diluent, the non-flammable LiFSI/MA-PFPN (1:2:2 by molar) electrolyte endows graphite||$LiNi_{0.65}Co_{0.15}Mn_{0.2}O_2$ full cells with excellent cycling performance at −20 °C, showing a high capacity retention of 94.6% after 300 cycles at 1 C [113]. $LiPO_2F_2$, characterized by its poor solubility in carboxylate and carbonate solvents and strong binding with Li^+, shows a prominent tendency to participate in the primary solvation sheath, thereby constructing inorganic-rich SEI [170–173]. To regulate the LT SEI formation on the surface of graphite anode, 0.2 M $LiPO_2F_2$ is introduced into the 0.5 M LiDFOB-0.5 M $LiPF_6$/MA-DFEC (9:1 by volume) weakly solvated electrolyte, in which the combination of LiDFOB and $LiBF_4$ guarantees the high-voltage tolerance and high ionic conductivity simultaneously [174]. The higher binding energy of $PO_2F_2^-$ with Li^+ than that of $DFOB^-$ allows the entrance of $PO_2F_2^-$ in the primary solvation sheath to replace $DFOB^-$, yielding the preferentially decomposition of $PO_2F_2^-$ to form a low-swelling, Li_3PO_4-rich SEI with favourable electron-blocking ability on graphite anode, and thus the suppression of solvent co-intercalation. As a result, the full cells coupling NCM811 cathode with graphite, graphite/SiO_x composites, and even pure SiO_x anodes exhibit stable cycling at −20 °C.

Siloxane analogues have attracted great attention due to their ability to form organic Si-O interphase component and remove hazardous species from the electrolyte. For instance, Jiang et al. [175] proposed trimethylsilyl isocyanate (Si-NCO) with the electron-withdrawing d-π conjugation as the scavenger to eliminate water in DOL-based electrolyte by a nucleophilic addition reaction, preventing DOL from a cationic ring-opening polymerization in the presence of inorganic salts (such as $LiBF_4$, $LiPF_6$, and LiDFOB). The 2.5 M $LiBF_4$/DOL-DME (7:3 by volume)-2 vol.% Si-NCO electrolyte endows Li||LCO cells with a capacity retention of 80% after 150 cycles at −40 °C.

Typically, LiDFOB has been widely reported as an effective electrolyte component for improving high-voltage stability due to its cost-effectiveness, outstanding solubility and thermal stability, as well as the capability to enhance the ionic conductivity of EEIs [176]. Moreover, it generates an electron-deficient difluoroborane under high working voltages and reacts with part of carbonate species at interface to produce highly elastic B-O based oligomers for accommodating the volume change of cathode. Piao et al. [177] designed a 1 M $LiPF_6$-0.1 M LiDFOB/FEC-FEMC (1:3 by volume) electrolyte with a B and F-containing solvation structure for stable operation of high-voltage LMBs. A robust and elastic B- and F-rich EEIs can be formed at both electrodes through preferentially decomposition of LiDFOB owing to its high HOMO and low LUMO energy levels, as well as the entrance of $DFOB^-$ in the inner solvation sheath of Li^+ with strong ion-ion interaction. The Li||$LiNi_{0.6}Co_{0.2}Mn_{0.2}O_2$ (NCM622) cells deliver a considerable capacity of 143.5 mAh g^{-1} at −20 °C. Lu et al. [178] introduced LiDFOB and TMSPi dual additives with the preferential oxidation into the 1 M $LiPF_6$/EC-EMC-DMC (1:2:2 by weight) base electrolyte for realizing all-climate high-voltage LIBs. Specially, the TMSPi additive participates in the first solvation shell of Li^+ to replace EMC and DMC, whereas the Li^+-$DFOB^-$ appears at a longer distance and the coordination of PF_6^- is enhanced in the outer shell, promoting the Li^+ desolvation, suppressing the HF generation, and conducive to forming a thin and robust CEI.

Gu et al. [179] proposed that the solubility of $LiNO_3$ in carbonate-based electrolytes could be increased by introducing electron donors to increase the local negative charge density of carbonyl oxygen (C=O) atoms in carbonate solvent molecules. Importantly, the heptafluorobutyramide (HFT) additive facilitates the dissolution of $LiNO_3$ in carbonate electrolytes due to the strong coordination between carbonyl groups and Li^+, whereas the Lewis basic -NH_2 in HFT can combine with the Lewis acidic PF_5 to suppress the HF generation [180]. Moreover, the first solvent sheath is transformed into the anion-dominated structure after adding HFT, significantly reducing Li^+ desolvation barrier. Besides, the preferentially reduction decomposition of HFT and $LiNO_3$ induces the formation of Li_3N/LiF-rich SEI on the Li metal anode. Thus, Li||LFP cells can sustain the capacity of 102.1 mAh g^{-1} after 500 cycles at −20 °C and 0.5 C. Piao et al. [181] combined the tetramethylurea (TMU) co-solvent with $LiNO_3$ additive in 1 M $LiPF_6$/EC-EMC (1:1 by volume)-2 wt.% FEC to ensure the preferential reduction of $LiNO_3$ on lithium metal anode and inhibit the HF generation by regulating the Li^+ solvation sheath and scavenging Lewis acid PF_5, which enables the excellent LT performance of Li||Cu half cells (96.14% at −15 °C and 1 mA cm^{-2}) and Li||LFP cells (32.5 mAh g^{-1} at −25 °C and 0.3 C). Similarity, a quasi-ionic liquid ([Li(15-crown-5)]NO_3) and $CuNO_3$ additives were utilized in LT LIBs [182,183].

Besides, the asymmetric 4,5-dicyano-2-(trifluoromethyl)imidazol-1-ide (TDI^-) anion, characterized by strong coordinating ability with Li^+ to accumulate at the cathode surface, is employed as an additive in 1 M LiFSI/DME electrolyte, allowing an interfacial high-concentration region to form the anion-rich solvation

structure and thus a low-resistance inorganic-dominated CEI [184]. The LiTDI-enhanced electrolyte guarantees remarkable performance of Li||NCM811 cells with 96.6% capacity retention after 700 cycles at −20 °C and 0.5 C. Driven by the bias-potential, the sodium perfluorooctanoate (NaPFO) additive dissolved into the 1 M LiFSI/THF electrolyte can reversibly self-assemble into an ordered molecular layer on the cathode surface due to its negatively charged carboxylic head group and the long perfluorinated alkyl chain tail, which enhances the oxidation stability of electrolyte [185]. Moreover, NaPFO significantly improves the electrolyte compatibility with Li metal at LTs due to the optimized SEI composition with higher LiF content. Thus, the 0.5 wt.% NaPFO-based electrolyte realizes high energy/power densities of Li||NCM811 cells at ultra-low temperatures. Lu et al. [186] synthesized lithium (trifluoromethanesulfinyl)(trifluoromethanesulfonyl)imide (LiSTFSI) with the asymmetric structure to serve as the additive in 1.0 M LiFSI-0.2 M $LiNO_3$-0.3 M LiSTFSI/DME-5 vol.% FEC electrolyte. The formation of a tough and resilient anion-derived CEI with an inorganic-dominated structure, consisting of the LiF-rich inorganic inner layer and the outer layer of N-S main-chained and negative-charged inorganic polymer which can accelerate the Li^+ desolvation, ensures extremely stable cycling of Li||NMC811 cells with 85.7% retention after 2000 cycles at −20 °C and 0.3 C.

The development of new additives incorporating specific elements such as F, B, S, Si, and N holds great potential for advancing the applicability of LT LIBs. It is important to acknowledge that these additives may undergo gradual consumption or degradation during repeated cycling, which could ultimately lead to a decline in capacity. The effectiveness of additives is inherently limited, and the long-term stability at subzero temperatures requires a careful and synergistic integration of various electrolyte components.

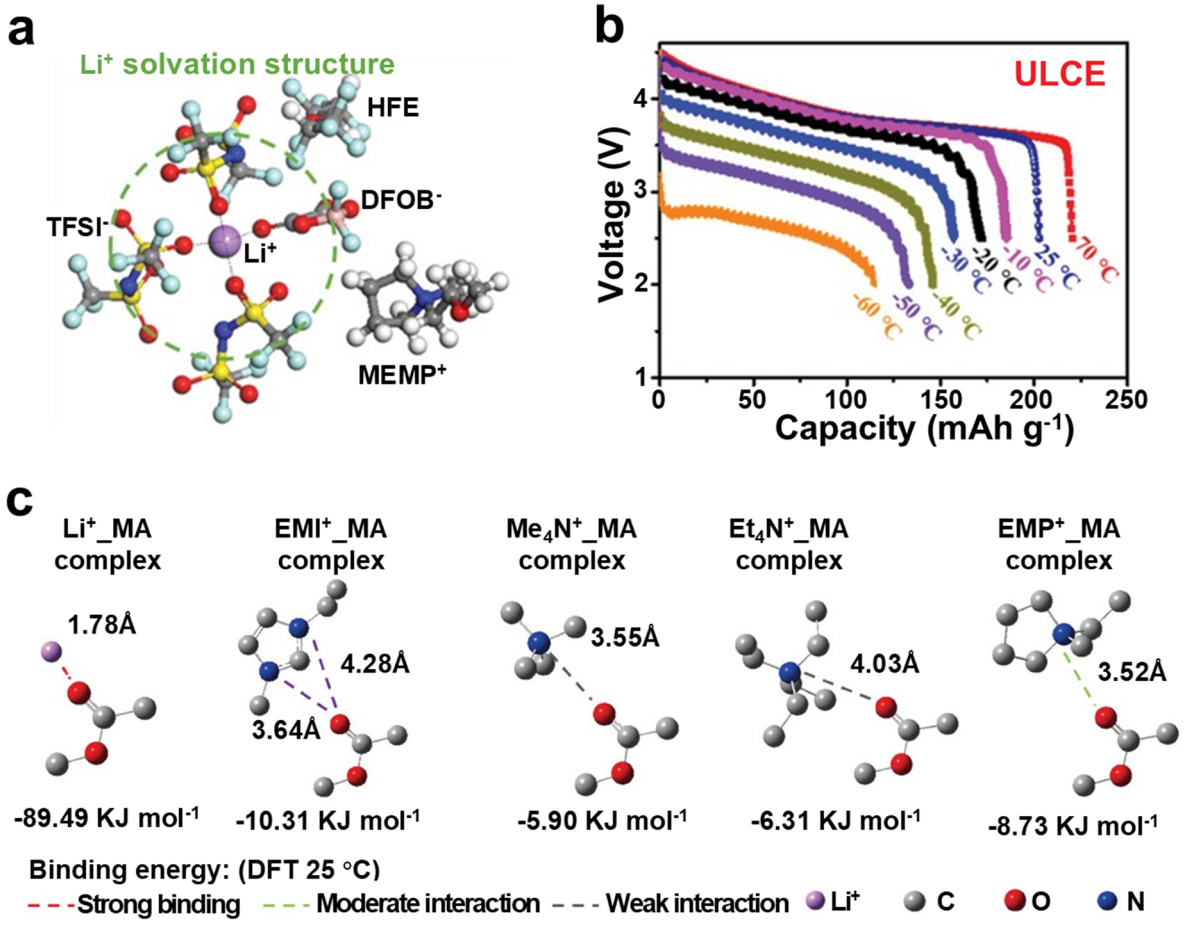

Figure 7. (**a**) Typical Li^+ solvation structure in ULCE extracted from MD simulation snapshot. (**b**) Discharge profiles of Li||NCM622 cells at different temperatures in ULCE. Reproduced from [187]. Copyright 2023 with permission from Wiley-VCH GmbH. (**c**) Interaction between different cations and MA solvent calculated by DFT method. Reproduced with permission [188]. Copyright 2024 with permission from Wiley-VCH GmbH.

4.3. Ionic Liquid-Based Electrolytes

Ionic liquids (ILs), as molten salts composed entirely of ions and liquid at room or near-RT, have garnered extensive attention as ideal candidates for next-generation high-performance electrolytes in energy storage

systems, which can attributed to their unique advantages, including wide ESW, high thermal stability, low vapor pressure, non-flammability, and remarkable structural tunability.

4.3.1. Ultralow-Concentration Ionic Liquid Electrolytes

In stark contrast to traditional HCEs, ultralow-concentration ionic liquid electrolytes (ULCILEs) leverage the properties of ILs by incorporating only a minute amount of lithium salt along with specific diluents to achieve exceptional LT performance. The core of this strategy lies in utilizing the trace amount of lithium salts as a functional component, while the diluent significantly reduces the overall viscosity. Simultaneously, this approach capitalizes on the non-volatility and electrochemical stability advantages inherent to ILs. ULCILEs are designed to optimize the Li^+ solvation environment, ensuring rapid desolvation kinetics and efficient ion transport even at cryogenic temperatures.

Wang et al. [187] developed an ultralow-concentration electrolyte composed of 0.1 M lithium difluoro(oxalato)borate (LiDFOB) dissolved in *N*-methyl-*N*-methoxyethylpyrrolidinium bis(trifluoromethylsulfonyl)imide ([MEMP][TFSI]) IL and TTE at a 1:2 volume ratio. The TTE diluent lowers the electrolyte viscosity, achieving an ionic conductivity of 4.1 mS cm^{-1} at 25 °C, while Li^+ coordinates mainly with $TFSI^-$ and $DFOB^-$ anions (Figure 7a). The $MEMP^+$ cations provide a cation shielding effect, where their high concentration allows them to gather at the Li anode surface and repel Li^+ ions, which ensures even Li^+ distribution and thus inhibits dendrite growth. Thanks to the combined effect of a robust anion-derived SEI (LiF, Li_2O, and Li_3N) and cation shielding effect, Li||NCM622 cells can deliver 115 mAh g^{-1} at –60 °C (Figure 7b). Although the design of low salt concentration improves the cost-effectiveness of IL-based electrolytes, long-term stability at high voltages needs further enhancement.

4.3.2. Localized High-Concentration Ionic Liquid Electrolytes

The strategy of LHCEs has also been widely applied to IL-based systems, offering a distinct approach to address the high viscosity and poor LT transport performance of ILs. The core of this strategy lies in ingeniously constructing a microheterogeneous structure: a high-concentration phase where lithium salt and the main ILs form compact, solvated Li-salt-IL clusters, interspersed with a low-concentration phase composed of the added non-solvating diluent (typically ethers or fluorinated ethers) that fills the space between these clusters. In this unique design, the diluent's critical role is not to directly participate in Li^+ solvation but to effectively lower the overall viscosity, while simultaneously confining Li^+ and its IL-solvation sheath to the localized high-concentration regions. This principle was first validated in conventional organic electrolytes, where it has been demonstrated to enable stable and efficient operation of LMBs even under harsh temperature conditions [95,189]. Its success in organic systems provides a robust theoretical foundation and strong research impetus for extending this concept to IL-based electrolytes.

For instance, Liu et al. [190] developed a locally concentrated ionic liquid electrolyte (LCILE) inspired by organic LHCEs, in which an EmimFSI-LiFSI ionic liquid was diluted with 1,2-difluorobenzene (dFBn) at a molar ratio of 2:2:1 to achieve LT performance. The anion-dominated solvation shell promotes the formation of a stable, inorganic-rich SEI (e.g., LiF, Li_3N) on the Li metal anode, which effectively suppresses Li dendrite growth. The surface of the LMA in Li||Li symmetric cells still maintain a dense and dendrite-free morphology after 50 cycles at –20 °C at 0.25 mA cm^{-2}. This LCILE enables a CE of 98.3% for Li plating/stripping and supports Li||$LiNi_{0.8}Co_{0.15}Al_{0.05}O_2$ cells with 70% capacity retention after 100 cycles at –20 °C. Furthermore, Qin et al. [188] developed a fast ion-conductor electrolyte consisting of N-ethyl-N-methylpyrrolidinium bis(fluorosulfonyl)imide (EMPFSI) as the primary organic ionic plastic crystal (OIPC) dissolved in MA with the 1.0 M concentration. This electrolyte is successfully applied in rechargeable all-organic batteries designed for –110 °C operation, utilizing polyimide (PI5) anode and polytriphenylamine (PTPAn) cathode. At the mechanistic level, this electrolyte design fundamentally leverages inherent weak interionic interaction of EMPFSI and gentle solvation capability of MA. Specifically, the EMP^+ cation of EMPFSI maintains a high ion diffusion coefficient of 2.8×10^{-8} cm^{-2} s^{-1} at −95 °C, ensuring rapid ion transport. Simultaneously, it exhibits an extremely low coordination binding energy with MA molecules (−8.73 kJ mol^{-1}), which effectively facilitates the ion desolvation process (Figure 7c). Benefiting from these properties, this electrolyte demonstrates exceptional anti-freezing capability and superior LT ion transport. Its melting point is as low as −108.4 °C, with a cold crystallization point further down at −125.7 °C. This electrolyte provides a significant ionic conductivity of 0.36 mS cm^{-1} at −110 °C. The assembled all-organic batteries, even under high load conditions, can deliver 65% of its theoretical capacity at −110 °C and 0.2 C.

Beyond optimizing electrochemical performance, a critical emerging challenge for LCILEs is the reliance on highly fluorinated diluents, which often fall under the category of per- and polyfluoroalkyl substances (PFAS) and raise significant environmental concerns. To address this issue, Xu et al. [191] recently reported a significant

advancement by developing a PFAS-free LCILE using anisole, a non-fluorinated aromatic compound, as the diluent. Similar to its fluorinated counterparts, anisole effectively reduces the high viscosity of the neat ionic liquid (from 67.5 to 6.1 mPa·s) and induces the characteristic nanophase segregation crucial for the LCILE concept. This design preserves the anion-dominated Li^+ solvation shell, resulting in a highly stable SEI and an exceptional CE of 99.7%.

4.4. Solid-State Electrolytes

Compared to liquid-based electrolytes, solid-state electrolytes (SSEs) are nonflammable, which significantly reduces the risks of fire and explosion in batteries. SSEs not only support fast charging without compromising safety but also pair well with high-voltage cathodes, enabling high theoretical energy density. Moreover, reduced side reactions at EEIs enhance the long-term stability of solid-state batteries. Importantly, SSEs exhibit superior performance under extreme temperature conditions, especially at LTs. However, several critical challenges arise when operating under LT conditions: (1) The ionic conductivity of SSEs declines significantly as the temperature drops, limiting ion transport efficiency and overall battery performance. (2) Poor interfacial compatibility between SSEs and electrodes becomes more pronounced at subzero temperatures, which leads to increased internal resistance and sluggish ion transfer kinetics, severely impacting battery efficiency. (3) At LTs, the SEI layer tends to exhibit structural instability. Uneven crystallization and fluctuations in its chemical composition can compromise its integrity, further exacerbating performance degradation under subzero-temperature conditions. Additionally, lithium metal anodes face the persistent challenge of uncontrolled dendrite growth at LTs, posing a severe threat to battery lifespan and safety. Addressing these issues is crucial for the development of next-generation solid-state batteries with reliable LT performance.

4.4.1. Solid Polymer Electrolytes

In conventional solid polymer electrolytes (SPEs), ion migration occurs through the segmental movement of polymer chains within amorphous regions. At LTs, the sluggish motion of these chains limits ion transport. The structural design of polymer chains is a key approach for improving the electrochemical performance of SPEs. Song et al. [192] developed a polymer electrolyte incorporating polar side chains with dynamic covalent bond (BE-GPE) for LT lithium-sulfur batteries. The BE-GPE was prepared by grafting the B-O dynamic bond-containing monomer 5-amino-2-(3-cyanophenyl)-1,3,2-dioxaborolane (CBN) and the diol monomer 3-amino-1,2-propanediol (APD) onto the polymer backbone via allyl glycidyl ether (AGE) ring-opening polymerization, subsequently crosslinked with pentaerythritol tetraacrylate (PETEA). By incorporating cyanide-functionalized dynamic side chains into the polymer framework, the B-O bonds associative exchange mechanism promotes chain migration, which dramatically decreases the desolvation energy barrier. The BE-GPE electrolyte shows high ionic conductivity of 1.95×10^{-3} S cm^{-1} at 0 °C. Poly(ethylene oxide) (PEO) is a commonly used polymer matrix in SPEs. However, the ionic conductivity of PEO-based electrolytes is only in the range of 10^{-8} to 10^{-7} S cm^{-1} at RT, which restricts their applications in LT environments [193]. To improve the ionic conductivity of PEO-based SPEs, incorporating plasticizers or reducing the crystallinity of PEO usually comes at the cost of mechanical strength. Lv et al. [194] developed a PEO-based composite electrolyte (KSCE) for LT lithium batteries through ultraviolet (UV) polymerizing PEO and methacryloyloxypropyltrimethoxysilane-modified SiO_2 (KS), which exhibited a high ionic conductivity of 1.73×10^{-4} S cm^{-1} at 0 °C, owing to the reduced crystallinity of PEO polymer chains and the synergistic effect of KS as Lewis acid centers. In this composite electrolyte, the formation of cross-linked networks not only reduces PEO crystallinity to enable fast Li^+ transport but also imparts strong mechanical properties, while KS, acting as Lewis acid centers, enhances lithium salt dissociation to boost ionic conductivity.

In-situ polymerization represents an alternative widely used approach for precisely modifying the structural characteristics of polymer segments [195]. He et al. [196] applied this method to create a quai-solid polymer electrolytes (QSPE) for wide-temperature LMBs. The *in-situ* polymerization of functionalized polyethylene glycol (A-PEG) in a low-melting organic solvent like DOL and lithium salt (LiTFSI) was used to fabricate D-QSPE. The incorporation of ethylene oxide (EO) and urethane units into polymer chain promotes rapid segmental dynamics in D-QSPE and ensures continuous coordination with Li^+, facilitating the creation of efficient Li^+ transport pathways. The weak binding energy between Li^+ and the solvent also contributes to Li^+ desolvation. The D-QSPE exhibits the ionic conductivity of 4.7×10^{-4} S cm^{-1} at −20 °C, which is higher than that of the commercial liquid ether-based electrolyte. Furthermore, the robust SEI derived from D-QSPE contains fewer organic components and a high content of LiF, resulting in the enhanced reaction kinetics and reduced side reactions. The as-assembled Li|D-QSPE|LFP cells show almost no capacity loss (92.8 mAh g^{-1}) under 0.1 C (1 C = 150 mA g^{-1}) after 550 cycles at −20 °C. Yu et al. [197] developed a QSPE system with high conductivity through *in-situ* fabrication for high-

energy LMBs at LTs. QSPEs were obtained by mixing and *in-situ* ring-opening polymerization of DOL monomer, LiTFSI, MP as the solvent, $LiPF_6$ as the initiator, and FEC. The as-prepared 1.0 M-40 QSPE (1.0 M LiTFSI with 40 vol.% of DOL) shows superior ionic conductivity under LT conditions (e.g., 1.0×10^{-3} S cm^{-1} at −30 °C, Figure 8a), along with remarkable Li^+ transfer number of 0.61 at the RT, which originates from the stronger binding energy between $TFSI^-$ and poly-DOL matrix compared to that between $TFSI^-$ and MP. Overall, the coordination environment of lithium ions can be tuned by modifying the structure of polymer molecular chains, resulting in a significant improvement in the ionic conductivity of SPEs [198].

By promoting interactions between fillers and the polymer matrix, filler blending is a straightforward and effective strategy to improve the ionic conductivity of SPEs. SN is a commonly used organic filler. Xu et al. [199] fabricated a homogeneous PEO-based solid-state electrolyte (Homo-SPE) for LT LMBs when the molar ratio between SN and PEO was approximately 1:4. The molecular size of SN aligns with the distance between Li^+ binding sites in PEO (Figure 8b). SN not only reduces the crystallinity of PEO but also weakens the interaction between EO chains and Li^+, endowing Homo-SPE with an impressive ionic conductivity of 2.1×10^{-5} S cm^{-1} at 0 °C. Park et al. [200] synthesized a fluorinated elastomeric electrolyte (F-PCEE) for LT and high-voltage LMBs through phase separation of 2,2,3,4,4,4-hexafluorobutyl acrylate (HFBA) and SN during polymerization. Most lithium ions reside within the SN phase due to its higher affinity for the hydrophilic SN than the hydrophobic HFBA, resulting in increased elasticity and high ionic conductivity at LTs. For comparison, BA-PCEE was prepared using fluorine-free BA monomers via a similar method. F-PCEE features a bicontinuous structure consisting of a fluorine-containing elastomer and SN plastic crystal phases, which serve as the mechanical scaffold and ion-conducting domains, respectively. The mechanical scaffold allows F-PCEE to remain elastic at −20 °C, while BA-PCEE undergoes irreversible plastic deformation below −10 °C. The ionic conductivity of F-PCEE is an order of magnitude higher than that of BA-PCEE at −20 °C. Additionally, the F-PCEE promotes the formation of a LiF-rich SEI layer, which suppresses Li-dendrite growth, enabling stable cycling of symmetric cells for over 1500 h at −10 °C and 1.0 mA cm^{-2}. More importantly, the Li|F-PCEE|NCM811 full cell retains 74.4% of its room-temperature capacity at −10 °C and 0.05 C (1 C = 200 mA g^{-1}).

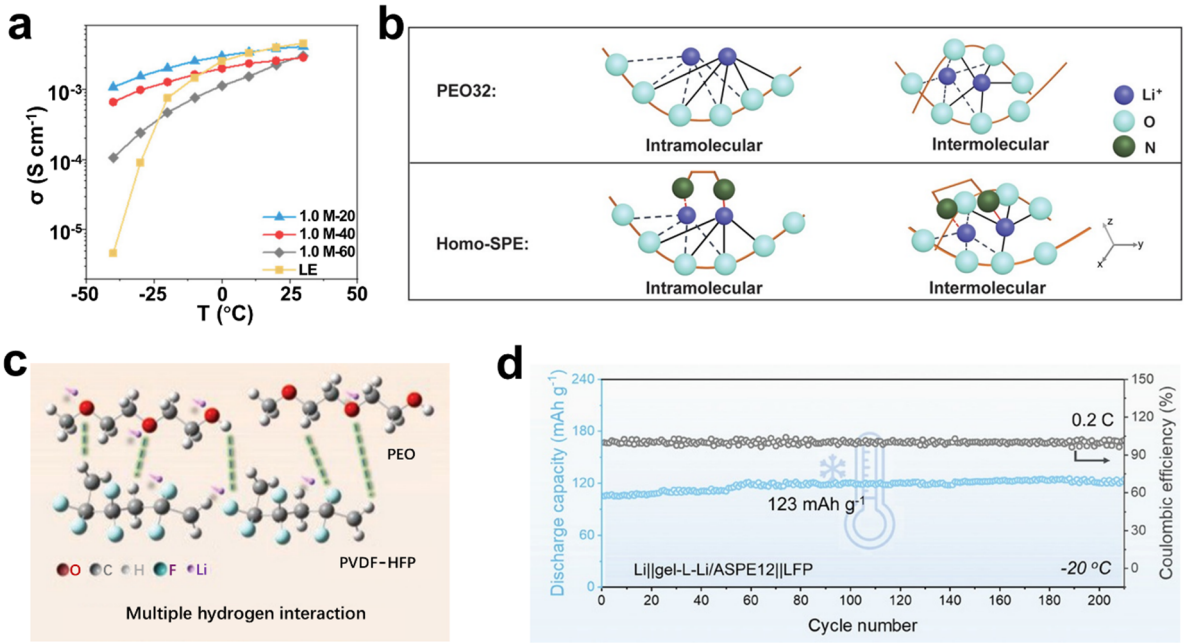

Figure 8. (**a**) Ionic conductivity of 1.0 M $LiPF_6$/EC-DMC (1:1 by volume, LE) and 1.0 M-X QSPEs, in which 1.0 M refers to 1.0 M LiTFSI and X represnets the volume ratio of DOL (DOL% = $V_{DOL}/(V_{DOL} + V_{FEC} + V_{MP})$), within a temperature range between −40 and 30 °C. Reproduced with permission [197]. Copyright 2021 with permission from Wiley-VCH GmbH. (**b**) Comparative study of Li^+ migration in PEO32 and Homo-SPE. Reproduced from [199]. Copyright 2020 with permission from Wiley-VCH GmbH. (**c**) The multiple hydrogen interaction between L-Li, PVDF-HFP, and PEO/LiTFSI. (**d**) Long-term cycling behavior of Li|gel-L-Li/ASPE12|LFP at −20 °C and 0.2 C. Reproduced from [201]. Copyright 2024 with permission from Wiley-VCH GmbH.

As natural resources deplete and the environment deteriorates, increasing attention has been directed toward sustainable development. Lignin, as an abundant renewable resource, exhibits excellent mechanical properties, which has been widely utilized in SPEs. Liu et al. [201] designed a lignin-based SPE (L-Li/ASPE12) for LT LMBs, which

was consisted of lignin-based single-ion lithium salt (L-Li), poly(vinylidene fluoride-co-hexafluoropropylene) (PVDF-HFP) as the framework, and PEO/LiTFSI as the filler through electrospinning, spraying and hot-pressing approach. The L-Li/ASPE12 membrane exhibits a high Young's modulus of 4.49 GPa, demonstrating robust mechanical properties, and high ionic conductivity of 0.13×10^{-3} S cm^{-1} at the RT. The sulfonate (SO_3^-) groups conjugated with the benzene ring in L-Li facilitate high Li^+ dissociation by repelling free anions and enable efficient Li^+ transport through nanofiber ionic bridge channels (Figure 8c). Then 20 μL of EDFA/FEC (9:1 by volume) was added into L-Li/ASPE12 to obtain a gel quasi-solid polymer electrolyte (gel-L-Li/ASPE12), and the as-assembled Li|gel-L-Li/ASPE12|LFP cells maintain a discharge capacity of 123 mAh g^{-1} at 0.2 C (1 C = 170 mA g^{-1}) and −20 °C over 210 cycles (Figure 8d).

Polymer electrolytes exhibit poor electrode wettability, which leads to a large interfacial resistance at LTs. Generally, adding low-melting-point organic solvents into polymers to create quasi-solid polymer electrolytes can significantly optimize solid-solid interface compatibility. However, there is always some side reactions at the interface. For example, in LMBs, the introduced organic solvents in quasi-all-solid-state electrolytes can react with lithium metal anode, which causes the formation of lithium dendrites and shortens the cycling lifespan. To suppress lithium dendrite, Li et al. [202] developed a quasi-solid-state polymer electrolyte that achieves a stable, low interfacial-impedance SEI for LT LMBs. The quasi-solid-state polymer electrolyte (named as TXE-FDMA-FEC-LiDFOB) was composed of the 2,2,2-trifluoro-N,N-dimethylacetamide (FDMA), 1,3,5-trioxane-based (TXE), FEC as the solvent, 1 M LiDFOB as both the lithium salt and initiator precursor. The TXE-FDMA-FEC-LiDFOB exhibits a high ionic conductivity of 2.2×10^{-3} S cm^{-1} at −20 °C. Owing to their low LUMO energy levels, FDMA and LiDFOB were preferentially decomposed to form a dual-layer SEI with less organic inner layer and amorphous outer layer. Notably, the addition of LiDFOB facilitates the formation of such a durable interphase on Li metal anodes while maintaining the Li^+ conductivity of electrolytes. Moreover, the *in-situ* constructed amorphous CEI can suppress interfacial side reactions, bulk and surface phase transformation, and even particle cracking in the cathode. The Li|TXE-FDMA-FEC-LiDFOB|LFP cells show good cycling stability, delivering a discharge capacity of about 95 mAh g^{-1} over 350 cycles at −20 °C and 17 mA g^{-1}.

Li et al. [203] prepared a dual-salt poly(tetrahydrofuran) (PTHF)-based electrolyte consisting of $LiPF_6$, LiDFOB, THF, FDMA, FEC and EO activator. LiDFOB was preferentially reduced to form conductive amorphous $Li_xBO_yF_z$ interlayer owing to its lowest LUMO. The $Li_xBO_yF_z$-rich SEI could suppress side reactions and enhance Li^+ transport across the SEI due to the high plasticity and low Li^+ migration energy barrier. Unlike the liquid electrolyte (1 M $LiPF_6$/EC-DMC,1:1 by volume), Li|PTHF-based|LFP coin cells achieve a high capacity of 94 mAh g^{-1} with near-zero capacity degradation over 250 cycles under 0.1 C (1 C = 150 mA g^{-1}) and −20 °C. An ideal interphase should possess properties such as electrochemical and chemical stability, ion conductive, flexible, and intimate with electrodes. Most of interphases *in-situ* formed at SSE/electrode interface fail to meet all these requirements simultaneously [194]. For this reason, designing an artificial interphase is a common strategy. Ren et al. [204] proposed that optimizing the weak interactions in bulk electrolytes and accelerating the interface desolvation at LTs could improve battery's performance in cold conditions. The dual salt eutectic polymer electrolyte (2MD PDSE) consisted of LiDFOB, LiTFSI, SN and DOL. They also constructed an artificial solid-state electrolyte interface (MEF@Li) by *in-situ* polymerizing methyl methacrylate (MMA), trimethylolpropane ethoxylate triacrylate (ETPTA), and F-porphyrin on the surface of the Li metal anode (Figure 9a). Because of the large specific surface area and porous structure, F-porphyrin can form continuous ion channels, which promotes ion transfer at the interface. The impedance of the MEF@Li-based symmetric cells with 2MD PDSE remains consistently lower than that with the 1 M $LiPF_6$/EC-DEC (1:1 by volume) electrolyte over a wide temperature range from −30 to 50 °C. The 2MD PDSE along with MEF@Li could balance ion transfer between the bulk electrolyte and interface, resulting in uniformly distributed Li^+ flux and electric fields to suppress the formation of Li dendrites. MEF@Li|2MD PDSE|LFP cells show negligible degradation after 200 cycles under 0.2 C (1 C = 144.3 mA g^{-1}) and −30 °C.

The sluggish interfacial kinetics at LTs significantly increase interfacial impedance, which hinders the Li^+ transport. Effective electrolyte-electrode interface engineering is crucial for quasi-solid batteries operating under extreme conditions. For example, Mo et al. [205] introduced methacryloxypropyltrimethoxysilane (MPS) into the pentaerythritol tetraacrylate (PETEA)-based gel polymer electrolyte (GPE) to promote interfacial adhesion. The terminal unsaturated C=C bond of MPS is copolymerized with the PETEA monomer during the *in-situ* polymerization, while its alkoxy groups can react with LiOH to form Si-O-Li covalent bonds on the surface of NCM811 cathode. Benefiting from the multistage bridges between the electrolyte and interface, MPS-GPE provides continuous Li^+ migration pathways and facilitates Li^+ transport kinetics at LTs, which shows a favorable ionic conductivity of 3.2×10^{-4} S cm^{-2} at −40 °C. MPS-GPE not only guarantees stable cycling of Li||Li symmetric

cells for more than 1200 h at −40 °C and 0.1 mA cm^{-2}, but also endows Li||NCM811 full cells with higher capacities than the GPE at LTs varied from −20 to −60 °C.

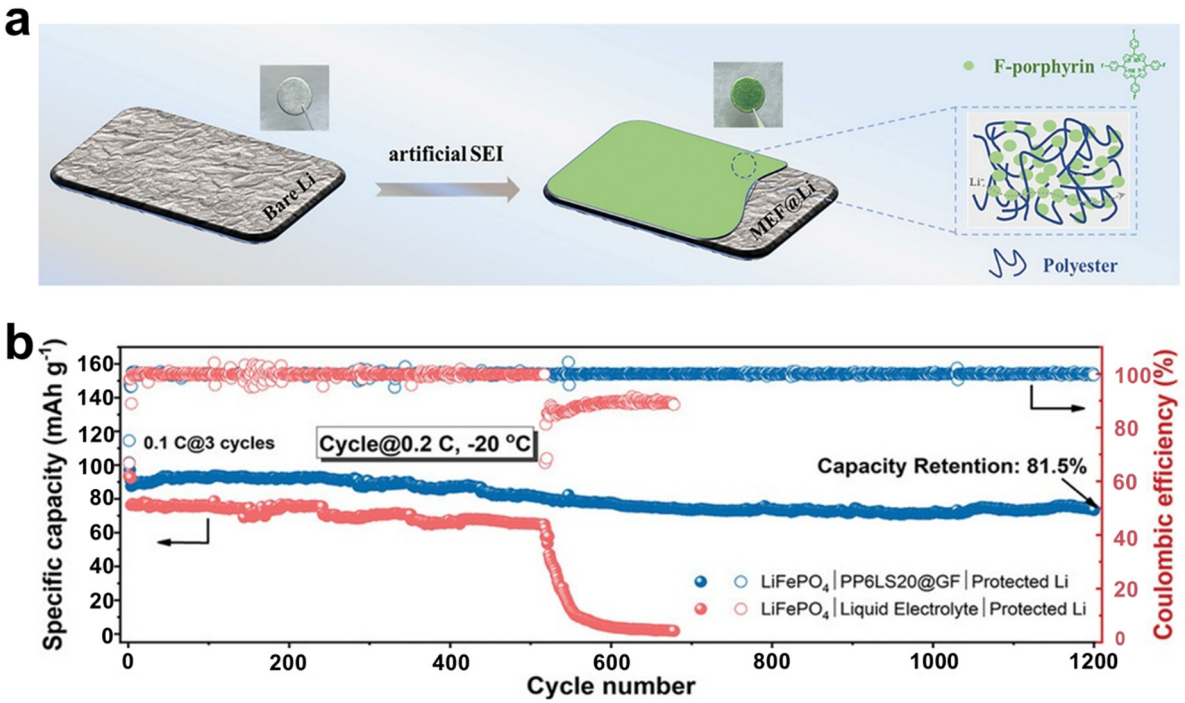

Figure 9. (**a**) Schematic representation of the engineered artificial SEI on Li metal with corresponding interfacial optical microscopy.-Reproduced from [204]. Copyright 2024 with permission from Wiley-VCH GmbH. (**b**) Cycling performance of protected Li|PP6LS20@GF|LFP cells with cathode loading of 3.5 mg cm^{-2} at −20 °C and 0.2 C. Reproduced from [206]. Copyright 2023 with permission from Wiley-VCH GmbH.

Although covalent bonding strategies show great promise in electrolyte-interface engineering, alternative approaches utilizing dynamic interactions have also emerged to address LT challenges. Huang et al. [206] fabricated a composite polymer electrolyte (denoted as PP6LS20@GF) consisting of polyether-b-amide (PEO-b-PA) as the polymer matrix, LiTFSI, SN as the plasticizer, and light-weight glass fiber mesh through a one-pot melt processing without solvent. Notably, this effective strategy that utilizes dynamic PA segments can create stable interfaces and fast ion channels, enhancing charge transfer kinetics, and thus PP6LS20@GF achieves a high ionic conductivity of 1.7×10^{-5} S cm^{-1} at −20 °C. The hydrogen bonding interactions between PA chain (−NH groups) and $TFSI^-$ anions significantly enhance the Li^+ transfer number, simultaneously suppressing cathode-side reactions and anode-side Li dendrite growth. The protected Li was obtained by immersing Li plates into 0.5 M LiTFSI/FEC for 5 h to form a LiF-rich protective layer on its surface. The protected Li|PP6LS20@GF|LFP cells show exceptional cycling performance, maintaining an average CE of 99.9% and 81.5% capacity retention after 1200 cycles at −20 °C and 0.2 C (1 C = 170 mAg^{-1}) (Figure 9b).

Up to now, smart strategies in improving the LT performance of SPEs-based LIBs (Table 2) mainly include polymer chain structure design, filler doping, *in-situ* polymerization, interface engineering and synergistic dual-salt systems to increase ionic conductivity and enhance interfacial stability. Future efforts should focus on exploring novel polymer electrolyte systems to develop materials with high ionic conductivity and structural stability, investigating interfacial mechanisms in depth to identify new modification strategies, and optimizing the SSEs fabrication process to meet practical LT application requirements.

Table 2. Summary of LT performance of representative SSE-based batteries.

Cell Configuration	Electrolyte Preparation	Ionic Conductivity (mS cm^{-1}) at LTs	Capacity (mAh g^{-1}) at LTs	Ref.
Li|BE-GPE|S	/	1.95 at 0 °C	791 after 200 cycles at 0 °C and 0.5 C	[192]
Li|KSCE|LFP	UV polymerization	0.173 at 0 °C	128.4 after 150 cycles at 0 °C and 0.2 C	[194]

Table 2. *Cont.*

Cell Configuration	Electrolyte Preparation	Ionic Conductivity (mS cm^{-1}) at LTs	Capacity (mAh g^{-1}) at LTs	Ref.
Li|D-QSPE|LFP	*In-situ* polymerization	0.45 at −20 °C	92.8 after 550 cycles at −20 °C and 0.1 C	[196]
Li|QSPE|NCM811	*In-situ* polymerization	1.0 at −30 °C	109 after 100 cycles at −20 °C and 0.2 C	[197]
Li|Homo-SPE|LFP	/	0.021 at 0 °C	118.6 after180 cycles at 0 °C and 0.1 C	[199]
Li|F-PCEE|NCM811	/	0.23 at −10 °C	~100 after150 cycles at −10 °C and 0.1 C	[200]
Li|gel-L-Li/ASPE12|LFP	Electrospinning, spraying and hot-pressing	0.13 at 25 °C	123 after 210 cycles at −20 °C and 0.2 C	[201]
Li|TXE-FDMA-FEC-LiDFOB|LFP	/	0.22 at −20 °C	95 after 350 cycles at −20 °C and 17 mA g^{-1}	[202]
Li|PTHF-based electrolyte|LFP	/	0.57 at −20 °C	94 after 250 cycles at −20 °C and 0.1 C	[203]
MEF@Li|2MD PDSE|LFP	/	0.0874 at −30 °C	66.2 after 200 cycles at −30 °C and 0.2 C	[204]
Li|MPS-GPE|NCM811	*In-situ* polymerization	0.32 at −40 °C	106 at −40 °C and 0.12 mA cm^{-1}	[205]
protected-Li|PP6LS20@GF|LFP	One-pot melt processing	0.017 at −20 °C	73.4 after 1200 cycles at −20 °C and 0.2 C	[206]
Li-In|$Li_{6.8}Si_{0.8}As_{0.2}S_5I$|$FeS_2$	Ball milling	3.74 at 0 °C	226.8 at −60 °C	[207]
Li|Li_6PS_5Cl|$LiNbO_3$@NCM523	/	2.0 at 25 °C	~80 at −40 °C and 20 μA cm^{-1} discharge	[208]
Li-In|Li_6PS_5Cl|Li_3InCl_6|Ni90	Ball milling	1.13 for Li_3InCl_6 at 25 °C	57.3 at −30 °C and 0.1 C	[209]
In-Li|Li-LaCeZrHfTa-Cl|NCM88	Mechanical milling	1.8 at 25 °C	102 after 390 cycles at −30 °C and 0.125 mA cm^{-2}	[210]
μSi|Li_6PS_5Cl|NCM811	Ball milling	1.5 at 25 °C	~1000 (based on μSi) at −20 °C and 0.3 mA cm^{-2}	[211]
Li-In|$Li_{5.5}PS_{4.5}Cl_{1.5}$|$LiNbO_3$@ $LiNi_{0.7}Co_{0.1}Mn_{0.2}O_2$	Mechanical milling	0.53 at −20 °C	79.3 at −20 °C and 0.05 C	[212]

4.4.2. Inorganic Solid Electrolytes

Inorganic solid-state electrolytes (SSEs) are pivotal for developing safe and high-performance LT all-solid-state batteries (ASSBs), primarily due to their non-flammable nature and potential to suppress lithium dendrite growth. Key categories investigated for LT applications include sulfide-based SSEs ($Li_{6.8}Si_{0.8}As_{0.2}S_5I$ (LASI-80Si) [207], $Li_{(7-x)}PS_{(6-x)}Cl_x$ ($x \approx 1$) [208], $Li_{5.5}PS_{4.5}Cl_{1.5}$ [213], etc.), and halide-based SSEs (e.g., Li_3InCl_6 (LIC) [209], $1.5LiCl\text{-}(LaCl_3 \cdot CeCl_3 \cdot ZrCl_4 \cdot HfCl_4 \cdot TaCl_5)_{0.2}$ (Li-LaCeZrHfTa-Cl) [210]) to a lesser extent for extreme LTs due to generally higher activation energies. A significant advantage over conventional liquid electrolytes is that inorganic SSEs generally do not freeze, maintaining their structural integrity at LTs [209,214].

Among inorganic SSEs, sulfide-based electrolytes are particularly attractive due to their high room-temperature ionic conductivities (often exceeding 10^{-3} S cm^{-1}, sometimes reaching 10^{-2} S cm^{-1}), good ductility, and relatively low Young's modulus. These properties stem from the larger ionic radius of sulfur compared to oxygen, leading to weaker Li^+-S^{2-} interactions and more facile ion transport. However, their chemical stability, particularly against moisture and high-voltage cathodes, remains a concern, which can be exacerbated at LTs where degradation product solubility might decrease. Despite their promise, the LT performance of sulfide-based SSEs often requires substantial optimization. A key challenge is their chemical and electrochemical instability when interfaced with high-voltage nickel-rich layered cathodes, leading to the formation of detrimental by-products (e.g., Li_2S, Li_3PO_4) during cycling. These by-products impede Li^+ transport, elevate interfacial resistance, and hasten capacity decay, issues exacerbated at LTs where reaction kinetics are already sluggish and interfacial contact may further degrade. To improve the LT suitability of sulfide-based ASSBs, primary strategies include: (1) selecting inherently more compatible cathode materials; and (2) engineering protective interfacial coatings between the cathode and the SSE. Lu et al. [207] reported a new superionic conductor LASI-80Si with an ionic conductivity of 10.4 mS cm^{-1} at the RT for an ASSB coupling with commercial FeS_2 cathode (Figure 10a). This

solid electrolyte can maintain good interfacial contact under constant stacking pressure to the FeS_2 cathode, effectively suppressing its large volume change during lithiation/delithiation. Meanwhile, the LASI-80Si||FeS_2 solid-solid structure could prevent the formation of soluble Li_2S_n (n = 4~8) species, thereby avoiding the shuttle effect of polysulfides often seen in liquid electrolytes. The structural design ensures the uniform distribution of Fe^0 nanoparticles within the cathode, which are generated during the discharge process. These small-sized Fe^0 nanoparticles possess a large specific surface area and high reactivity, which provide an electron transport pathway to facilitates the conversion reaction between Li_2S and S. The excellent thermal stability and low activation energy of the LASI-80Si electrolyte allow FeS_2|LASI-80Si|Li-In ASSBs to deliver a high discharge capacity of 226.8 mAh g^{-1} at –60 °C and 0.15 mA cm^{-2}.

Beyond optimizing cathode interfaces, sulfide-based SSEs also offer unique advantages in stabilizing high-capacity anodes that typically suffer from severe interfacial issues in liquid electrolytes, thereby enabling their operation across a wide temperature range. Tan et al. [211] demonstrated that sulfide SSEs (e.g., Li_6PS_5Cl-type) could enable the stable cycling of high-loading (99.9 wt.%), carbon-free micron-sized silicon (μSi) anodes. They found that the passivating interface formed between the sulfide SSE and μSi, coupled with the elimination of carbon additives (which were shown to promote SSE decomposition), effectively suppressed continuous SEI growth and irreversible lithium loss. This approach allows μSi|SSE|NCM811 full cells to achieve remarkable performance, including operation at –20 °C, high current densities (up to 5 mA cm^{-2} at RT), and excellent cycle life (80% capacity retention after 500 cycles at 5 mA cm^{-2}).

Halide-based SSEs offer a compelling balance, exhibiting good ionic conductivity, wider electrochemical stability windows, and often better air stability than sulfides [209,210]. To address the interfacial instability issue, Lu et al. [209] introduced a Li_2ZrO_3 (LZO) protective coating layer on the $LiNi_{0.90}Co_{0.05}Mn_{0.05}O_2$ (Ni90) cathode to suppress unfavourable interfacial reactions and the formation of byproducts (e.g., Li_2S and Li_3PO_4) under LT conditions when paired with the Li_6PS_5Cl (LPSC) electrolyte. The introduction of the Li_2ZrO_3 coating enabled the Ni90@LZO|LPSC|Li-In ASSB to achieve low overpotential while effectively mitigating capacity degradation at LTs. To further enhance LT performance, the Li_3InCl_6 (LIC) electrolyte was utilized to replace the LPSC electrolyte and a LZO coating layer. The formation of a highly stable interface in the Ni90|LIC|LPSC|Li-In ASSB results in the enhanced ionic conductivity and reduced activation energy at the cathode/SSE interface. The Li^+ transport through the CEI and charge transfer across the CEI was significantly accelerated. Compared to Ni90@LZO|LIC|LPSC|Li-In and Ni90|LPSC|Li-In ASSBs, the Ni90|LIC|LPSC|Li-In ASSB exhibits the lowest overpotential and highest capacity retention when the temperature drops from 30 to −30 °C (Figure 10b,c). Doping cations or anions is a widely adopted strategy to optimize the synthesis method and improve the crystal structure of non-sulfide-based SSEs for enhancing the ionic conductivity at LTs. For example, Li et al. [210] used a mechanical milling method, with $LaCl_3$ and $CeCl_3$ as framework materials and LiCl as the lithium ion source, while introducing $ZrCl_4$, $HfCl_4$, and $TaCl_5$ to increase structural disorder. By optimizing the composition and milling time, the ionic conductivity of the Li-LaCeZrHfTa-Cl electrolyte was significantly increased to 10^{-3} S cm^{-1} at the RT. The In-Li||$LiNi_8Co_8Mn_4O_{20}$ (NCM88) cells maintain a reversible capacity of 100 mAh g^{-1} after 390 cycles at 0.125 mA cm^{-2} and –30 °C.

While the primary focus of this section is on purely inorganic SSEs, it is noteworthy that inorganic nanomaterials also play a critical role as functional fillers in composite electrolytes to boost LT performance [215]. Li et al. [216] designed a composite gel electrolyte (designated as F-CGE-6 wt %) for wide-temperature solid-state LMBs by integrating 6 wt.% magnesium-doped lithium fluoride nanocrystals ($Mg_xLi_{1-2x}F$) as functional nanofillers into a fluorinated polymer matrix. This polar polymer matrix was prepared by the *in-situ* polymerization of ethoxylated trimethylolpropane triacrylate (ETPTA) and 2,2,3,4,4,4-hexafluorobutyl methacrylate (HFBMA), and synergistically combined with the plasticizer to form this novel electrolyte. Mechanism investigations reveal that Mg^{2+} doping induces lattice distortion and electronic rearrangement, which enhances the reactivity of LiF. This structural modification strengthens interfacial interactions between nano-fillers and fluorinated polymers, triggering the release of F-ions that rapidly form a LiF-dominated SEI with significantly reduced Li^+ diffusion barriers. The synergistic functionalities of the designed electrolyte mainly include cation-mediated salt dissociation and coordination regulation. On the one hand, positively charged $Mg_xLi_{1-2x}F$ surfaces facilitate LiTFSI dissociation through strong anion adsorption, achieving high ionic conductivity (1.37 mS cm^{-1}) and Li^+ transference number (0.58) of the F-CGE-6 wt % electrolyte at the RT. On the other hand, fluorinated polymer segments weaken Li^+-solvent coordination via electron-withdrawing effects, enabling stable operation over a wide temperature range (−20~80 °C). The *in-situ* optical microscopy shows the formation of dendritic protrusions during the lithium plating process in a conventional gel electrolyte (n-GPE), whereas the LiF-rich SEI layer induced by the F-CGE-6 wt.% electrolyte effectively suppresses Li dendrite growth (Figure 10d), resulting in uniform and compact lithium deposition morphology. This observation validates the enhanced interfacial stability

enabled by the composite electrolyte design. The LFP-based solid-state LMBs show excellent performance at −20 °C, achieving a high capacity retention of 95% after 500 cycles at 0.2 C.

Inorganic SSEs have demonstrated significant advancements for LT battery applications. Nevertheless, critical challenges persist across all inorganic SSE families. These include mitigating detrimental interfacial side reactions (especially with high-voltage cathodes, which can be kinetically hindered but still problematic at LTs, improving ion transport efficiency at ultra-low temperatures, and ensuring sufficient and stable physical contact at solid-solid interfaces under thermal cycling and volume changes [212].

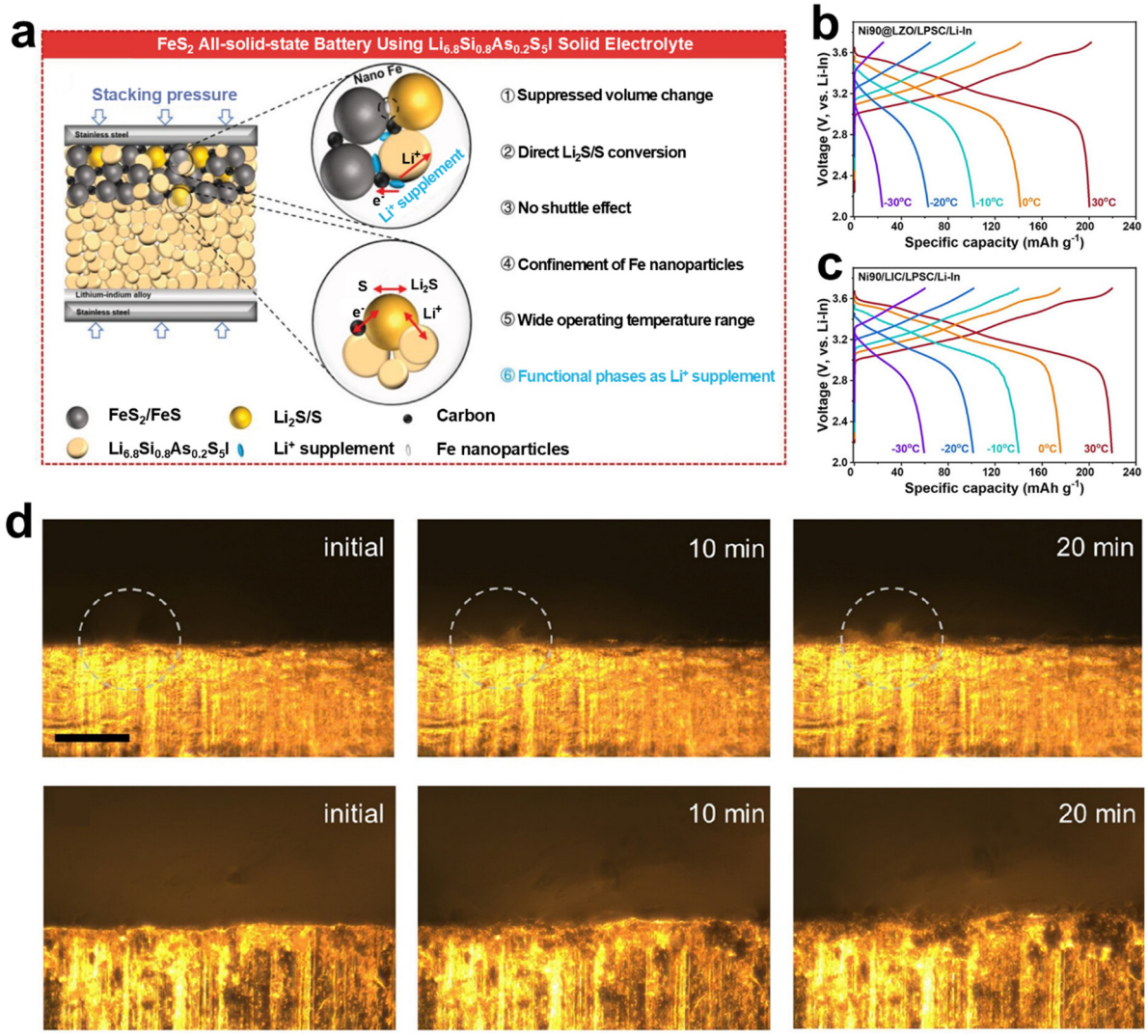

Figure 10. (**a**) The configuration of ASSB coupling with commercial FeS_2 cathode and the LASI-80Si SE that effectively overcomes the challenges encountered by FeS_2 in conventional LIBs. Reproduced from [207]. Copyright 2023 with permission from Wiley-VCH GmbH. The charge-discharge curves of the second cycle for (**b**) Li-In|LPSC|Ni90@LZO and (**c**) Li-In|LIC/LPSC|Ni90@LZO ASSBs within the temperature range of −30 to 30 °C. Reproduced from [209]. Copyright 2024 with permission from American Chemical Society. *In-situ* optical images of the electrodeposited Li on lithium metal of symmetric Li||Li cells assembled with (**d**) the n-GPE and the F-CGE-6 wt.% electrolytes at 1 mA cm^{-2}. Scale bar: 200 μm. Reproduced from [216]. Copyright 2024 with permission from American Chemical Society.

5. Advanced Characterization for Low-Temperature Electrolytes

Recent advances in electrolytes for LT LIBs have been primarily driven by an increasingly comprehensive understanding of solvation structures, electrochemical kinetics, and interfacial chemistry at EEIs [217,218]. These insights have been enabled by the rapid development of advanced characterization tools.

The solvation structure plays a pivotal role in determining key properties of LT electrolytes, including bulk ionic conductivity, ESW, and the desolvation energy barrier. Small angle X-ray scattering (SAXS), which is sensitive to clusters and networks formed in liquids, can provide insights into the mesoscopic properties of

electrolytes [219]. Spectroscopic characterizations such as conventional nuclear magnetic resonance (NMR), Fourier transform infrared (FTIR), and Raman spectroscopy are effective approaches to investigate the solvation structure of electrolytes [37,220]. In addition, polarized light microscopes can be employed to study the isotropy and anisotropy of the liquid before and after freezing by directly observing its morphology changes [221]. Importantly, Xu et al. [222] developed an *in-situ* liquid secondary ion mass spectrometry (Figure 11a) to investigate the anion-solvation interaction in weakly solvating bis(3-fluoropropyl)ether (BFPE)-based three 0.5 M electrolytes containing different anions ($TFSI^-$, FSI^-, and $FTFSI^-$) which showed similar dissociation energies towards Li^+. The depth profiles (Figure 11b) show the detection of $[BFPE\text{-}FTFSI]^-$, $[BFPE\text{-}FSI]^-$, and $[BFPE\text{-}TFSI]^-$ clusters after penetration the Si_3N_4 film at about 50 s, suggesting an association between the anion and BFPE solvent, and the strength of anion-solvation interaction follows the order of $[BFPE\text{-}FTFSI]^-$ > $[BFPE\text{-}FSI]^-$ > $[BFPE\text{-}TFSI]^-$. More importantly, the mass spectra collected at 100 s (Figure 11c) present the signals of $[BFPE\text{-}TFSI]^-$ ($m/z = 418$), $[BFPE\text{-}FSI]^-$ ($m/z = 318$), and $[BFPE\text{-}FTFSI]^-$ ($m/z = 468$), and the higher intensity of $[BFPE\text{-}FTFSI]^-$ further confirms stronger BFPE-$FTFSI^-$ interaction. Experimental results further demonstrate that the anion solvation, especially for asymmetric $FTFSI^-$ anion, effectively enhances the Li^+ transfer number, decreases the organic component in SEI, and accelerates the Li^+ desolvation kinetics, resulting in the highly improved Li plating/stripping CE at −30 °C.

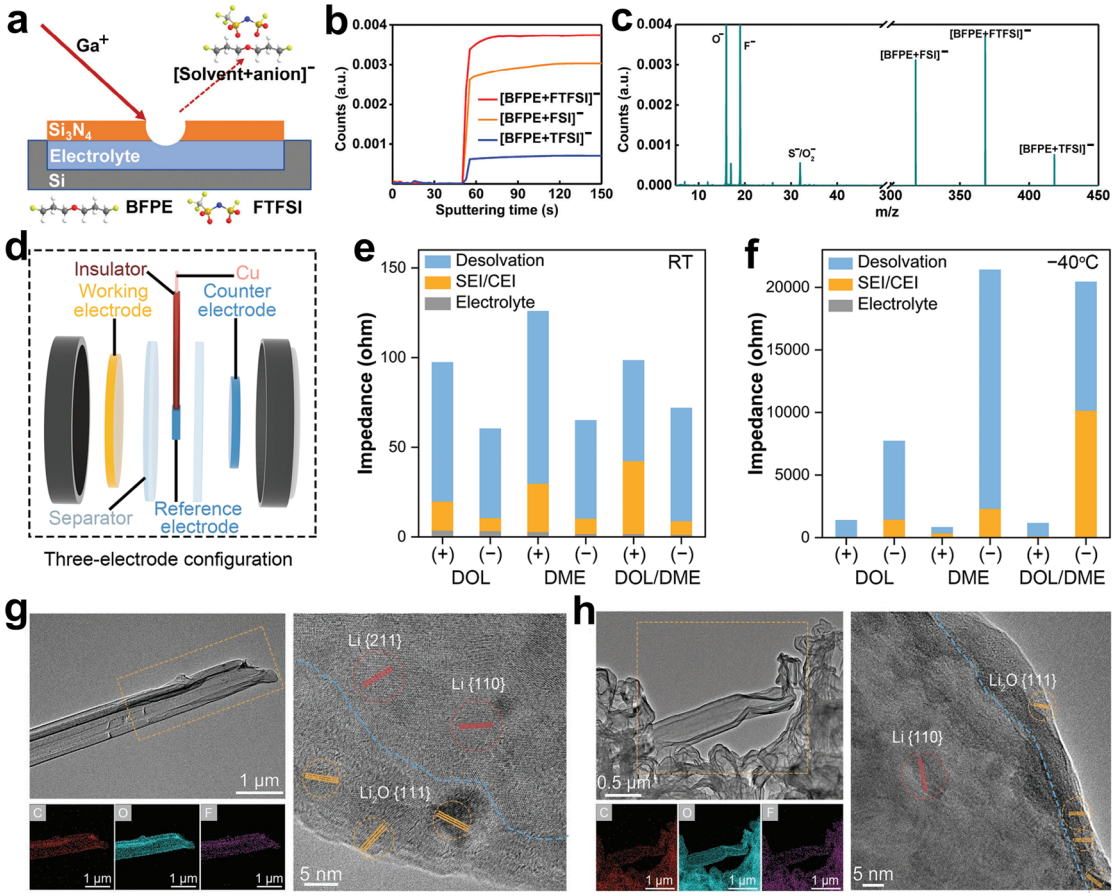

Figure 11. (**a**) Schematic setup of an *in-situ* liquid SIMS cell assembled by silicon support grids with silicon nitride membranes. (**b**) Depth profiles and (**c**) mass spectra of 0.5 M LiFSI+0.5 M LiFTFSI+0.5 M LiTFSI in BFPE electrolytes in the negative ion mode. Reproduced from [222]. Copyright 2024 with permission from Wiley-VCH GmbH. (**d**) Schematic model of the three-electrode cell for EIS measurement. (**e**,**f**) The impedance of desolvation, SEI/CEI, and electrolyte with respect to cathode and anode at the RT and −40 °C. Low- magnification and high-resolution cryo-TEM images of SEI derived from LiTFSI/DOL electrolyte at the (**g**) RT and (**h**) −40 °C. Reproduced from [223]. Copyright 2023 with permission from Wiley-VCH GmbH.

The reliable operation of LT LIBs is critically governed by the chemical composition and spatial structure of EEIs. The formation of stable, ion-conductive, and low-impedance EEIs is essential for achieving long-term cycling stability and maintaining high energy density of LT LIBs. Elucidating the interfacial chemistry through advanced characterization techniques, and establishing clear correlations between interfacial structure/composition and electrochemical performance at subzero temperatures, are of great importance for guiding the rational design of

interface chemistry that are inherently adaptive to subzero-temperature environments. Electrochemical measurements of LIBs are conventionally conducted using a two-electrode configuration, which yields only the overall electrochemical response of the coupled system. This configuration limits the capability to distinguish the individual behavior of the cathode and anode, hindering accurate assessment of their respective electrochemical properties. To address this limitation, three-electrode configurations incorporating the integrated reference electrode (RE) have been developed to facilitate the precise, independent evaluation of the kinetics and stability characteristics of each electrode during cycling. Moreover, the three-electrode setup plays a pivotal role in accurately determining the ESW of the electrolyte and in real-time monitoring of the voltage profiles of individual electrodes during battery operation at sub-zero temperatures. For instance, McDowell's group fabricated three-electrode coin cells consisting of alloy materials (antimony, silicon, and tin) as the working electrode (WE), Li metal as the counter electrode (CE), and a small piece of Li metal as the RE placed between the other electrodes to investigate the realistic electrochemical performance of the above alloy electrodes at temperatures down to –40 °C, owing to the large overpotentials originating from the Li counter electrode under such LT conditions [224]. In particular, three-electrode EIS has been increasingly employed to differentiate the respective contributions of the cathode and anode to the overall impedance increase, especially under LT conditions. Based on the three-electrode EIS measurement (Figure 11d), Zhang's team disclosed that the desolvation process dominates the total cell resistance under both the RT and −40 °C conditions, exceeding the impedance contributions from the SEI/CEI and bulk electrolytes (Figure 11e,f) [223]. At the RT, the cathode exhibits a higher resistance contribution than the anode. When the temperature turns to −40 °C, the cell resistance is primarily attributed to the anode, highlighting a temperature-dependent shift in the rate-limiting interfacial process. Among three ether-based electrolytes with the LiFSI concentration of 1 M, the DOL-based electrolyte enables the lowest value of anode impedance at −40 °C. Nevertheless, the practical application of three-electrode cell systems is still constrained by the challenges associated with constructing stable and durable RE for long-term cycling, and current relevant studies primarily utilize this configuration to monitor the evolution of electrodes during the initial cycles. Besides, the DRT-based timescale diagnosis provides a powerful characterization to decouple complicated kinetic processes in LT battery system [225].

Unlike X-ray photoelectron spectroscopy (XPS) and time-of-flight secondary ion mass spectrometry (TOF-SIMS), cryogenic transmission electron microscopy (cryo-TEM) enables non-destructive, atomic-resolution characterization of air- and electron-beam-sensitive interfacial films, allowing detailed visualization of the structure and composition of EEIs, which can provide valuable insights for the design of LT electrolytes. In Zhang's previous study [223], when the temperature decreased from RT to −40 °C, Li deposits in the LiFSI-DOL electrolyte exhibited a pronounced transition to wizened and thinner dendritic morphologies, accompanied by a significant decrease in SEI thickness and a substantial decline in the polymer matrix content (Figure 11g,h). Nevertheless, three ether-based electrolytes produce similar SEI, indicating comparable Li^+ transport kinetics across the SEI. It can be summarized that the differences in LT Li-metal battery performance primarily arise from variations in the desolvation process rather than Li deposition morphology or SEI properties. As a result, the full cell composed of the high-loading NCM523 (3.2 mAh cm^{-2}) cathode and limited Li anode (50 μm, ≈10 mAh cm^{-2}) retain 66% of the room-temperature capacity at −40 °C. Besides, operando NMR spectroscopy and fluorescence probe have been developed to visually and even semi-quantitatively detect metallic lithium deposition at LT and fast-charging conditions [226,227].

6. Conclusions and Perspectives

In recent years, substantial progress has been achieved in the development of LIBs capable of stable operation at subzero temperatures through advanced electrolyte engineering. Extensive experimental and theoretical studies have demonstrated that LT performance degradation originates from the coupled mismatch among solvation structures, interfacial chemistry, and ion-transport dynamics under cold conditions. A deeper mechanistic understanding of temperature-dependent solvation configurations, interphase formation, and transport-reaction coupling is driving the transition from empirical optimization toward mechanism-guided electrolyte design. This review systematically analyzes the critical bottlenecks of LIBs at subzero temperatures and comprehensively summarizes electrolyte regulation strategies, including aqueous electrolytes, organic electrolytes, ionic liquid-based electrolytes, and solid electrolytes, reflecting the emerging trend of multidimensional and synergistic design.

The low-temperature performance of LIBs is governed by the interplay among solvation thermodynamics, desolvation kinetics, interfacial reaction pathways, ion migration mechanisms, and the mechanical stability of EEIs. As temperature decreases, electrolyte viscosity increases and ionic conductivity declines, while ion association is enhanced, leading to a higher fraction of CIPs and AGGs in the solvation structure and a reduced population of

effective charge carriers. Meanwhile, desolvation at the Helmholtz plane becomes sluggish, increasing charge-transfer resistance. If the SEI and CEI are mechanically fragile or structurally inhomogeneous, thermal contraction during cooling may induce cracking, which further deteriorates interfacial stability. Therefore, rational low-temperature design requires simultaneous regulation of solvation chemistry and interphase architecture.

Solvation-structure engineering has emerged as a central strategy for enhancing LT performance. By judiciously selecting low-freezing-point solvents, such as ethers, selected nitriles, or branched carbonates, in combination with weakly coordinating or charge-delocalized anions and functionally targeted additives, the coordination environment within the primary solvation shell can be tuned to lower desolvation energy barriers and promote the formation of inorganic-rich, robust interphases. However, practical systems inevitably involve multi-objective trade-offs. Increased anion participation in the solvation sheath may facilitate stable interphase formation but can also elevate viscosity or narrow the oxidative stability window. Highly fluorinated solvents often improve interfacial robustness but raise cost and environmental concerns. Thus, next-generation cold-resistant electrolytes should achieve holistic optimization across solvation strength, ionic transport kinetics, electrochemical stability, safety, and sustainability.

Several electrolyte design principles are increasingly shaping the field. First, constructing a "weakly coordinated yet structurally defined" solvation environment has become a key direction. The synergistic combination of moderately donating solvents with charge-delocalized anions can reduce desolvation barriers while preserving low-temperature fluidity. In LHCE systems, it is essential to maintain localized high-concentration solvation structures without excessive ion clustering that would impede ionic transport, while also carefully controlling diluent content, volatility, and environmental impact. Second, interphase engineering is shifting toward functionally graded architectures. Bilayer or gradient EEI structures, comprising an outer dense inorganic layer (e.g., LiF- or Li_2O-rich) for enhanced antifreeze and reduced resistance, and an inner organic or ionomeric layer for mechanical compliance, can accommodate thermal stress and sustain continuous ion-conduction pathways during cooling and rewarming. Third, cooperative additives, such as nitrate-, borate-, or halide-containing species, can direct preferential reductive or oxidative decomposition to construct inorganic-dominated interphases while suppressing solvent-derived side reactions. When integrated with artificial interphase fabrication techniques, such as molecular layer deposition and plasma-assisted surface modification, these strategies offer a pathway toward more predictable and tunable interfacial chemistry across wide temperature ranges.

Despite these advances, mechanistic understanding under subzero conditions remains constrained by methodological limitations. Solvation rearrangement and interphase evolution at low temperatures involve strongly coupled temporal and spatial scales, which are difficult to capture simultaneously with conventional characterization tools. Although theoretical simulations provide molecular-level insights, they rely on approximate force fields and limited sampling, and often struggle to reproduce non-equilibrium electrochemical processes under realistic conditions. The development of high-resolution operando cryogenic characterization techniques, together with multiscale modeling frameworks that integrate first-principles calculations and machine learning (ML)-based interatomic potentials, will be crucial for enabling predictive electrolyte design. Data-driven approaches are also accelerating electrolyte discovery. By constructing databases that incorporate solvent descriptors, solvation energies, transport coefficients, and interphase compositions, ML models can identify promising electrolyte formulations under multi-objective constraints. A closed-loop optimization framework that integrates computational screening, automated synthesis, and operando cryogenic diagnostics has the potential to substantially shorten development cycles and enhance design efficiency for LT electrolytes.

From an engineering perspective, many low-temperature electrolyte systems demonstrate outstanding performance in coin cells, yet their scalability and manufacturability remain critical challenges. Highly fluorinated systems incur high cost, and LHCEs require stringent control over composition and moisture, complicating large-scale production. Therefore, future studies should prioritize validation in pouch cells and large-format prototypes under application-relevant conditions, including controlled cooling rates, stack pressure, and long-term cycling in dynamic thermal environments, to evaluate interfacial stability and safety risks. Moreover, co-designing electrolyte chemistry with thermal management strategies, such as self-heating architectures, interfacial coatings, and optimized current collectors, will be essential to mitigate lithium plating and dendrite growth exacerbated by sluggish desolvation kinetics at low temperatures. Establishing standardized testing protocols for subzero operation is equally important. Systematic reporting of ionic conductivity $\sigma(T)$, viscosity with Vogel-Fulcher-Tammann (VFT) fitting parameters, cation transference numbers, interfacial charge-transfer resistance, and activation energies will enable meaningful cross-comparison among systems. In addition, CE for lithium plating/stripping at low temperatures, impedance evolution during cooling and rewarming, and post-mortem analysis of deposition morphology following standardized LT pulse protocols should become routine metrics.

Cross-chemistry benchmarking using identical electrode configurations and cell formats will facilitate the extraction of universal design principles.

Looking forward, the design of low-temperature electrolytes is expected to evolve toward a more predictive, sustainable, and application-oriented paradigm. Key future directions include: (i) the development of fluorine-lean or fluorine-free electrolyte systems to balance interfacial stability with cost and environmental considerations; (ii) precise solvation-structure manipulation through coordinated ion-solvent-additive design to achieve decoupled optimization of ionic transport and interphase formation; (iii) the exploration of emerging electrolyte systems, such as deep eutectic and high-entropy electrolytes, for enhanced adaptability under extreme temperature conditions; and (iv) the establishment of data-driven design frameworks that integrate machine learning with high-throughput experiments and operando characterization. Together, these strategies are expected to accelerate the transition from trial-and-error discovery to rational electrolyte engineering, ultimately enabling robust LIB operation across wide temperature ranges.

In summary, the realization of safe, durable, and sustainable subzero LIBs requires a system-level strategy that treats solvation chemistry and interfacial evolution as dynamically coupled, temperature-dependent processes. Supported by advanced operando characterization, multiscale theoretical modeling, and AI-assisted materials discovery, future research is poised to deliver fluorine-lean, manufacturable electrolyte systems that simultaneously achieve high ionic conductivity, robust interphase stability, and environmental compatibility. Such advances will expand the operational envelope of LIBs in extreme climates and enable more resilient and versatile energy storage technologies.

Funding

This work received financial support from Natural Science Foundation of Zhejiang Province (LD25B060001), Open Project of the State Key Laboratory of Environment-Friendly Energy Materials (23kfhg09), Key Laboratory Open Fund Project of Jiangxi Province for Persistent Pollutants Control and Resources Recycle (ES202480187), the Fundamental Research Funds for the Provincial Universities of Zhejiang (2024YW103), and the College Students Innovation and Entrepreneurship Training Program in Zhejiang Province (S202510356045).

Conflicts of Interest

The authors declare no conflict of interest.

Use of AI and AI-Assisted Technologies

No AI tools were utilized for this paper.

References

1. Nagasubramanian, G. Electrical characteristics of 18650 Li-ion cells at low temperatures. *J. Appl. Electrochem.* **2001**, *31*, 99–104.
2. Smart, M.C.; Ratnakumar, B.V.; Chin, K.B.; et al. Lithium-ion electrolytes containing ester cosolvents for improved low temperature performance. *J. Electrochem. Soc.* **2010**, *157*, A1361–A1374.
3. Zhang, S.; Xu, K.; Jow, T.R. A new approach toward improved low temperature performance of Li-ion battery. *Electrochem. Commun.* **2002**, *4*, 928–932.
4. Li, Y.; Wong, K.; Dou, Q.; et al. Improvement of lithium-ion battery performance at low temperature by adopting ionic liquid-decorated PMMA nanoparticles as electrolyte component. *ACS Appl. Energy Mater.* **2018**, *1*, 2664–2670.
5. Zhao, Y.; Hu, Z.; Zhao, Z.; et al. Strong solvent and dual lithium salts enable fast-charging lithium-ion batteries operating from −78 to 60 °C. *J. Am. Chem. Soc.* **2023**, *145*, 22184–22193.
6. Liu, B.; Li, B.; Guan, S. Effect of fluoroethylene carbonate additive on low temperature performance of Li-ion batteries. *Electrochem. Solid-State Lett.* **2012**, *15*, A77–A79.
7. Fan, X.; Ji, X.; Chen, L.; et al. All-temperature batteries enabled by fluorinated electrolytes with non-polar solvents. *Nat. Energy* **2019**, *4*, 882–890.
8. Ramanujapuram, A.; Yushin, G. Understanding the exceptional performance of lithium-ion battery cathodes in aqueous electrolytes at subzero temperatures. *Adv. Energy Mater.* **2018**, *8*, 1802624.
9. Lin, Z.; Liu, J. Low-temperature all-solid-state lithium-ion batteries based on a di-cross-linked starch solid electrolyte. *RSC Adv.* **2019**, *9*, 34601–34606.
10. Qin, M.; Zeng, Z.; Wu, Q.; et al. Microsolvating competition in Li^+ solvation structure affording PC-based electrolyte with fast kinetics for lithium-ion batteries. *Adv. Funct. Mater.* **2024**, *34*, 2406357.

11. Lu, W.; Xie, K.; Pan, Y.; et al. Effects of carbon-chain length of trifluoroacetate co-solvents for lithium-ion battery electrolytes using at low temperature. *J. Fluorine Chem.* **2013**, *156*, 136–143.
12. Ein-Eli, Y.; Thomas, S.R.; Chadha, R.; et al. Li-ion battery electrolyte formulated for low-temperature applications. *J. Electrochem. Soc.* **1997**, *144*, 823.
13. Abraham, K.M.; Goldman, J.L. The use of the reactive ether, Tetrahydrofuran (THF), in rechargeable lithium cells. *J. Power Sources* **1983**, *9*, 239–245.
14. Smart, M.C.; Ratnakumar, B.V.; Whitcanack, L.D.; et al. Improved low-temperature performance of lithium-ion cells with quaternary carbonate-based electrolytes. *J. Power Sources* **2003**, *119–121*, 349–358.
15. Zhou, L.; Xu, M.; Lucht, B.L. Performance of lithium tetrafluorooxalatophosphate in methyl butyrate electrolytes. *J. Appl. Electrochem.* **2013**, *43*, 497–505.
16. Yang, C.; Ren, Y.; Wu, B.; et al. Formulation of a new type of electrolytes for $LiNi_{1/3}Co_{1/3}Mn_{1/3}O_2$ cathodes working in an ultra-low temperature range. *Adv. Mat. Res.* **2012**, *455–456*, 258–264.
17. Mikhaylik, Y.V.; Akridge, J.R. Low temperature performance of Li/S batteries. *J. Electrochem. Soc.* **2003**, *150*, A306–A311.
18. Zhang, S.; Xu, K.; Jow, T.R. The low temperature performance of Li-ion batteries. *J. Power Sources* **2003**, *115*, 137–140.
19. Chandrasekaran, R.; Koh, M.; Ozhawa, Y.; et al. Electrochemical cell studies on fluorinated natural graphite in propylene carbonate electrolyte with difluoromethyl acetate (MFA) additive for low temperature lithium battery application. *J. Chem. Sci.* **2009**, *121*, 339–346.
20. Smart, M.C.; Ratnakumar, B.V.; Surampudi, S. Electrolytes for low-temperature lithium batteries based on ternary mixtures of aliphatic carbonates. *J. Electrochem. Soc.* **1999**, *146*, 486–492.
21. Suo, L.; Han, F.; Fan, X.; et al. "Water-in-Salt" electrolytes enable green and safe Li-ion batteries for large scale electric energy storage applications. *J. Mater. Chem. A* **2016**, *4*, 6639–6644.
22. Rustomji, C.S.; Yang, Y.; Kim, T.K.; et al. Liquefied gas electrolytes for electrochemical energy storage devices. *Science* **2017**, *356*, eaal4263.
23. Holoubek, J.; Liu, H.; Wu, Z.; et al. Tailoring electrolyte solvation for Li metal batteries cycled at ultra-low temperature. *Nat. Energy* **2021**, *6*, 303–313.
24. Yue, J.; Zhang, J.; Tong, Y.; et al. Aqueous interphase formed by CO_2 brings electrolytes back to salt-in-water regime. *Nat. Chem.* **2021**, *13*, 1061–1069.
25. Xu, J.; Zhang, J.; Pollard, T.P.; et al. Electrolyte design for Li-ion batteries under extreme operating conditions. *Nature* **2023**, *614*, 694–700.
26. Lu, D.; Li, R.; Rahman, M.M.; et al. Ligand-channel-enabled ultrafast Li-ion conduction. *Nature* **2024**, *627*, 101–107.
27. Yang, J.; Wang, S.; Song, S.; et al. Cyclable micron-sized silicon-based lithium-ion batteries at −40 °C enabled by temperature-dependent solvation regulation. *Adv. Mater.* **2025**, *37*, 2501807.
28. Kunze, M.; Jeong, S.; Appetecchi, G.B.; et al. Mixtures of ionic liquids for low temperature electrolytes. *Electrochim. Acta* **2012**, *82*, 69–74.
29. Wang, X.; Yang, L.; Ahmad, N.; et al. Colloid electrolyte with changed Li^+ solvation structure for high-power, low-temperature lithium-ion batteries. *Adv. Mater.* **2023**, *35*, 2209140.
30. Landesfeind, J.; Gasteiger, H.A. Temperature and concentration dependence of the ionic transport properties of lithium-ion battery electrolytes. *J. Electrochem. Soc.* **2019**, *166*, A3079–A3097.
31. Zhang, W.; Lu, Y.; Wan, L.; et al. Engineering a passivating electric double layer for high performance lithium metal batteries. *Nat. Commun.* **2022**, *13*, 2029.
32. Wang, H.; Yu, D.; Kuang, C.; et al. Alkali metal anodes for rechargeable batteries. *Chem* **2019**, *5*, 313–338.
33. Thenuwara, A.C.; Shetty, P.P.; McDowell, M.T. Distinct nanoscale interphases and morphology of lithium metal electrodes operating at low temperatures. *Nano Lett.* **2019**, *19*, 8664–8672.
34. Yu, D.; Zhu, Q.; Cheng, L.; et al. Anion solvation regulation enables long cycle stability of graphite cathodes. *ACS Energy Lett.* **2021**, *6*, 949–958.
35. Li, Z.; Yao, N.; Yu, L.; et al. Inhibiting gas generation to achieve ultralong-lifespan lithium-ion batteries at low temperatures. *Matter* **2023**, *6*, 2274–2292.
36. Liao, B.; Li, H.; Xu, M.; et al. Designing low impedance interface films simultaneously on anode and cathode for high energy batteries. *Adv. Energy Mater.* **2018**, *8*, 1800802.
37. Mo, Y.; Liu, G.; Yin, Y.; et al. Fluorinated solvent molecule tuning enables fast-charging and low-temperature lithium-ion batteries. *Adv. Energy Mater.* **2023**, *13*, 2301285.
38. Zhang, S.; Xu, K.; Jow, T.R. Electrochemical impedance study on the low temperature of Li-ion batteries. *Electrochim. Acta* **2004**, *49*, 1057–1061.
39. Abe, T.; Fukuda, H.; Iriyama, Y.; et al. Solvated Li-ion transfer at interface between graphite and electrolyte. *J. Electrochem. Soc.* **2004**, *151*, A1120–A1123.
40. Abraham, D.P.; Heaton, J.R.; Kang, S.-H.; et al. Investigating the low-temperature impedance increase of lithium-ion

cells. *J. Electrochem. Soc.* **2008**, *155*, A41–A47.
41. Xu, K.; Cresce, A.V.; Lee, U. Differentiating contributions to "Ion Transfer" barrier from interphasial resistance and Li^+ desolvation at electrolyte/graphite interface. *Langmuir* **2010**, *26*, 11538–11543.
42. Li, J.; Yuan, C.; Guo, Z.; et al. Limiting factors for low-temperature performance of electrolytes in $LiFePO_4$/Li and graphite/Li half cells. *Electrochim. Acta* **2012**, *59*, 69–74.
43. Li, Q.; Lu, D.; Zheng, J.; et al. Li^+-desolvation dictating lithium-ion Battery's low-temperature performances. *ACS Appl. Mater. Interfaces* **2017**, *9*, 42761–42768.
44. Yao, Y.-X.; Yao, N.; Zhou, X.-R.; et al. Ethylene-carbonate-free electrolytes for rechargeable Li-ion pouch cells at sub-freezing temperatures. *Adv. Mater.* **2022**, *34*, 2206448.
45. Zhu, Q.; Cheng, L.; Sun, X.; et al. LiC_6@Li as a promising substitution of Li metal counter electrode for low-temperature battery evaluation. *Adv. Mater.* **2025**, *37*, 2419041.
46. Zhang, G.; Wei, X.; Han, G.; et al. Lithium plating on the anode for lithium-ion batteries during long-term low temperature cycling. *J. Power Sources*, **2021**, *484*, 229312.
47. Wang, C.; Xie, Y.; Huang, Y.; et al. Li_3PO_4-enriched SEI on graphite anode boosts Li^+ de-solvation enabling fast-charging and low-temperature lithium-ion batteries. *Angew. Chem. Int. Ed.* **2024**, *63*, e202402301.
48. Zhang, H.; Wu, X.; Kong, W.; et al. Tailoring electrolyte solvation of dimethyl sulfite with fluoride dominant via electrolyte engineering for enabling low-temperature batteries. *Energy Storage Mater.* **2025**, *74*, 103955.
49. Hu, H.; Li, J.; Zhang, Q.; et al. Non-concentrated electrolyte with weak anion coordination enables low Li-ion desolvation energy for low-temperature lithium batteries. *Chem. Eng. J.* **2023**, *457*, 141273.
50. Qin, N.; Chen, J.; Lu, Y.; et al. Trace $LiBF_4$ enabling robust LiF-rich interphase for durable low-temperature lithium-ion pouch cells. *ACS Energy Lett.* **2024**, *9*, 4843–4851.
51. Luo, L.; Chen, K.; Chen, H.; et al. Enabling ultralow-temperature (−70 °C) lithium-ion batteries: Advanced electrolytes utilizing weak-solvation and low-viscosity nitrile cosolvent. *Adv. Mater.* **2023**, *36*, 2308881.
52. Wang, C.; Zhou, S.; Xu, Z.; et al. A weakly-solvating propylene carbonate electrolyte for high-voltage and low-temperature lithium-ion batteries. *Angew. Chem. Int. Ed.* **2025**, *137*, e202510351.
53. Wang, Z.; Han, R.; Huang, D.; et al. Co-intercalation-free ether-based weakly solvating electrolytes enable fast-charging and wide-temperature lithium-ion batteries. *ACS Nano* **2023**, *17*, 18103–18113.
54. Ma, T.; Ni, Y.; Wang, Q.; et al. Optimize lithium deposition at low temperature by weakly solvating power solvent. *Angew. Chem. Int. Ed.* **2022**, *61*, e202207927.
55. Yin, Y.; Zheng, T.; Chen, J.; et al. Uncovering the function of a five-membered heterocyclic solvent-based electrolyte for graphite anode at subzero temperature. *Adv. Funct. Mater.* **2023**, *33*, 2215151.
56. Zhang, W.; Jiang, G.; Zou, W.; et al. A microscopically heterogeneous colloid electrolyte of covalent organic nanosheets for ultrahigh-voltage and low-temperature lithium metal batteries. *Energy Environ. Sci.* **2024**, *17*, 2642–2650.
57. Cai, G.; Yin, Y.; Xia, D.; et al. Sub-nanometer confinement enables facile condensation of gas electrolyte for low-temperature batteries. *Nat. Commun.* **2021**, *12*, 3395.
58. Li, N.; Gao, K.; Fan, K.; et al. Customization nanoscale interfacial solvation structure for low-temperature lithium metal batteries. *Energy Environ. Sci.* **2024**, *17*, 5468–5479.
59. Yang, Y.; Li, Z.; Yang, Z.; et al. Ultrafast lithium-ion transport engineered by nanoconfinement effect. *Adv. Mater.* **2025**, *37*, 2416266.
60. Shi, S.; Lu, P.; Liu, Z.; et al. Direct calculation of Li-ion transport in the solid electrolyte interphase. *J. Am. Chem. Soc.* **2012**, *134*, 15476–15487.
61. Ramasubramanian, A.; Yurkiv, V.; Foroozan, T.; et al. Lithium diffusion mechanism through solid-electrolyte interphase in rechargeable lithium batteries. *J. Phys. Chem. C* **2019**, *123*, 10237–10245.
62. Zhang, Q.; Pan, J.; Lu, P.; et al. Synergetic effects of inorganic components in solid electrolyte interphase on high cycle efficiency of lithium ion batteries. *Nano Lett.* **2016**, *16*, 2011–2016.
63. Sun, S.-Y.; Zhang, X.-Q.; Wang, Y.-N.; et al. Understanding the transport mechanism of lithium ions in solid-electrolyte interphase in lithium metal batteries with liquid electrolytes. *Mater. Today* **2024**, *77*, 39–65.
64. Yin, X.; Li, B.; Liu, H.; et al. Solvent-derived organic-rich SEI enables capacity enhancement for low-temperature lithium metal batteries. *Joule* **2025**, *9*, 101823.
65. Xu, H.; Hu, R.; Yan, H.; et al. Solvation structure-tunable phase change electrolyte for stable lithium metal batteries. *ACS Energy Lett.* **2022**, *7*, 3761–3769.
66. Mo, Y.; Liu, G.; Chen, J.; et al. Unraveling the temperature-responsive solvation structure and interfacial chemistry for graphite anodes. *Energy Environ. Sci.* **2024**, *17*, 227–237.
67. Wang, Y.; Yang, H.; Hu, T.; et al. Designing electrolytes by thermodynamics. *Natl. Sci. Rev.* **2025**, *12*, nwaf100.
68. Wang, Q.; Zhao, C.; Yao, Z.; et al. Entropy-driven liquid electrolytes for lithium batteries. *Adv. Mater.* **2023**, *35*, 2210677.
69. Ye, G.; Zhu, L.; Ma, Y.; et al. Molecular design of solid polymer electrolytes with enthalpy−entropy manipulation for Li

metal batteries with aggressive cathode chemistry. *J. Am. Chem. Soc.* **2024**, *146*, 27668–27678.
70. Ren, K.-F.; Du, Y.-F.; Guo, J.-X.; et al. Gibbs free energy regulation to decrease desolvation barrier for ultralow-temperature lithium metal batteries at −40 °C. *Small* **2025**, *21*, 2505027.
71. Zhang, W.; Xia, H.; Zhu, Z.; et al. Decimal solvent-based high-entropy electrolyte enabling the extended survival temperature of lithium-ion batteries to −130 °C. *CCS Chemistry* **2021**, *3*, 1245–1255.
72. Kim, S.C.; Wang, J.; Xu, R.; et al. High-entropy electrolytes for practical lithium metal batteries. *Nat. Energy* **2023**, *8*, 814–826.
73. Qu, Z.; Xue, P.; Hu, X.; et al. Strongly and weakly solvating solvents co-coordinated electrolyte for stable lithium metal batteries. *ACS Energy Lett.* **2025**, *10*, 2913–2923.
74. Suo, L.; Oh, D.; Lin, Y.; et al. How solid-electrolyte interphase forms in aqueous electrolytes. *J. Am. Chem. Soc.* **2017**, *139*, 18670–18680.
75. Zheng, J.; Tan, G.; Shan, P.; et al. Understanding thermodynamic and kinetic contributions in expanding the stability window of aqueous electrolytes. *Chem* **2018**, *4*, 2872–2882.
76. Dubouis, N.; Lemaire, P.; Mirvaux, B.; et al. The role of the hydrogen evolution reaction in the solid–electrolyte interphase formation mechanism for ''Water-in-Salt'' electrolytes. *Energy Environ. Sci.* **2018**, *11*, 3491–3499.
77. Suo, L.; Borodin, O.; Gao, T.; et al. "Water-in-salt" electrolyte enables high-voltage aqueous lithium-ion chemistries. *Science* **2015**, *350*, 938–943.
78. Wang, H.; Zhang, H.; Cheng, Y.; et al. All-NASICON LVP-LTP aqueous lithium ion battery with excellent stability and low-temperature performance. *Electrochim. Acta* **2018**, *278*, 279–289.
79. Shang, Y.; Chen, N.; Li, Y.; et al. Tiny-Ligand Solvation Electrolyte Enabled Fast-Charging Aqueous Batteries. *Angew. Chem. Int. Ed.* **2025**, *137*, e202423808.
80. Shang, Y.; Chen, S.; Chen, N.; et al. A universal strategy for high-voltage aqueous batteries via lone pair electrons as hydrogen bond-breaker. *Energy Environ. Sci.* **2022**, *15*, 2653–2663.
81. Ma, Z.; Xie, Z.; Liu, J.; et al. Distinct roles: Co-solvent and additive synergy for expansive electrochemical range and low-temperature aqueous batteries. *Energy Storage Mater.* **2024**, *66*, 103203.
82. Shang, Y.; Chen, N.; Li, Y.; et al. Decoding the entropy-performance relationship in aqueous electrolytes for lithium-ion batteries. *Adv. Energy Mater.* **2025**, *15*, 2406118.
83. Kim, H.-I.; Shin, E.; Kim, S.-H.; et al. Aqueous eutectic lithium-ion electrolytes for wide-temperature operation. *Energy Storage Mater.* **2021**, *36*, 222–228.
84. Jiang, L.; Hu, Y.-C.; Ai, F.; et al. Rational design of anti-freezing electrolyte concentrations via freeze concentration process. *Energy Environ. Sci.* **2024**, *17*, 2815–2824.
85. Li, X.; Li, M.; Liu, Y.; et al. Fast interfacial defluorination kinetics enables stable cycling of low-temperature lithium metal batteries. *J. Am. Chem. Soc.* **2024**, *146*, 17023–17031.
86. Piao, N.; Wang, J.; Gao, X.; et al. Designing temperature-insensitive solvated electrolytes for low-temperature lithium metal batteries. *J. Am. Chem. Soc.* **2024**, *146*, 18281–18291.
87. Lin, Y.; Yang, Z.; Zhang, X.; et al. Activating ultra-low temperature Li-metal batteries by tetrahydrofuran-based localized saturated electrolyte. *Energy Storage Mater.* **2023**, *58*, 184–194.
88. Gu, R.; Zhang, D.; Zhu, S.; et al. An ether-based electrolyte solvation strategy for long-term stability and ultra-low temperature Li-metal batteries. *Adv. Funct. Mater.* **2024**, *34*, 2310747.
89. Ren, X.; Zhang, X.; Shadike, Z.; et al. Designing advanced in situ electrode/electrolyte interphases for wide temperature operation of 4.5 V Li||$LiCoO_2$ batteries. *Adv. Mater.* **2020**, *32*, 2004898.
90. Xu, R.; Zhang, S.; Shen, X.; et al. Unlocking the polarization and reversibility limitations for stable low-temperature lithium metal anodes. *Small Struct.* **2023**, *4*, 2200400.
91. Zhang, X.; Zou, L.; Xu, Y.; et al. Advanced electrolytes for fast-charging high-voltage lithium-ion batteries in wide-temperature range. *Adv. Energy Mater.* **2020**, *10*, 2000368.
92. Yoon, S.G.; Cavallaro, K.A.; Park, B.J.; et al. Controlling solvation and solid-electrolyte interphase formation to enhance lithium interfacial kinetics at low temperatures. *Adv. Funct. Mater.* **2023**, *33*, 2302778.
93. Zhang, J.; Zhang, H.; Deng, L.; et al. An additive-enabled ether-based electrolyte to realize stable cycling of high-voltage anode-free lithium metal batteries. *Energy Storage Mater.* **2023**, *54*, 450–460.
94. Lai, P.; Zhang, Y.; Huang, B.; et al. Revealing the evolution of solvation structure in low-temperature electrolytes for lithium batteries. *Energy Storage Mater.* **2024**, *67*, 103314.
95. Holoubek, J.; Kim, K.; Yin, Y.; et al. Electrolyte design implications of ion-pairing in low-temperature Li metal batteries. *Energy Environ. Sci.* **2022**, *15*, 1647–1658.
96. Zheng, X.; Cao, Z.; Luo, W.; et al. Solvation and interfacial engineering enable −40 °C operation of Graphite/NCM batteries at energy density over 270 Wh kg^{-1}. *Adv. Mater.* **2023**, *35*, 2210115.
97. Fu, H.; Ye, X.; Zhang, Y.; et al. Toward ultralow temperature lithium metal batteries: Advancing the feasibility of 1,3-

dioxolane based localized high-concentration electrolytes via lithium nitrate. *Adv. Energy Mater.* **2024**, *14*, 2401961.
98. Sun, N.; Li, R.; Zhao, Y.; et al. Anionic coordination manipulation of multilayer solvation structure electrolyte for high-rate and low-temperature lithium metal battery. *Adv. Energy Mater.* **2022**, *12*, 2200621.
99. Shi, J.; Xu, C.; Lai, J.; et al. An amphiphilic molecule-regulated core-shell-solvation electrolyte for Li-metal batteries at ultra-low temperature. *Angew. Chem.* **2023**, *135*, e202218151.
100. Zhao, Z.; Wang, A.; Chen, A.; et al. Leveraging ion pairing and transport in localized high-concentration electrolytes for reversible lithium metal anodes at low temperatures. *Angew. Chem. Int. Ed.* **2024**, *63*, e202412239.
101. Holoubek, J.; Yu, K.; Wu, J.; et al. Toward a quantitative interfacial description of solvation for Li metal battery operation under extreme conditions. *Proc. Nat. Acad. Sci. USA* **2023**, *120*, e2310714120.
102. Wu, J.; Li, M.; Ma, L.; et al. Engineering densely packed ion-cluster electrolytes for wide-temperature lithium-sulfurized polyacrylonitrile batteries. *ACS Nano* **2024**, *18*, 32984–32994.
103. Cui, Z.; Wang, D.; Guo, J.; et al. Push-pull electrolyte design strategy enables high-voltage low-temperature lithium metal batteries. *J. Am. Chem. Soc.* **2024**, *146*, 27644–27654.
104. Liu, L.; Shadike, Z.; Cai, X.; et al. Regulating the solvation structure of an acetonitrile-based electrolyte for Li/NMC811 batteries cycled at low temperature. *J. Mater. Chem. A* **2024**, *12*, 6947–6954.
105. Feng, T.; Yang, G.; Zhang, S.; et al. Low-temperature and high-voltage lithium-ion battery enabled by localized high-concentration carboxylate electrolytes. *Chem. Eng. J.* **2022**, *433*, 134138.
106. Jiang, Z.; Zeng, Z.; Liang, X.; et al. Fluorobenzene, a low-density, economical, and bifunctional hydrocarbon cosolvent for practical lithium metal batteries. *Adv. Funct. Mater.* **2020**, *31*, 2005991.
107. Liu, C.; Li, Z.; Jiang, L.; et al. Dipole-dipole interactions in electrolyte to facilitate Li-ion desolvation for low-temperature Li-ion batteries. *J. Energy Chem.* **2025**, *104*, 678–686.
108. Jiang, Z.; Zeng, Z.; Zhai, B.; et al. Fluorobenzene-based diluted highly concentrated carbonate electrolyte for practical high-voltage lithium metal batteries. *J. Power Sources* **2021**, *506*, 230086.
109. Lei, S.; Zeng, Z.; Yan, H.; et al. Nonpolar cosolvent driving LUMO energy evolution of methyl acetate electrolyte to afford lithium-ion batteries operating at −60 °C. *Adv. Funct. Mater.* **2023**, *33*, 2301028.
110. Huang, A.; Ma, Z.; Kumar, P.; et al. Low-temperature and fast-charging lithium metal batteries enabled by solvent-solvent interaction mediated electrolyte. *Nano Lett.* **2024**, *24*, 7499–7507.
111. He, R.; Zhang, Q.; Hu, Y.; et al. Partially sacrificial hybrid diluent regulated electrolytes boosting wide-temperature Li metal batteries. *Energy Storage Mater.* **2024**, *73*, 103836.
112. Dong, L.; Luo, D.; Zhang, B.; et al. All-fluorinated electrolyte engineering enables practical wide-temperature-range lithium metal batteries. *ACS Nano* **2024**, *18*, 18729–18742.
113. Lei, S.; Zeng, Z.; Liu, M.; et al. Nonflammable cosolvent enables methyl acetate-based electrolyte for 4.6 V-class lithium-ion batteries operating at −60 °C. *Chem. Eng. J.* **2023**, *478*, 147180.
114. Qin, M.; Liu, M.; Zeng, Z.; et al. Rejuvenating propylene carbonate-based electrolyte through nonsolvating interactions for wide-temperature Li-ions batteries. *Adv. Energy Mater.* **2022**, *12*, 2201801.
115. Yi, X.; Fu, H.; Rao, A.M.; et al. Safe electrolyte for long-cycling alkali-ion batteries. *Nat. Sustain.* **2024**, *7*, 326–337.
116. Dong, X.; Lin, Y.; Li, P.; et al. High-Energy Rechargeable Metallic Lithium Battery at –70 °C Enabled by a Cosolvent Electrolyte. *Angew. Chem. Int. Ed.* **2019**, *58*, 5623–5627.
117. Lai, P.; Huang, B.; Deng, X.; et al. A localized high concentration carboxylic ester-based electrolyte for high-voltage and low temperature lithium batteries. *Chem. Eng. J.* **2023**, *461*, 141904.
118. He, S.; Liu, S.; Cai, S.; et al. The high-fluorinated bi-molecular combination enables high-energy lithium batteries under challenging environment. *Chem. Eng. J.* **2024**, *493*, 152640.
119. Wang, K.; Gao, S.; Li, L.; et al. Enhanced low-temperature resistance of lithium-metal rechargeable batteries based on electrolyte including ethyl acetate and LiDFOB Additives. *Chem. Eur. J.* **2024**, *30*, e202400803.
120. Su, F.; Lin, Y.; Dou, X.; et al. Compact ion-pair aggregates dominated electrolytes enable high-performance low-temperature lithium-ion batteries. *Angew. Chem. Int. Ed.* **2025**, *64*, e202510647.
121. Lin, S.; Hua, H.; Lai, P.; et al. A multifunctional dual-salt localized high-concentration electrolyte for fast dynamic high-voltage lithium battery in wide temperature range. *Adv. Energy Mater.* **2021**, *11*, 2101775.
122. Chen, Y.; Yu, Z.; Rudnicki, P.; et al. Steric effect tuned ion solvation enabling stable cycling of high-voltage lithium metal battery. *J. Am. Chem. Soc.* **2021**, *143*, 18703–18713.
123. Yang, Y.; Li, Y.; Zhang, J.; et al. Co-intercalation-free graphite anode enabled by an additive regulated interphase in an ether-based electrolyte for low-temperature lithium-ion batteries. ACS Appl. *Mater. Interfaces* **2024**, *16*, 10116–10125.
124. Liu, X.; Zhang, J.; Yun, X.; et al. Anchored weakly-solvated electrolytes for high-voltage and low-temperature lithium-ion batteries. *Angew. Chem. Int. Ed.* **2024**, *63*, e202406596.
125. Zhu, X.; Chen, J.; Liu, G.; et al. Non-fluorinated cyclic ether-based electrolyte with quasi-conjugate effect for high-performance lithium metal batteries. *Angew. Chem. Int. Ed.* **2025**, *64*, e202412859.

126. Ma, Y.; Huang, M.; Xue, Y.; et al. A fully methylated cyclic ether solvent enables graphite anode cycling at low temperatures. *ACS Appl. Mater. Interfaces* **2024**, *16*, 23362–23373.
127. Wang, Y.; Liu, J.; Ji, H.; et al. Optimizing Si-O conjugation to enhance interfacial kinetics for low-temperature rechargeable lithium-ion batteries. *Adv. Mater.* **2024**, *37*, 202412155.
128. Li, Z.; Yao, Y.-X.; Zheng, M.; et al. Electrolyte Design Enables Rechargeable LiFePO4/Graphite Batteries from −80 °C to 80 °C. *Angew. Chem. Int. Ed.* **2025**, *64*, e202409409.
129. Lin, W.; Li, J.; Wang, J.; et al. Weak-coordination electrolyte enabling fast Li^+ transport in lithium metal batteries at ultra-low temperature. *Small* **2023**, *19*, 202207093.
130. Han, R.; Wang, Z.; Huang, D.; et al. High-energy-density lithium metal batteries with impressive Li^+ transport dynamic and wide-temperature performance from −60 to 60 °C. *Small* **2023**, *19*, 2300571.
131. Weng, S.; Zhang, X.; Yang, G.; et al. Temperature-dependent interphase formation and Li^+ transport in lithium metal batteries. *Nat. Commun.* **2023**, *14*, 4474.
132. Cui, Z.; Liu, C.; Manthiram, A. Enabling stable operation of lithium-ion batteries under fast-operating conditions by tuning the electrolyte chemistry. *Adv. Mater.* **2024**, *36*, 2409272.
133. Zou, Y.; Cheng, F.; Lu, Y.; et al. High performance low-temperature lithium metal batteries enabled by tailored electrolyte solvation structure. *Small* **2023**, *19*, 2203394.
134. Yang, Y.; Fang, Z.; Yin, Y.; et al. Synergy of weakly-solvated electrolyte and optimized interphase enables graphite anode charge at low temperature. *Angew. Chem. Int. Ed.* **2022**, *61*, e202208345.
135. Luo, L.; Chen, K.; Cao, R.; et al. Ethyl fluoroacetate with weak Li^+ interaction and high oxidation resistant induced low-temperature and high-voltage graphite//$LiCoO_2$ batteries. *Energy Storage Mater.* **2024**, *70*, 103438.
136. Cao, Z.; Zheng, X.; Zhou, M.; et al. Electrolyte solvation engineering toward high-rate and low-temperature silicon-based batteries. *ACS Energy Lett.* **2022**, *7*, 3581–3592.
137. Chen, C.; Zhang, S.; Xu, C.; et al. Wide-temperature and high-voltage Li||$LiCoO_2$ cells enabled by a nonflammable partially-fluorinated electrolyte with fine-tuning solvation structure. *J. Energy Chem.* **2025**, *101*, 608–618.
138. Wang, Z.; Sun, Z.; Shi, Y.; et al. Ion-dipole chemistry drives rapid evolution of Li ions solvation sheath in low-temperature Li batteries. *Adv. Energy Mater.* **2021**, *11*, 2100935.
139. Tan, S.; Borodin, O.; Wang, N.; et al. Synergistic anion and solvent-derived interphases enable lithium-ion batteries under extreme conditions. *J. Am. Chem. Soc.* **2024**, *146*, 30104–30116.
140. Xiao, P.; Zhao, Y.; Piao, Z.; et al. A nonflammable electrolyte for ultrahigh-voltage (4.8 V-class) Li||NCM811 cells with a wide temperature range of 100 °C. *Energy Environ. Sci.* **2022**, *15*, 2435–2444.
141. Cai, G.; Holoubek, J.; Li, M.; et al. Solvent selection criteria for temperature-resilient lithium–sulfur batteries. *Proc. Nat. Acad. Sci. USA* **2022**, *119*, e2200392119.
142. Li, H.; Kang, Y.; Wei, W.; et al. Branch-chain-rich Diisopropyl ether with steric hindrance facilitates stable cycling of lithium batteries at−20 °C. *Nano-Micro Lett.* **2024**, *16*, 197.
143. Liu, T.; Feng, J.; Shi, Z.; et al. Diminishing ether-oxygen content of electrolytes enables temperature-immune lithium metal batteries. *Sci. China Chem.* **2023**, *66*, 2700–2710.
144. Huang, Y.; Fang, H.; Geng, J.; et al. Anionic solvation transition at low temperatures for reversible anodes in lithium-oxygen batteries. *J. Am. Chem. Soc.* **2024**, *146*, 26516–26524.
145. Mao, S.; Zhang, J.; Mao, J.; et al. Anionic aggregates induced interphase chemistry regulation toward wide-temperature silicon-based batteries. *Adv. Energy Mater.* **2024**, *14*, 2401979.
146. Zhang, H.; Zeng, Z.; Ma, F.; et al. Cyclopentylmethyl ether, a non-fluorinated, weakly solvating and wide temperature solvent for high-performance lithium metal battery. *Angew. Chem. Int. Ed.* **2023**, *62*, e202300771.
147. Chen, X.; Li, Z.; Zhao, H.; et al. Dominant solvent-separated ion pairs in electrolytes enable superhigh conductivity for fast-charging and low-temperature lithium ion batteries. *ACS Nano* **2024**, *18*, 8350–8359.
148. Zhang, J.; Li, Q.; Zeng, Y.; et al. Weakly solvating cyclic ether electrolyte for high-voltage lithium metal batteries. *ACS Energy Lett.* **2023**, *8*, 1752–1761.
149. Li, Z.; Liao, Y.; Ji, H.; et al. A tetrahydropyran-based weakly solvating electrolyte for low-temperature and high-voltage lithium metal batteries. *Adv. Energy Mater.* **2024**, *15*, 2404120.
150. Gu, R.; Zhang, D.; Xu, S.; et al. Thermoresponsive ether-based electrolyte for wide temperature operating lithium metal batteries. *Nat. Commun.* **2025**, *16*, 5474.
151. Yu, R.; Li, Z.; Zhang, X.; et al. Electrolyte design for inorganic-rich solid-electrolyte interfaces to enable low-temperature Li metal batteries. *Chem. Commun.* **2022**, *58*, 8994–8997.
152. Li, Z.; Rao, H.; Atwi, R.; et al. Non-polar ether-based electrolyte solutions for stable high-voltage non-aqueous lithium metal batteries. *Nat. Commun.* **2023**, *14*, 868.
153. Tan, L.; Chen, S.; Chen, Y.; et al. Intrinsic nonflammable ether electrolytes for ultrahigh-voltage lithium metal batteries enabled by chlorine functionality. *Angew. Chem. Int. Ed.* **2022**, *61*, e202203693.

154. Yu, Z.; Wang, H.; Kong, X.; et al. Molecular design for electrolyte solvents enabling energy-dense and long-cycling lithium metal batteries. *Nat. Energy* **2020**, *5*, 526–533.
155. Yu, Z.; Rudnicki, P.E.; Zhang, Z.; et al. Rational solvent molecule tuning for high-performance lithium metal battery electrolytes. *Nat. Energy* **2022**, *7*, 94–106.
156. Chen, Y.; He, Q.; Zhao, Y.; et al. Breaking solvation dominance of ethylene carbonate via molecular charge engineering enables lower temperature battery. *Nat. Commun.* **2023**, *14*, 8326.
157. Ma, P.; Xue, C.; Wang, K.-H.; et al. Molecular structure optimization of fluorinated ether electrolyte for all temperature fast charging lithium-ion battery. *ACS Energy Lett.* **2024**, *9*, 6144–6152.
158. Chen, J.; Lu, H.; Kong, X.; et al. Interphase engineering via solvent molecule chemistry for stable lithium metal batteries. *Angew. Chem. Int. Ed.* **2024**, *63*, e202317923.
159. Zhang, G.; Chang, J.; Wang, L.; et al. A monofluoride ether-based electrolyte solution for fast-charging and low-temperature non-aqueous lithium metal batteries. *Nat. Commun.* **2023**, *14*, 1081.
160. Chen, Y.-P.; Niu, Y.-L.; Zheng, Z.; et al. Origin of anion-rich solvation structures in siloxane electrolytes. *Angew. Chem. Int. Ed.* **2025**, *64*, e202508152.
161. Zou, Y.; Ma, Z.; Liu, G.; et al. Non-flammable electrolyte enables high-voltage and wide-temperature lithium-ion batteries with fast charging. *Angew. Chem. Int. Ed.* **2023**, *62*, e202216189.
162. Liang, P.; Li, J.; Dong, Y.; et al. Modulating interfacial solvation via ion dipole interactions for low-temperature and high-voltage lithium batteries. *Angew. Chem. Int. Ed.* **2025**, *64*, e202415853.
163. Liang, P.; Hu, H.; Dong, Y.; et al. Competitive coordination of ternary anions enabling fast Li-ion desolvation for low-temperature lithium metal batteries. *Adv. Funct. Mater.* **2024**, *34*, 2309858.
164. Cheng, F.; Zhang, W.; Li, Q.; et al. High chaos induced multiple-anion-rich solvation structure enabling ultrahigh voltage and wide temperature lithium-metal batteries. *ACS Nano* **2023**, *17*, 24259–24267.
165. Thenuwara, A.C.; Shetty, P.P.; Kondekar, N.; et al. Efficient low-temperature cycling of lithium metal anodes by tailoring the solid-electrolyte interphase. *ACS Energy Lett.* **2020**, *5*, 2411–2420.
166. Huang, J.; Li, Y.; Liu, J.; et al. Interphase-designable additive-enabled ethylene carbonate-free electrolyte for wide-temperature, long-cycling, high-voltage lithium metal batteries. *Adv. Funct. Mater.* **2024**, *34*, 2406215.
167. Zhu, H.; Zhang, Q.; Wang, K.; et al. Minimizing solvent-coordination in ether electrolytes for lithium metal batteries under extreme operating conditions. *Adv. Mater.* **2025**, *37*, 202505892.
168. Li, Y.; Wen, B.; Li, N.; et al. Electrolyte Engineering to Construct Robust Interphase with High Ionic Conductivity for Wide Temperature Range Lithium Metal Batteries. *Angew. Chem. Int. Ed.* **2025**, *64*, e202414636.
169. Zhang, Z.; Hu, J.; Hu, Y.; et al. Lithium fluorosulfonate-induced low-resistance interphase boosting low-temperature performance of commercial graphite/$LiFePO_4$ pouch batteries. *J. Colloid Interface Sci.* **2024**, *669*, 305–313.
170. Chen, N.; Feng, M.; Li, C.; et al. Anion-dominated conventional-concentrations electrolyte to improve low-temperature performance of lithium-ion batteries. *Adv. Funct. Mater.* **2024**, *34*, 2400337.
171. Shangguan, X.; Xu, G.; Cui, Z.; et al. Additive-assisted novel dual-salt electrolyte addresses wide temperature operation of Lithium–Metal batteries. *Small* **2019**, *15*, 1900269.
172. Li, L.; Lv, W.; Chen, J.; et al. Lithium difluorophosphate ($LiPO_2F_2$): An electrolyte additive to help boost low-temperature behaviors for lithium-ion batteries. *ACS Appl. Energy Mater.* **2022**, *5*, 11900–11914.
173. Dong, L.; Yan, H.-J.; Liu, Q.-X.; et al. Quantification of charge transport and mass deprivation in solid electrolyte interphase for kinetically-stable low-temperature lithium-ion batteries. *Angew. Chem. Int. Ed.* **2024**, *63*, e202411029.
174. Liang, J.-Y.; Zhang, Y.; Xin, S.; et al. Mitigating swelling of the solid electrolyte interphase using an inorganic anion switch for low-temperature lithium-ion batteries. *Angew. Chem. Int. Ed.* **2023**, *62*, e202300384.
175. Jiang, H.-Z.; Yang, C.; Chen, M.; et al. Electrophilically trapping water for preventing polymerization of cyclic ether towards low-temperature Li metal battery. *Angew. Chem. Int. Ed.* **2023**, *62*, e202300238.
176. Zhang, L.-J.; He, J.-Z.; Yan, X.; et al. Enhancing low-temperature electrolyte performance through intermittent discharge for improved LiODFB additive film formation. *J. Electroanal. Chem.* **2024**, *957*, 118124.
177. Piao, Z.; Ren, H.-R.; Lu, G.; et al. Stable operation of lithium metal batteries with aggressive cathode chemistries at 4.9 V. *Angew. Chem. Int. Ed.* **2023**, *62*, e202300966.
178. Lu, Z.; Liu, D.; Dai, K.; et al. Tailoring solvation chemistry in carbonate electrolytes for all-climate, high-voltage lithium-rich batteries. *Energy Storage Mater.* **2023**, *57*, 316–325.
179. Gu, S.; Zhang, Y.; Li, M.; et al. Internal electron-donation allocation design for intrinsic solubilization of lithium nitrate in ester electrolyte for stable lithium metal batteries. *Angew. Chem. Int. Ed.* **2025**, *64*, e202410020.
180. Jiang, J.; Li, M.; Liu, X.; et al. Multifunctional additives to realize dendrite-free lithium deposition in carbonate electrolytes toward low-temperature Li metal batteries. *Adv. Energy Mater.* **2024**, *14*, 2400365.
181. Piao, Z.; Xiao, P.; Luo, R.; et al. Constructing a stable interface layer by tailoring solvation chemistry in carbonate electrolytes for high-performance lithium-metal batteries. *Adv. Mater.* **2022**, *34*, 2108400.

182. He, Z.; Tu, H.; Sun, G.; et al. High ion-conductive interphase enabled by nitrate-ionic liquid additive for low-temperature lithium metal batteries. *Adv. Funct. Mater.* **2025**, *35*, 2414569.
183. Lin, Y.; Su, F.; Jiang, J.; et al. Copper nitrate enables high-performance lithium-ion batteries at low temperature. *Energy Storage Mater.* **2024**, *70*, 103484.
184. Ou, Y.; Zhu, D.; Zhou, P.; et al. Self-compartmented electrolyte design for stable cycling of lithium metal batteries under extreme conditions. *Angew. Chem. Int. Ed.* **2025**, *64*, e202504632.
185. Zhang, W.; Lu, Y.; Cao, Q.; et al. A reversible self-assembled molecular layer for lithium metal batteries with high energy/power densities at ultra-low temperatures. *Energy Environ. Sci.* **2024**, *17*, 4531–4543.
186. Lu, Y.; Cao, Q.; Zhang, W.; et al. Breaking the molecular symmetricity of sulfonimide anions for high-performance lithium metal batteries under extreme cycling conditions. *Nat. Energy* **2025**, *10*, 191–204.
187. Wang, Z.; Zhang, H.; Xu, J.; et al. Advanced ultralow-concentration electrolyte for wide-temperature and high-voltage Li-metal batteries. *Adv. Funct. Mater.* **2022**, *32*, 2112598.
188. Qin, J.; Liu, Y.; Li, G.; et al. Plastic crystal fast ion-conductor electrolyte enabled ultra-low temperature rechargeable organic battery. *Adv. Energy Mater.* **2024**, *14*, 2400731.
189. Kim, S.; Pol, V.G. Tailored solvation and interface structures by tetrahydrofuran-derived electrolyte facilitates ultralow temperature lithium metal battery operations. *ChemSusChem* **2023**, *16*, e202202143.
190. Liu, X.; Mariani, A.; Diemant, T.; et al. Locally concentrated ionic liquid electrolytes enabling low-temperature lithium metal batteries. *Angew. Chem. Int. Ed.* **2023**, *62*, e202305840.
191. Liu, X.; Mariani, A.; Diemant, T.; et al. PFAS-free locally concentrated ionic liquid electrolytes for lithium metal batteries. *ACS Energy Lett.* **2024**, *9*, 3049–3057.
192. Song, W.; Li, B.; Qu, Y.; et al. Dynamic migration-pulling polymer electrolyte design strategy for low-temperature Lithium–Sulfur batteries. *Angew. Chem. Int. Ed.* **2025**, *64*, e202505095.
193. Li, R.; Hua, H.; Yang, X.; et al. The deconstruction of a polymeric solvation cage: A critical promotion strategy for PEO-based all-solid polymer electrolytes. *Energy Environ. Sci.* **2024**, *17*, 5601–5612.
194. Lv, F.; Liu, K.; Wang, Z.; et al. Ultraviolet-cured polyethylene oxide-based composite electrolyte enabling stable cycling of lithium battery at low temperature. *J. Colloid Interface Sci.* **2021**, *596*, 257–266.
195. Lu, P.; Zhou, Z.; Xiao, Z.; et al. Materials and chemistry design for low-temperature all-solid-state batteries. *Joule* **2024**, *8*, 635–657.
196. He, Y.; Shan, X.; Li, Y.; et al. In-situ formation of quasi-solid polymer electrolyte for wide-temperature applicable Li-metal batteries. *Energy Storage Mater.* **2024**, *68*, 103281.
197. Yu, J.; Lin, X.; Liu, J.; et al. In situ fabricated quasi-solid polymer electrolyte for high-energy-density lithium metal battery capable of subzero operation. *Adv. Energy Mater.* **2022**, *12*, 2102932.
198. Zhang, X.; Cui, X.; Li, Y.; et al. A star-structured polymer electrolyte for low-temperature solid-state lithium batteries. *Small Methods* **2024**, *8*, 2400356.
199. Xu, S.; Sun, Z.; Sun, C.; et al. Homogeneous and fast ion conduction of PEO-based solid-state electrolyte at low temperature. *Adv. Funct. Mater.* **2020**, *30*, 2007172.
200. Park, J.; Seong, H.; Yuk, C.; et al. Design of fluorinated elastomeric electrolyte for solid-state lithium metal batteries operating at Low Temperature and High Voltage. *Adv. Mater.* **2024**, *36*, 2403191.
201. Liu, Y.; Wang, P.; Yang, Z.; et al. Lignin derived ultrathin all-solid polymer electrolytes with 3D single-ion nanofiber ionic bridge framework for high performance lithium batteries. *Adv. Mater.* **2024**, *36*, 2400970.
202. Li, Z.; Yu, R.; Weng, S.; et al. Tailoring polymer electrolyte ionic conductivity for production of low-temperature operating quasi-all-solid-state lithium metal batteries. *Nat. Commun.* **2023**, *14*, 482.
203. Li, Z.; Li, Z.; Yu, R.; et al. Dual-salt poly(tetrahydrofuran) electrolyte enables quasi-solid-state lithium metal batteries to operate at 30 °C. *J. Energy Chem.* **2024**, *96*, 456–463.
204. Ren, W.; Shang, X.; Lin, Y.; et al. Regulating interfacial Li deposition at low-temperature through eliminating Li^+ transfer mismatching by artificial modifying the interface in solid state battery. *Adv. Energy Mater.* **2025**, *15*, 2405284.
205. Mo, S.; An, H.; Liu, Q.; et al. Multistage bridge engineering for electrolyte and interface enables quasi-solid batteries to operate at –40 °C. *Energy Storage Mater.* **2024**, *65*, 103179.
206. Huang, X.; Huang, S.; Wang, T.; et al. Polyether-b-amide based solid electrolytes with well-adhered interface and fast kinetics for ultralow temperature solid-state lithium metal batteries. *Adv. Funct. Mater.* **2023**, *33*, 2300683.
207. Lu, P.; Xia, Y.; Huang, Y.; et al. Wide-temperature, long-cycling, and high-loading pyrite all-solid-state batteries enabled by argyrodite thioarsenate superionic conductor. *Adv. Funct. Mater.* **2022**, *33*, 2211211.
208. Morino, Y. Impact of surface coating on the low temperature performance of a sulfide-based all-solid-state battery cathode. *Electrochemistry* **2022**, *90*, 027001.
209. Lu, P.; Gong, S.; Wang, C.; et al. Superior low-temperature all-solid-state battery enabled by high-ionic-conductivity and low-energy-barrier interface. *ACS Nano* **2024**, *18*, 7334–7345.

210. Li, X.; Xu, Y.; Zhao, C.; et al. The universal super cation-conductivity in multiple-cation mixed chloride solid-state electrolytes. *Angew. Chem. Int. Ed.* **2023**, *62*, e202306433.
211. Tan, D.H.S.; Chen, Y.-T.; Yang, H.; et al. Carbon-free high-loading silicon anodes enabled by sulfide solid electrolytes. *Science* **2021**, *373*, 1494–1499.
212. Peng, L.; Ren, H.; Zhang, J.; et al. $LiNbO_3$-coated $LiNi_{0.7}Co_{0.1}Mn_{0.2}O_2$ and chlorine-rich argyrodite enabling high-performance solid-state batteries under different temperatures. *Energy Storage Mater.* **2021**, *43*, 53–61.
213. Peng, L.; Yu, C.; Zhang, Z.; et al. Chlorine-rich lithium argyrodite enabling solid-state batteries with capabilities of high voltage, high rate, low-temperature and ultralong cyclability. *Chem. Eng. J.* **2022**, *430*, 132896.
214. Wang, X.; Jin, S.; Shi, L.; et al. Toward enhancing low temperature performances of lithium-ion transport for Metal-Organic framework-based solid-state electrolyte: Nanostructure engineering or crystal morphology controlling. *ACS Appl. Mater. Interfaces* **2024**, *16*, 33954–33962.
215. Akimoto, J.; Akao, T.; Nagai, H.; et al. Low-temperature sintering of a garnet-type $Li_{6.5}La_3Zr_{1.5}Ta_{0.5}O_{12}$ solid electrolyte and an all-solid-state lithium-ion battery. *ACS Appl. Mater. Interfaces* **2023**, *15*, 18973–18981.
216. Li, J.; Zhu, R.; Zhang, T.; et al. Integrating activated inorganic fluoride nanocrystals with polar polymer for wide-temperature solid lithium metal batteries. *ACS Energy Lett.* **2024**, *9*, 4044–4052.
217. Xu, J. Electrolyte Design via Temperature-Responsive Solvation Structures for All-Climate Batteries. *Chem. Mater.* 2026. https://doi.org/10.1021/acs.chemmater.5c03090.
218. Sun, S.; Wang, K.; Hong, Z.; et al. Electrolyte Design for Low-Temperature Li-Metal Batteries: Challenges and Prospects. *Nano-Micro Lett.* **2024**, *16*, 35.
219. Guo, D.; Wang, J.; Cui, Z.; et al. Low-Temperature Sodium-Sulfur Batteries Enabled by Ionic Liquid in Localized High Concentration Electrolytes. *Adv. Funct. Mater.* **2024**, *34*, 2409494.
220. Zhang, H.; Zhao, Y.; Li, X.; et al. Wide-Temperature Electrolyte Design via Cation-Anion Solvation Engineering for 4.6 V Lithium-Ion Batteries. *Adv. Sci.* **2025**, *12*, e03151.
221. Nian, Q.; Wang, J.; Liu, S.; et al. Aqueous Batteries Operated at –50 °C. *Angew. Chem. Int. Ed.* **2019**, *58*, 16994–16999.
222. Xu, J.; Koverga, V.; Phan, A.; et al. Revealing the Anion-Solvent Interaction for Ultralow Temperature Lithium Metal Batteries. *Adv. Mater.* **2024**, *36*, 2306462.
223. Jin, C.-B.; Yao, N.; Xiao, Y.; et al. Taming Solvent-Solute Interaction Accelerates Interfacial Kinetics in Low-Temperature Lithium-Metal Batteries. *Adv. Mater.* **2023**, *35*, 2208340.
224. Cavallaro, K.A.; Sandoval, S.E.; Yoon, S.G.; et al. Low-Temperature Behavior of Alloy Anodes for Lithium-Ion Batteries. *Adv. Energy Mater.* **2022**, *12*, 2201584.
225. Lu, Y.; Zhao, C.-Z.; Huang, J.-Q.; et al. The timescale identification decoupling complicated kinetic processes in lithium batteries. *Joule* **2022**, *6*, 1172–1198.
226. Araujo, L.A.; Sarou-Kanian, V.; Sicsic, D.; et al. Operando nuclear magnetic resonance spectroscopy: Detection of the onset of metallic lithium deposition on graphite at low temperature and fast charge in a full Li-ion battery. *J. Magn. Reson.* **2023**, *354*, 107527.
227. Xu, G.; Wang, M.; Song, Y.; et al. Visualized Detection of Lithium Plating on Graphite Anodes Cycled Under Low Temperature and Fast Charging. *Adv. Funct. Mater.* **2025**, *35*, 2412614.